UNIVERSITE MOHAMMED V

FACULITE DES SCIENCES
Rabat

N° d'ordre : 2729

THESE DE DOCRORAT

Présentée par

Sufyan Saleh Ahmed NAJI

Discipline: Physique informatique.
Spécialité : Matière condensée et modélisation des systèmes

A theoretical study on physical properties of 2D hexagonal nanostructured materials

Soutenue le 23 Septembre 2014
Devant le jury :

Président :

Abdelilah BENYOUSSEF	PES, Faculté des Sciences, Rabat

Examinateurs :

Lahoucine BAHMAD	PES, Faculté des Sciences, Rabat
Mohamed BENAISSA	PH, Faculté des Sciences, Rabat
Youssef EL AMRAOUI	PES, Faculté des Sciences et Techniques, Errachidia
Abdallah EL KENZ	PES, Faculté des Sciences, Rabat
Hamid EZ-ZAHRAOU	PES, Faculté des Sciences, Rabat
El Kebir HLIL	PES, Institut NEEL, CNRS, Grenoble, France
Mohamed LOULIDI	PES, Faculté des Sciences, Rabat

Dedication

To

My father and mother

My wife Abeer

My children NOOR and Mohammed

To my brothers and sisters

To all my professors and teachers

To all my friends

Acknowledgement

This thesis has been carried out at the Laboratory of Magnetism and High Energy Physics (LMPHE), Faculty of Science, Mohammed V University – Rabat, under the supervision of prof. Abdelilah Benyoussef.

First and foremost, praises and thanks go to Allah, the Almighty, for his unlimited and uncountable blessings in my whole life and throughout my research work especially.

On this page, I would like to express my very great appreciation, deep gratitude and sincere thanks to my supervisor, the chairman of the jury prof. Abdelilah Benyoussef, for giving me this opportunity to learn from his valuable expertise and to have the fruitful discussions with him. He always had time to answer my questions and he patiently provided the vision, encouragement and advise necessary for me to proceed throughout my research period. It is my privilege to be his student.

Besides my supervisor, I would like also to offer my thanks to the thesis committee for reviewing my thesis and giving their insightful and useful comments.

I would like to thank Prof. Lahoucine Bahmad from Faculty of Science Rabat, for reviewing my PhD thesis.

I would like also to express my thanks to Prof. Abdallah EL Kenz from Faculty of Science Rabat , for reporting and reviewing this thesis.

I would like to thank Prof. Hamid EZ-Zahraouy from Faculty of Science Rabat, for reviewing this PhD thesis.

I would like also to offer my thanks to Prof. Mohamed Loulidi from Faculty of Science Rabat, for reviewing this thesis.

I would also like to extend my thanks to Prof. Mohamed Benaissa from Faculty of Science Rabat, for reviewing my thesis.

I would like also to express my thanks to Prof. El Kebir Hlil from University of Joseph Fourier, Grenoble, Institut Néel, France, for reporting and reviewing this PhD thesis.

I would like also to offer my thanks Prof. Youssef EL Amraoui from Faculty of Science and Technology, Errachidia, for reviewing this thesis.

I would like also to offer my special thanks to all the professors of our laboratory for their valuable suggestions and discussions.

I would also like to extend my thanks to the researchers Dr. H. Labrim, prof. A. Belhaj, Mr. M. Bhihi, Dr. B. Khalil for the interesting discussions and contributions. My thanks also go to my colleagues especially, Ms. F. El Hallani, Mr. D. Larhris, Mr. M. Lakhal, Miss M. El khatabi, Miss. H. Zaari, Mr. M. Abdellaoui, Mr. M. Boujnah, and Mr. N. Lakouari

I would like to thank the two following groups: prof. M. Richter and FPLO group and prof. P. Blaha, prof. K. Schwartz and WIEN2K group, for the support of FPLO and WIEN2K packages and for useful discussions.

Special thanks should be given to my wife Abeer, my daughter Noor and my son Mohammad, for their support, patience and encouragement throughout my study.

Finally, I wish to thank my parents and my siblings, for their support and encouragement.

Abstract

In this thesis, we have theoretically investigated, using ab initio calculations, the electronic structure of graphene, silicene and germanene nanostructures.

We have shown first that, the inter-distances variation of the graphene bilayer affects the electronic properties that drastically depend on stacking arrangements. The interactions in such system lead to the opening of the band gap energy making this system extremely appealing for electronic devices and optoelectronics applications. A similar study has been also extended to silicene and germanene like bilayer systems which give close behaviors and results.

We have also engineered a double hexagonal structure model based on the adsorbed materials (Fe, Co, or Ni) atoms interacting with a graphene sheet. A close inspection shows that Fe-graphene and Co-graphene systems are ferromagnetic with strong spin polarizations, while Ni-system remains a non-magnetic metal. Monte Carlo calculations show that Co-graphene system has a high critical temperature making it a very useful in spintronic field. Besides that, we have proposed and examined a new hexagonal structure for C, Si and Ge atoms. It is found that, this new hexagonal structure modified the usual electronic properties, appearing in the single hexagonal geometries.

Keywords: Graphene, silicene and germanene nanostructures, ab initio calculations, Monte Carlo simulation, opening of the band gap energy, ferromagnetic with a strong spin polarization.

Résumé

Dans cette thèse, nous avons étudié théoriquement, en utilisant des calculs *ab* initio, la structure électronique des nanostructures graphène, silicene et germanene.

Nous avons montré tout d'abord que, la variation de l'inter-distance de la bicouche de graphène affecte les propriétés électroniques qui dépendent fortement des configurations d'empilement. Les interactions, dans un tel système, conduisent à l'ouverture de l'énergie de la bande interdite qui rend ce système extrêmement attrayant pour des dispositifs électroniques et des applications optoélectroniques. Une étude similaire a été également étendue au silicene et germanene comme des systèmes bicouches qui donnent des comportements et des résultats proches.

Nous avons également conçu un modèle de la double structure hexagonale sur la base des éléments adsorbées (Fe, Co, ou Ni) interagissant avec une feuille de graphène. On constate que les systèmes Co-graphène et Fe-graphène sont ferromagnétiques avec une forte polarisation des spins, tandis que le système Ni-graphène reste non magnétique. Des calculs Monte Carlo montrent que le système Co-graphène a une haute température critique ; cette caractéristique est très utile dans le domaine de la spintronique.

En plus de cela, nous avons proposé et examiné une nouvelle structure hexagonale pour les atomes C, Si et Ge. Il se trouve que, cette nouvelle structure hexagonale a modifié les propriétés électroniques, figurant dans les géométries hexagonales simples.

Mots-clefs: Nanostructures, graphène, silicene et germanene, calculs ab initio, la simulation Monte Carlo, l'ouverture de l'énergie de la bande interdite, ferromagnétiques avec une forte polarisation des spins.

Résumé Détaillé

Cette thèse porte sur l'étude théorique, basée sur le calcul *ab* initio et la simulation Monte Carlo, des propriétés physiques des nanostructures mono et bicouche à base de graphène, silicene et germanene. Ainsi que la proposition et l'étude d'une nouvelle structure « hexagonale » à base d'atomes de carbone, silicium et germanium.

Le premier chapitre de cette thèse est une introduction générale sur le graphène, comme cristal de carbone, avec ses propriétés physiques, des techniques de sa synthèse et d'autres matériaux similaires comme le silicene et le germanene. Afin de montrer l'utilité du graphene nous avons listé quelques applications actuelles et autres à l'échelle pilote.

Le deuxième chapitre introduit le cadre théorique y compris les différentes approximations et approches de calcul *ab* initio et simulation Monte Carlo sur lesquelles le calcul s'était basé dans cette thèse.

Le troisième chapitre de cette thèse propose une étude d'un modèle monocouche. En effet, nous avons présenté les systèmes modélisés correspondant à une seule couche de graphène, silicene et germanene avec deux différentes géométries (plan et boucle) utilisant le calcul ab initio avec les approximations appropriées inclus dans le code FPLO9.00-34. Les principaux résultats obtenus sont : les paramètres optimaux de maille, la densité d'états et les structures de bandes de ces systèmes. Ses résultats montrent aussi que le modèle à boucle est plus stable dans le cas de silicene et germanene.

Le 4ème chapitre adresse l'étude de la structure électronique de deux feuilles parallèles de graphène par le biais du calcul ab initio mises en œuvre dans le code FPLO9.00-34 avec l'approximation de la densité locale LDA (Local Density Approximation). Dans ces systèmes la 1ère couche est statique et interagit avec une couche supplémentaire (2ème couche) qui est placée à une distance d dans la direction normale z de la configuration d'empilement (AB). En se basant sur ce modèle, nous avons constaté que la variation de la distance verticale ne modifie pas la bande interdite, pendant que la variation de la distance diagonale de la bicouche de graphène, affecte les propriétés électroniques qui dépendent fortement des arrangements d'empilage intermédiaires entre les configurations (AA) et (AB). Nous avons aussi remarqué que le système bicouche se comporte comme deux plans de graphène isolés pour les grandes distances. Dans le

cas de courtes distances, les états dans les cônes de Dirac appartenant aux deux couches interagissent entre eux. Ces interactions conduisent à l'ouverture de la bande d'énergie interdite ce qui rend ce système extrêmement attractif pour les dispositifs électroniques et les applications optoélectroniques. Les résultats des arrangements d'empilage intermédiaires fournissent également une nouvelle façon théorique d'étudier et de décrire le désordre dans le système bicouche de graphène qui pourrait se produire au cours de la production d'échantillons.

Le 5ème chapitre s'est focalisé sur l'étude de la structure électronique des deux plans parallèles de silicene et germanene, ayant une géométrie hexagonale, en utilisant le calcul ab initio basé sur le code FPLO9.00-34 avec l'approximation de la densité locale LDA. Pour le cas de silicene, nous avons trouvé que la bande interdite peut être ouverte simplement en faisant varier la distance entre deux couches parallèles de silicium à partir d'une distance supérieure à la longueur de liaison de Van der Waals. Alors que dans le cas de germanene, la bande interdite peut être ouverte en faisant varier la distance entre deux couches parallèles de germanene seulement pour les géométries boucles. Ces comportements rendent le silicene et le germanene attrayant autant que dispositifs électroniques et des applications optoélectroniques.

Dans le sixième chapitre, nous avons également conçu, utilisant le calcul ab initio basé sur le code WIEN2K-12 avec l'approximation du gradient généralisé (GGA), un modèle de la double structure hexagonale sur la base des éléments adsorbés (Fe, Co, ou Ni) interagissant avec une feuille de graphène. Nous constatons que les systèmes Co-graphène et Fe-graphène sont ferromagnétiques avec une forte polarisation des spins, tandis que le système Ni-graphène reste non magnétique. Des calculs Monte Carlo montrent que le système Co-graphène a une haute température critique ; cette caractéristique est très utile dans le domaine de la spintronique.

Le dernier chapitre, propose et examine, utilisant le calcul ab initio sur le code FPLO9.00-34 avec l'approximation du gradient généralisé (GGA), une nouvelle structure hexagonale pour les atomes de carbone, silicium et germanium. Cette nouvelle structure a modifié les propriétés électroniques, figurant dans les géométries hexagonales simples. Ceci est corrélé à une augmentation du nombre des atomes voisins qui interagissent dans la nouvelle structure. Nous avons conclu alors que cette augmentation crée de nouveaux états au niveau de l'énergie de Fermi, conduisant à un recouvrement entre les bandes de valence et de conduction. Ceci implique que les deux systèmes se comportent comme un métal.

List of Publications

Publications related to this thesis

1. **S. Naji**, A. Belhaj, H. Labrim, M. Bhihi, A. Benyoussef, A. El Kenz. Adsorption of Co and Ni on Graphene with Double Hexagonal Symmetry: Electronic and Magnetic properties. ***Journal of Physical Chemistry C*** **J. Phys. Chem. C,** 2014, 118 (9), pp 4924–4929.

2. **S. Naji,** M. Bhihi, H. Labrim, A. Belhaj, A. Benyoussef, A. El Kenz, M. Loulidi, On Distance Variation Effects on Graphene Bilayers. ***Journal of chemistry and physics of solids***, 75 (6), 2014, 739–745.

3. **S. Naji**, A. Belhaj, H. Labrim, M. Bhihi, A. Benyoussef, A. El Kenz. Electronic and magnetic properties of iron adsorption on graphene with double hexagonal geometry ***Int. J. Quantum Chem.*** 2014, 114, 463–467.

4. **S. Naji,** A. Belhaj, H. Labrim, A. Benyoussef, A. El Kenz, New hexagonal structure for silicon atoms, ***the European Physical Journal B*** vol. 85,11(2012) 373.

5. **S. Naji,** A. Belhaj, H. Labrim, A. Benyoussef, A. El Kenz, Electronic structure of graphene and germanene based on double hexagonal structure, ***Modern Mod. Phys. Lett.*** B 27, 1350212 (2013).

6. **S.Naji**, B. Khalil, H. Labrim, M. Bhihi, A. Belhaj, A. Benyoussef, M. Lakhal, A. El Kenz, Interdistance Effects on Flat and Buckled Silicene Like-bilayer***s. Journal of Physics: Conference Series, 3rd International Meeting on Silicene (IMS-3);*** 491 (2014) 012006.

7. **S.Naji**, M. Bhihi, H. Labrim, A. Belhaj, A. Benyoussef, M. Lakhal, A. El Kenz, First-Principles Study of Interdistance Effects on Germanene Like-bilayers, submitted.

Other publications

1. **S. Naji** , A. Benyoussef, A. El Kenz , H. Ez-Zahraouy and M. Loulidi , Monte Carlo study of phase transitions and magnetic properties of $LaMnO_3$: ***Heisenberg model physica A***, 391(2012)3885.

2. **S. Naji**, A. Belhaj, H. Labrim, L. Bahma, A. Benyoussef, A. El Kenz, Phases Diagrams and Magnetic Properties of Tri-layer Superlattices: Mean Field Study. ***Physica A,***399 (2014) 106–112.

3. **S. Naji,** A. Belhaj, H. Labrim, M. Bhihi, A. Benyoussef, A. El Kenz, New Statistical Lattice Model from Double Honeycomb Structure. ***Int. J. Mod. Phys. B*** 28, 1450086 (2014).

4. **S. Naji**, A. Belhaj, H. Labrim, L. Bahmad, A. Benyoussef, A. El Kenz, Monte Carlo study of phase diagrams and magnetic properties of trilayer superlattices . ***Acta Physica Polonica Series B,*** 45, (2014) 947.

5. F. El Hallani, **S. Naji,** H. Ez-Zahraouy, and A. Benyoussef, First-principles study of the magnetic stability and the exchange couplings of LaMn2O5,***J. Appl. Phys.*** 114, 163909 (2013).

6. B. Khalil, **S. Naji,** H. Labrim ,M. Bhihi, A. G. El Hachimi, M. Lakhal, A. Belhaj, A. Benyoussef, A. El Kenz, Magnetic Properties of SrO Doped with 3d Transition Metals, ***journal of superconductivity and novel magnetism DOI*** 10.1007/s10948-013-2241-1. (2013).

7. O. El Rhazouan, A. Benyoussef**, S. Naji,** A. El kenz, Magnetic properties of double perovskite Sr2CrReO6: Mean field approximation and Monte Carlo simulation, ***Physica A,*** 397(2014)31.

8. M. Bhihi, M. Lakhal, **S. Naji**, H. Labrim, A. Belhaj, A. Benyoussef, A. El Kenz, M. Loulidi, B. Khalil, O. Mounkachi, M. Abdellaoui, E. K. Hlil, First Principle Calculations

for improving Desorption Temperature in Mg16H32 Doped with Ca, Sr and Ba Elements. ***Accepted Bulletin of Materials Science*** (2014).

9. M. Lakhal, M. Bhihi, H. Labrim, A. Benyoussef, **S. Naji**, A. Belhaj, B. Khalil, M. Abdellaoui, O. Mounkachi, M. Loulidi, A. El kenz, Kinetic Monte Carlo and density functional study of hydrogen diffusion in magnesium hydride MgH2, ***International Journal of Hydrogen Energy,*** 38, 20, (2013), 8350–8356.

10. A. Slassi, **S. Naji,** A. Benyoussef, M. Hamedoun, A. El Kenz, On the transparent conducting oxide Al doped ZnO: First Principles and Boltzmann equations study. ***Journal of Alloys and Compounds,*** 605 (2014) 118–123.

List of Figures:

List of Tables:

List of Abbreviations

0D	Zero Dimensional
1D	One Dimensional
2D	Two Dimensional
2DM	Two Dimensional Material
3D	Three Dimensional
AFM	Atomic Force Microscopy
APW	Augmented Plan Wave
BZ	Brillouin Zone
CC	Coupled Cluster
CI	Configuration Interaction
CVD	Chemical Vapor Deposition
DRAM	Dynamic Random Access Memory
DFT	Density Functional Theory
DOS	Density Of States
FET	Field Effect Transistor
FeRAM	Ferroelectric Random Access Memory
FPLO	Full-Potential Local-Orbital Minimum-Basis
GGA	Generalized Gradient Approximation
HOPG	Highly Oriented Pyrolytic Graphite
ITO	Indium Tin Oxide
LAPW	Linear Augmented Plan Wave
LCAO	Linear Combination Of Atomic-Like Orbitals
LCD	Liquid Crystal Display
LDA	Local Density Approximation
LEDs	Light-Emitting Diodes
LMTO	Linear Muffin-Tin Orbitals
MCSCF	Multi-Configurational Self-Consistent Field
MP	Møller–Plesset Perturbation Theory
MRAM	Magneto-Resistive Random Access Memory
MRDCI	Multi-Reference Single And Double Configuration Interaction
MTO	Muffin-Tin Orbitals
NEVPT	N-Electron Valence State Perturbation Theory
NVM	Nonvolatile Data Memory
O LEDs	Organic Light-Emitting Diodes
QCI	Quadratic Configuration Interaction
OPW	Orthonormal Plane Waves
QHE	Quantum Hall Effect
PAW	Projector Augmented Wave
PBE	Perdew-Burke-Ernzerhof
P-W	Perdew And Wang
Rf	Radio Frequency
RRAM	Resistance-Switching Random Access Memory
STM	Scanning Tunneling Microscopy
TCs	Transparent Conducting
TM	Transition Metals

Contents

Part I: Graphene: Basic Survey

Part II: Computational Methods

Part III: Physical properties of 2D hexagonal nanostructured materials: A theoretical study

General Introduction

General Introduction

Since the discovery of the graphene from bulk natural graphite by Novoselov et al. [**1**], the two dimensional materials (2DM) become the most promised research topics in condensed matter physics and related areas including high energy physics. [**1**], [**2**], [**3**], [**4**] [**5**]. [**6**], [**7**], [**8**], [**9**] [**10**], [**11**], [**12**].This discovery led to a revolution in research topics including the investigation of, the outstanding properties of such material, the possible applications and the other 2D layered materials. In fact, graphene has some fascinating physical properties that makes it extremely appealing for applications These properties include extraordinary high room-temperature electron mobility [**13**] , high Young's modulus and intrinsic strength [**14**], extremely high thermal conductivity [5], an excellent optical transparence [**15**] , complete impermeability to any gases [**16**], highest current density at room temperature (a million times higher than copper) [**17**]. It has to be mentioned that, the Nobel Prize in Physics 2010 was awarded to Andre Geim and Konstantin Novoselov from the University of Manchester for groundbreaking experiments regarding the two-dimensional material graphene.

Furthermore, a special interest is to investigate the particular materials composed of atoms appearing in the fourth group of Mendeleev chemistry table [**18**], [**19**]. This includes only the graphene-like 2D buckled Nano sheets silicene and germanene .These counterparts of graphene, have evolved from theoretical predictions [**18**] to experimental observations [**6**] [**12**] [**20**], [**21**], only within a few years. Theoretical calculations have shown that they exhibit electronic characteristics similar to those of graphene [**11**].It has been shown that such honeycomb-structured models play crucial role placed in Nano-science and Nano-technology. Moreover, it has been suggested that, these structures could be considered as the most stable material systems used in the semiconductor electronic applications [**5**], [**22**], [**23**].

On the theoretical side, due to the continuous advances in computer technology, nowadays the computational modeling and simulation could be considered as a third stream together with pure theory and experiment to scientific investigation. They provide a modeling of physical phenomenon from a broad range of perspectives, from the electronic structure methods to the macroscopic end. The computational methods of different structures of materials and their

properties, in different scales, can be very valuable and useful for developing materials and their applications. As these methods offer acceptable accuracy in prediction of materials properties, they are widely used in the development of new materials and for interpretation of experimental results.

More precisely, the possibility to predict novel materials like, nano-systems and to calculate their basic chemical and physical properties is quite remarkable with falling back on the elementary interactions and the most accurate electronic structure methods for their simulation. Acutely, the Nobel Prize in chemistry 1998 was awarded, , in the field of electronic structure approaches, jointly to Walter Kohn for his work developing the foundations of the density functional theory DFT and John Pople for his groundbreaking work on developing a quantum chemistry computer code for calculating the electronic structure of atoms and molecules.

It might be convenient now to remind that, the down-scaling of microelectronic devices associated with the increase of the hardware capacities involves technological challenges such as Moore's law. On the other side, it has been found, recently, that, the systems based on the graphene physics are interesting for the electron-device community see refs. [**24**], [**25**] and references therein. In particular, the systems based on transistors have been extensively investigated and they are considered as an alternative option for the silicon electronic applications. However, one of the main challenges of graphene is its zero band gap energy, therefore, in order to use the graphene in semiconductor electronics, such as in transistors , the band gap should be opened [**26**] . In this context, the first goal of this thesis is to present our contribution to these activities by considering a new way for discussing the opening of the band gap energy using distance variation effects on two parallel sheets of the graphene placed in various stacking arrangements.

Moreover, the study of these intermediate configurations, describing the disorder in the bilayer of the graphene, should be interesting. It may occur during the production of samples and that it can influence quite strongly on the electronic properties. Effectively, such structures have been observed experimentally by STM on graphite surfaces [**27**], [**28**]. It has also been revealed experimentally that the Moiré patterns appear when the graphene plane is the considered cleaved graphite [**29**]. Therefore, the second goal of this thesis is, in the same chapter, to define a special

direction in which all possible intermediate arrangements between (AB) and (AA) configurations can be covered .The choice of this direction is motivated from the fact that this is the only direction that can produce the (AA) configuration starting from the (AB) one.
Another issue and as a bonus, the opening of the band gap energy using distance variation effects on two parallel sheets of the graphene is extend to the graphene counterparts like-bilayer; silicene and germanene.

Furthermore, many efforts have been devoted to study the interaction of the metal adatoms in the graphene-like models [**30**], [**31**], [**32**], [**33**], [**34**]. This interaction can be used for many potential applications including the building of the nano-magnetic materials. Precisely, the interaction of the magnetic atoms with the graphene like materials can produce half-metallic systems which have been considered as interesting tools for the spintronic device applications [**35**], [**36**], [**37**]. More precisely, several potential applications of spintronic could be spin field-effect transistor (spin-FET) [**38**], spin-light emitting diode (spin-LED) [**39**], magneto-resistive random access memory (MRAM) [**40**]. However, a lot of research still needs to be done to understand all the processes involved in this field. So, another main goal of this thesis is concerned with the theoretical investigation of the interaction between adatoms (Fe, Co, or Ni) and graphene with a double hexagonal symmetry, which might be useful for this kind of applications. Properties such as binding energies, magnetic moments, spin polarization, critical temperature and exchange mechanism will be examined with the density functional theory calculations and Monte Carlo simulations.

The last issue in this thesis is to examine, theoretically, a new hexagonal structure for monolayer C, Si and Ge atoms. This extended structure is based on a double hexagonal flat geometry which is associated with the two dimensional root system of the exceptional Lie algebra G_2 and motivated by several experimental observations [**41**], [**42**].

The organization of this thesis is as follows: Chapter 1 will present an introduction to the graphene, as one of the crystalline carbon allotropes, properties, counterparts, synthesis and applications.

Chapter 2 will focus on the needed background of the computational methods for the calculations that are performed in later chapters.

Chapter 3 will give a preliminary survey on the single layer of graphene, silicene and germanene.

Chapter 4 will deal with the opening of the band gap energy using distance variation effects on two parallel sheets of the graphene placed in various stacking arrangements.

Chapter 5 will treat, using distance variation effects, the opening of the band gap of silicene- and germanene-like bilayer.

Chapter 6 will investigate the electronic and magnetic properties of the adsorption of Fe, Co and Ni on the graphene with a double hexagonal symmetry.

Chapters 7 will examine, theoretically, a new hexagonal structure for flat monolayer C, Si and Ge atoms which is associated with the two dimensional root system of the exceptional Lie algebra $G_{2.}$

Finally we close this thesis by the conclusion and outlook.

Graphene: Basic Survey

1. Graphene: Basic Survey

1.1. Carbon bonding and allotropes:

Carbon is one of the most flexible elements in terms of the number of compounds. In fact, it forms the basis of all organic molecules, which makes it the most important element for life on our planet, and exists in over 95% of the known chemical compounds overall [**43**]. This strong capability is due to the types of bonds and the number of different bonding elements. Carbon, like the fourth group elements of Mendeleev table, has six electrons with the ground state atomic configuration is $1s^2$, $2s^2 2p^2$. Two electrons form a closed $1s^2$ shell while the remaining four electrons are available to form covalent bonds. In order to get covalent bonds in the presence of some atoms, such as other carbon atoms, it should be excite one electron from the 2s to the third 2p orbital, as the energy difference between them is almost 4.2eV [**44**], providing four unpaired electrons that are able to form bonds. These four atomic orbitals can be mixed together to form four or three energetically equivalent hybrid orbitals. This process is called hybridization. The kind of this hybridization can be sp^2 or sp^3 hybridization. In the sp^2 hybridization, two of the 2p-orbitals and one 2s-orbital take part in the hybridization process. This hybridization makes three energetically equivalent sp2-hybrid orbitals, which adopt a trigonal planar geometry with bond angles of 120°, and one unchanged p-orbital that sets at right angles to the plane of the hybrid orbitals. However, in the sp^3 hybridization, the four orbital can be mixed together to form four energetically equivalent sp^3-hybrid orbitals adopting a tetrahedral geometry with bond angles of 109°, as shown schematically in Figure 1.1 .

The crystalline carbon allotropes, i.e. those crystalline materials which entirely consist of carbon atoms, can be divided into two classes according to the type of bonds. Diamond or graphitic structures are formed, when all carbon atoms either have sp^3-hybridization or sp^2-hybridization, respectively. It should be mentioned that, there is another class of non-crystalline carbon allotropes contains the amorphous carbons which consist of mixtures of sp^2- and sp^3-hybridized carbon atoms.

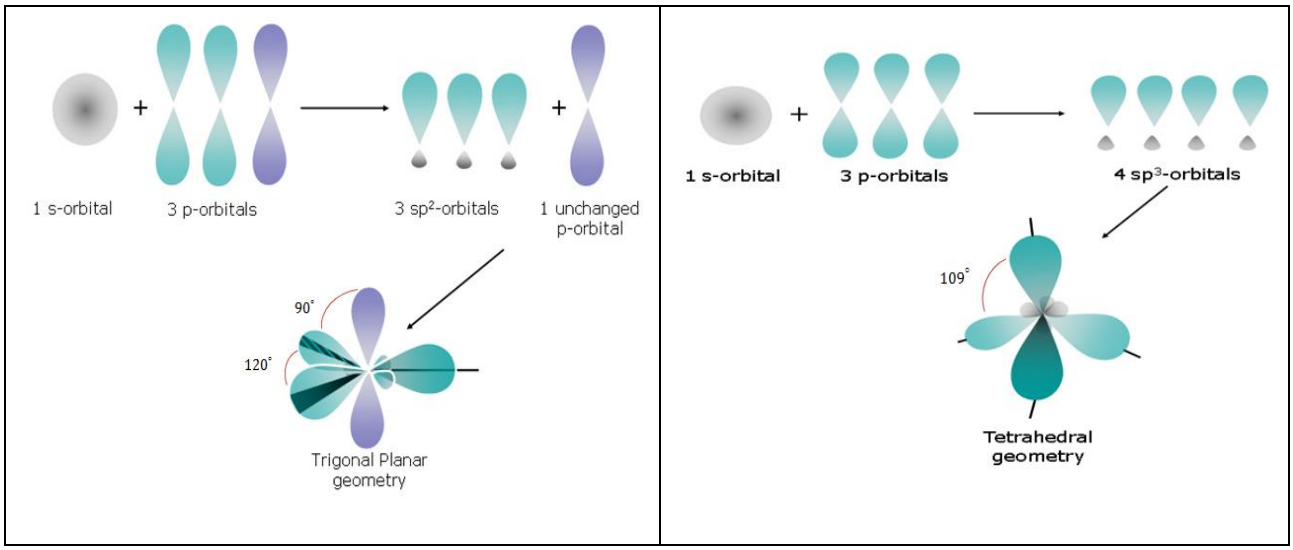

Figure 1.1: schematic representation of sp^2 (left) and sp^3 hybridizations (right).

A schematic overview of these different crystalline carbon allotropes is given in Figure 1.2. These crystalline allotropes span all three spatial dimensions from 0D fullerene and carbon nano-flake, 1D carbon nanotubes and nanoribbons, 2D graphene to 3D graphite and diamond. These materials are briefly described in the following.

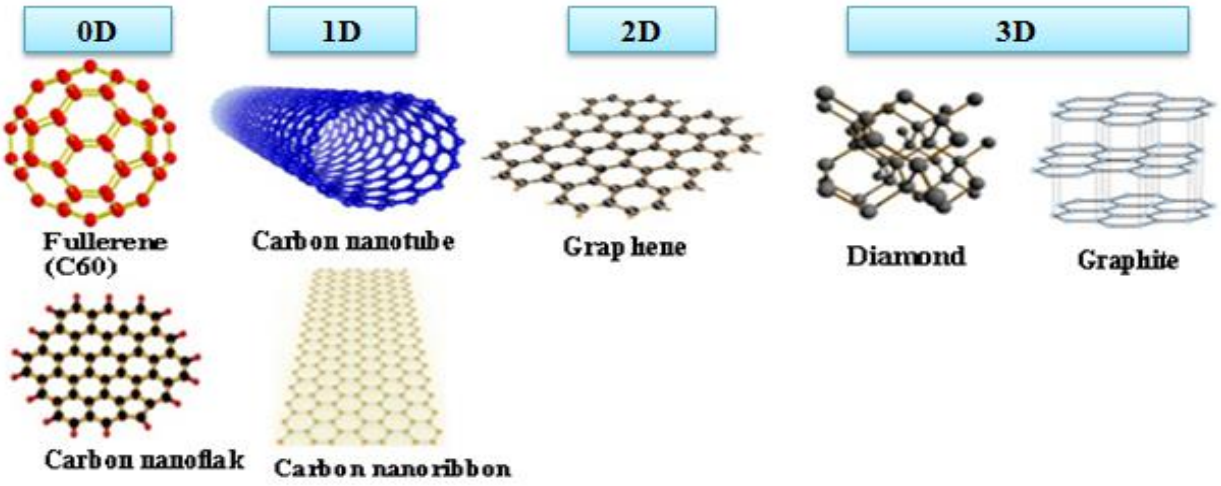

Figure 1.2 : The different crystalline carbon allotropes.

1.1.1. Diamond

Diamond is the most famous carbon allotrope, the highest thermal conductive and the strongest bulk materials. These exceptional properties are results from the strong covalent bonding between its atoms. In diamond, each atom has four bonding partners forming equivalent sp3-bonds at distance of 1.545 Å, leading to different crystal structures. Nearly all diamonds have the usual cubic structure but a very small percentage show a hexagonal structure related to wurtzite and these are called lonsdaleite. For pressures above 60 $kbar$, the cubic diamond is the thermodynamically stable form of carbon. Diamond is a slightly more compact structure; hence its density is greater than that of graphite. Like graphite, it is relatively unreactive but does burn in air at 600-800°C. All diamond materials are excellent insulators that characterized by an exceptional hardness and a large band gap giving them their transparent appearance. Such properties make them very useful for both industrial applications and jewelry.

1.1.2. Graphite

Graphite is the most stable carbon allotrope, under standard conditions, and the most common in nature consequently. At very high temperatures and pressures (roughly 2000℃ and 5 GPa), it can be transformed into diamond. It is known for a long time as a writing material tools and lubricants to its unusual layered structure at the nano scale. As shown in Figure 1.2, the graphite structure consists of layers of covalently bonded carbon atoms which are held together by weak van der Waals interaction. The intra-layer bonding exceeds the interlayer bonding in strength by several orders of magnitude which can be demonstrated by the intra-layer bond length of 1.42 Å as compared to 3.35 Å for the interlayer bonds. In most graphite (α-graphite), these layers are arranged in as ABABAB... but in the less common form of graphite, β-form (rhombohedral), the stacking is ABCABCABC... although all the carbon-carbon distances remain the same as in the α-form.

Even though graphite is 3D in nature, it can often be regarded as a $(2 + 1)$ D material. Unlike diamond, graphite is an electrical conductor and due to the electrons and phonons can propagate much faster along the layers than from one layer to another, the thermal, electrical and other properties of graphite are highly anisotropic. The graphite forms of the heavier elements are not known and the structures of silicon, germanium, and tin are related to the diamond structure above.

1.1.3. Fullerene

Fullerene is a closed cage molecule builds up from carbon atoms, which was first discovered in 1985. Fullerenes have different forms, such as hollow sphere, ellipsoid and many other shapes. Spherical fullerenes are also called buckyballs like C_{60} which consists of consists of 12 pentagons and 20 hexagons. From the structural point of view fullerenes are similar to graphite, with hexagonal carbon ring but they may also contain pentagonal or heptagonal rings. In the past two decades the discovery fullerenes attracted a lot of attention in physics, chemistry, mathematics, architecture and engineering. For their discovery of fullerene, Nobel Prize in Chemistry 1996 was awarded jointly to Robert F. Curl Jr., Sir Harold W. Kroto and Richard E. Smalley.

1.1.4. Carbon nanotubes

Single-walled carbon nanotube is a one-dimensional (1D) form of carbon and it was discovered in 1991 by S. Iijima [**45**]. It can be thought of as rolled up monolayer sheet of graphene (see Figure 1.2 and Figure 1.4) and, consequently, many of their properties can be derived from those of graphene. These sheets are also rolled at specific and discrete ("chiral") angles, and the combination of the rolling angle and radius decides the nanotube properties; for example, whether the individual nanotube shell is a metal or semiconductor. Carbon nanotubes have unusual properties, which are valuable for the fields of materials science and technology. In particular, owing to their extraordinary thermal conductivity and mechanical and electrical properties, carbon nanotubes find applications as additives to various structural materials.

1.1.5. Carbon nanoribbons

Graphene nanoribbons have one-dimensional structures with hexagonal two dimensional carbon lattices, which are stripes of graphene with ultra-thin width ($< 50\,nm$). Graphene nanoribbons can be divided into two kinds: Armchair and Zigzag and depending on this termination style, graphene nanoribbons present different electronic properties ranging from normal semiconductors to spin-polarized half metals, which open the possibility of graphene nanoribbons as electronic devices. In fact, Armchair graphene nanoribbons show semiconducting behaviors with a direct energy gap, while the zigzag graphene nanoribbons have been predicted to have a magnetic insulating ground state with ferromagnetic ordering at each zigzag edge, and

antiparallel spin orientation between the two edges. The importance of one-dimensional quantum confinement effect and edge states are crucial in determining its properties .Since graphene nanoribbons have large surface-volume ratio and special edge states, their properties can be also modified by many methods, such as doping and adsorption [**46**], [**47**] [**48**], [**49**], [**50**].

1.1.6. Carbon nano-flakes

Another zero-dimensional (0-D) form of graphene, which may be called graphene nano-flakes or graphene nano-dots. Graphene nano-flakes have a great potential for a variety of applications especially in magnetic and electronic devices which differ from those of 2D and 1D graphene structures. These potential applications arise because graphene nano-flakes not only have edge states, but also corner states, and may also be cut into a much larger variety of different shapes which can play a very important role in determining their electronic and magnetic properties [**47**]. Besides these edges and corners, the effect of defects is also important and may introduce new properties such as magnetism. However, these defects often degrade the nano-flakes properties. Due to the finite size, defects can dominate, depending on defect size and density, the structure and its properties. Furthermore, functional groups attached to the graphene nano-flakes can also open new opportunities for technological applications including spintronic, sensors and transistors see [**47**] and references therein.

1.1.7. Graphene

Graphene is a two-dimensional (2D) form of crystalline carbon and it is the first perfect 2D materials with single-atom thickness arranged in a honeycomb lattice. In 2004, it is the first experimental isolation of graphene from bulk natural graphite by Noveselov et al [**1**]. This experiment led to a revolution in research including the investigation of the fascinating properties of such material and the possible applications. These fascinating properties including extremely high intrinsic electron mobility at room-temperature electron mobility > 1.0×10^5 $cm^2V^{-1}s^{-1}$ [**13**] , highest current density at room temperature (a million times higher than copper) [**17**], extraordinary high thermal conductivity (about 3.000 $Wm^{-1}K^{-1}$) [5], optical absorption of exactly $\pi\alpha \approx 2.3\%$ (in the infrared limit, where α is the fine structure constant) [**15**] , the strongest and the most stretchable known material with a Young's modulus of 1TPa and intrinsic strength

of 130 GPa [**14**], complete impermeability to any gases [**16**] and others [**51**] . Due to these properties, graphene offers and promises a lot of different applications, such as nano-electronics, optical devices, sensors, composites, batteries, energy generation and hydrogen storage, [**52**], [**53**], [**54**], [**25**], [**55**], [**56**], [**57**], [**58**], [**59**], [**60**] and references therein. The Nobel Prize in Physics 2010 was awarded to Andre Geim and Konstantin Novoselov from the University of Manchester for groundbreaking experiments of the 2D material graphene.

Since the mid-30s of the past century, it was convinced, according to the theoretical works of Peierls [**61**], Landau [**62**] and Mermin and Wagner [**63**], [**64**],that, 2D crystals are thermodynamically unstable and strictly cannot exist at any finite temperature due to the thermal fluctuations that destroy the long range order leading to melt the 2D crystals. This thought was confirmed by experimental observations like the decreasing melting temperature for films with the decreasing thickness. Moreover the failure of creating thin films , since these films became unstable and tend to separate and clump up rather than form perfect layers, seemed to provide also strong support for this theory.

It came therefore as a big surprise when Novoselov, Geim et al. at Manchester University succeeded to isolate a stable single layer of carbon atoms and some other 2D materials in 2004. [**1**]. Currently the stability of graphene can be explained by postulating small out-of-plane corrugations (see Figure 1.3) due the anharmonic coupling between its bending and stretching modes [**65**], [**66**]. These corrugations have been observed on a lateral scale around 10 nm and are believed to suppress thermal vibrations [**65**]. An alternative explanation is found by considering the graphene layer is kept in its metastable state by van der Waals interaction with a supporting substrate and the strong intra-layer bonds which prevent the defects formation.

Moreover, the graphene, can form the basis of all these other graphitic allotropes (see Figure 1.4) graphite, which is a three-dimensional crystal consisting of relatively weakly coupled graphene layers; nanotubes, which may be represented as scrolls of graphene; and buckyballs, spherical molecules made from graphene with some hexagonal rings replaced by pentagonal rings.

In a graphene layer the carbon atoms are distributed at the edges of regular hexagons (see Figure 1.5 (a)). This structure is often called a honeycomb lattice. However, the honeycomb lattice is not a Bravais lattice and from a crystallographic point of view, it has to be described by

a triangular lattice with two atoms per unit cell. These two atoms are often referred to as A and B atoms. The unit cell of the lattice is a rhomboid defined by the vectors:

$$a_1 = \left(\frac{\sqrt{3a}}{2}, \frac{a}{2}\right), \qquad a_2 = \left(\frac{\sqrt{3a}}{2}, \frac{-a}{2}\right) \tag{1.1}$$

Each carbon atom (A or B) is covalently bonded by σ-bond to its three nearest neighbors and the separation distance a_{C-C} between type A (B) and the nearest type B (A) atoms is approximately 1.42 Å and given by :

$$a_{C-C} = \frac{\sqrt{3}}{a} \tag{1.2}$$

The reciprocal lattice of graphene is also a hexagonal lattice (see Figure 1.5 (b)) that can be defined by the reciprocal vectors as:

$$b_1 = \left(\frac{2\pi}{\sqrt{3a}}, \frac{2\pi}{a}\right), b_2 = \left(\frac{2\pi}{\sqrt{3a}}, \frac{-2\pi}{a}\right) \tag{1.3}$$

with $|b_1| = |b_2| = 4\pi/\sqrt{3}a$. The first Brillouin zone (BZ) has sides length $b_{BZ} = |b_1|/\sqrt{3} = 4\pi/3a$ is shown by the shaded area in Figure 1.5 (b). The Γ-point is at the center of this zone, and the vectors describing the location of the special high-symmetric points with respect to the zone center are given by:

$$\Gamma M = \left(\frac{2\pi}{\sqrt{3a}}, 0\right), \Gamma K = \left(\frac{2\pi}{\sqrt{3a}}, \frac{2\pi}{3a}\right) \tag{1.4}$$

There are six K-points and six M-points within the Brillouin zone.

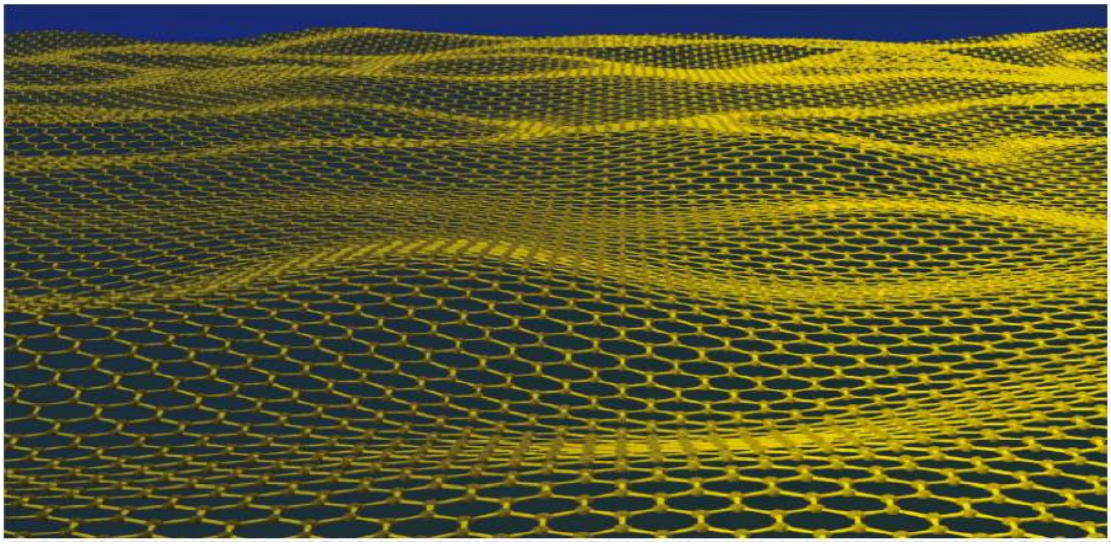

Figure 1.3: Simulated model for the crumpling of a graphene monolayer in the third dimension. (Figure from Ref. [3] (journal cover).)

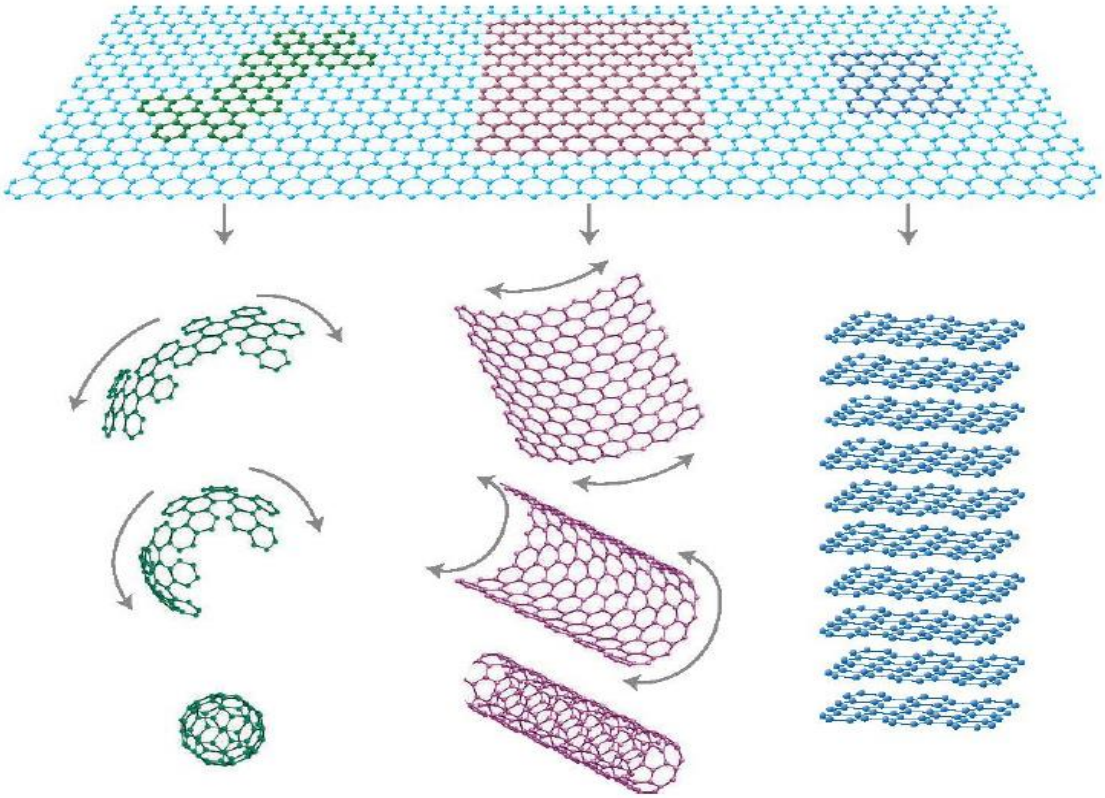

*Figure 1.4: Graphene forms the basis of the other graphitic carbon allotropes; from left to right: fullerene, carbon nanotube, and graphite. (Taken from ref [**2**].)*

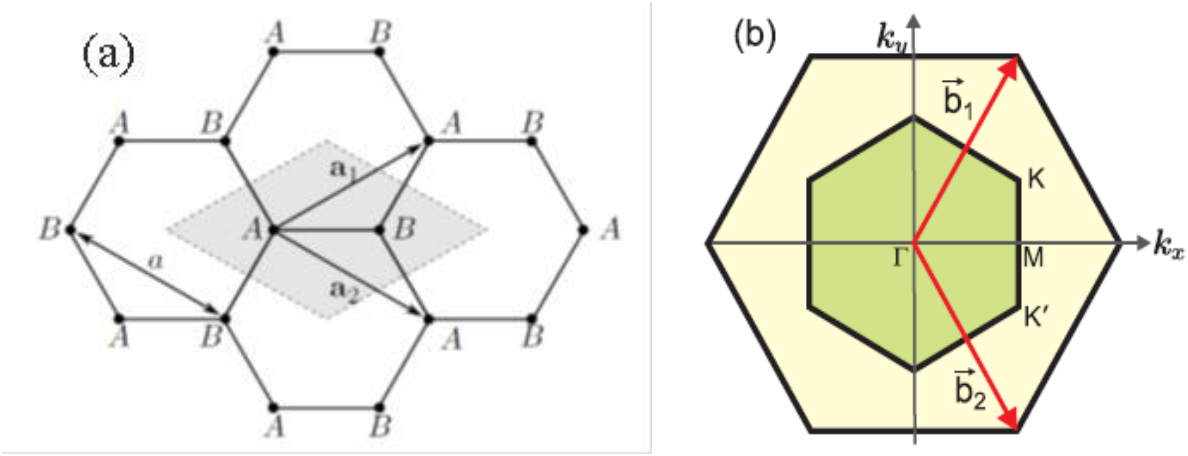

Figure 1.5: (a) The honeycomb lattice of graphene. The unit cell in gray contains two atoms denoted as A and B (b) the reciprocal lattice with the hexagonal first BZ shown in green and the second BZ shown in yellow. The special high-symmetry points labeled as Γ, M, and K located at the center, midpoint of the side, and corner of the hexagon respectively.

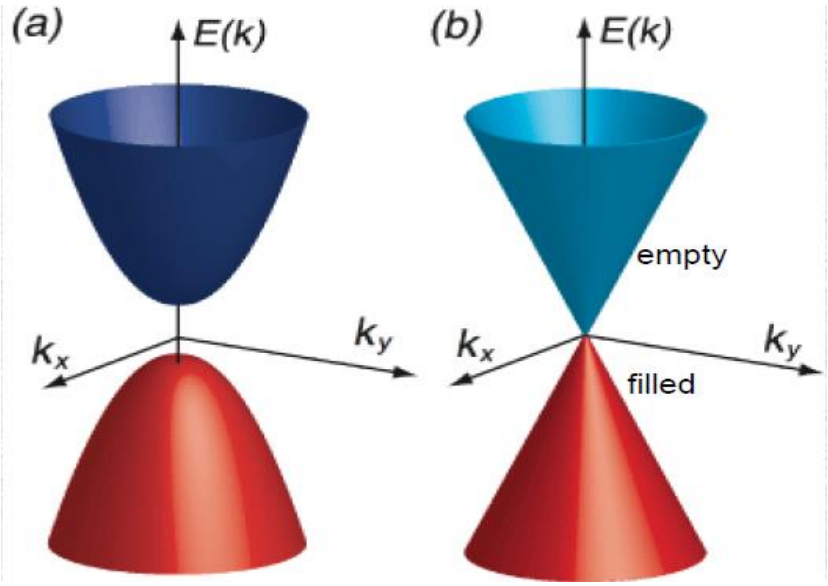

Figure 1.6 : Schematic view of band structure for (a) ordinary semiconductors or insulators (b) graphene around K-point.

In 1947, the first electronic structures calculations for a single graphite layer obtained by P. R. Wallace [**67**] in the framework of a simple tight-binding model. Further this model was developed by McClure in1957 [**68**] and by Slonczewski and Weiss in1958 [**69**]. The electronic structures of graphene is consist from the σ-states that form occupied and empty bands with a huge gap, whereas π states form a single band, with a conical self-crossing point in K. This conical point is a characteristic of the peculiar electronic structure of graphene and the origin of its unique electronic properties. In particular, near the so-called Dirac points the system has a linear energy dispersion i.e.

$$E = \pm h v_F k \qquad [1.5]$$

Where k and v_F are momentum and Fermi velocity respectively. Linear dispersion behavior indicates that the charge carriers near Dirac point become like massless fermionic fields satisfying the relativistic Dirac-like equation [**23**]. On K-points, the usual graphene material is considered as a gapless semi-conductor see Figure 1.6.

In 1984, G.W. Semenoff [**70**] showed the possibility of a (2+1)D quantum electrodynamics analog with graphene as a condensed matter system by a Hamiltonian consists of two decoupled copies of the Dirac equation at low energy, which are related by time reversal. The existence of such Dirac fermions in single layer graphene confirmed finally in 2005 by two papers appeared in Nature [**71**], [**72**] . The charge carriers of graphene and its unique electronic structure leads to a number of interesting physical effects, such as the minimal electrical conductivity, anomalous quantum Hall effect, Klein tunneling, the universal optical conductivity and the strong nonlinear electromagnetic response [**53**], [**73**].

1.2. Graphene Counterparts:

Since the discovery of the graphene from bulk natural graphite by Novoselov et al [**1**], the two dimensional materials (2DM) become the most promised research topics in condensed matter physics and related areas including high energy physics. This discovery led to an explosion in research topics including the investigation of, the outstanding properties of such material, the possible applications and the other 2D layered materials [**1**], [**2**], [**3**], [**4**] [**5**]. [**6**], [**7**], [**8**], [**9**] [**10**],

[**11**], [**12**]. These 2D layered materials including graphan, fluorographene, boron-nitride, transition metal oxides, metal chalcogenides and other 2D materials have gained huge interest for their particular electronic structure ranging from insulator to metal to superconductor. A large variety of layered materials with weak van der Waals-like inter-layer bonds and strong intra-layer bonds exists which could potentially be exfoliated into 2D materials. These have different properties such as superconductivity [**74**], topological insulator effect [**75**], [**76**] , and thermoelectricity [**77**] [41]. Furthermore, a special interest is to investigate the particular materials composed of atoms appearing in the fourth group of Mendeleev chemistry table [**18**], [**19**]. This includes only the graphene-like 2D buckled Nano sheets silicene and germanene. These graphene counterparts have evolved from theoretical predictions [**18**] to experimental observations [**6**], [**12**], [**20**], [**21**], only with a few years. It has been shown that such honeycomb-structured models play crucial role placed in Nano-science and Nano-technology. Moreover, it has been suggested that, they could be considered as the most stable material systems used in the semiconductor electronic applications [**5**], [**22**], [**23**].

More precisely, there has been a great interest in studying the silicene since it involves properties similar to those of the graphene [**5**], [**6**], [**10**] . For this reason, the silicene, which is a monolayer of the silicon atoms forming a 2D honeycomb lattice, can be also viewed as an alternative potential candidate for nanotechnology applications. This material has been synthesized and modeled using different approaches [**78**], [**79**], [**80**], [**81**], [**82**], [**83**], [**84**].

Recently, the electronic properties of two-dimensional hexagonal materials of germanium and numerical calculations on the ground state properties of germanene have been also done using first-principles method [**85**], [**86**], [**87**], [**88**], [**89**]. In particular, it has been found that the buckled germanene is more stable than the planar one involving an electronic structure similar to graphene with linear energy dispersion around the K point [**86**].More recently, the 2D buckled and nearly flat germanene sheets have been, also, fabricated with two different surface substrates [**20**], [**21**].

In the present thesis, I focus my studied basically on graphene and as extension of some works on silicene and germane.

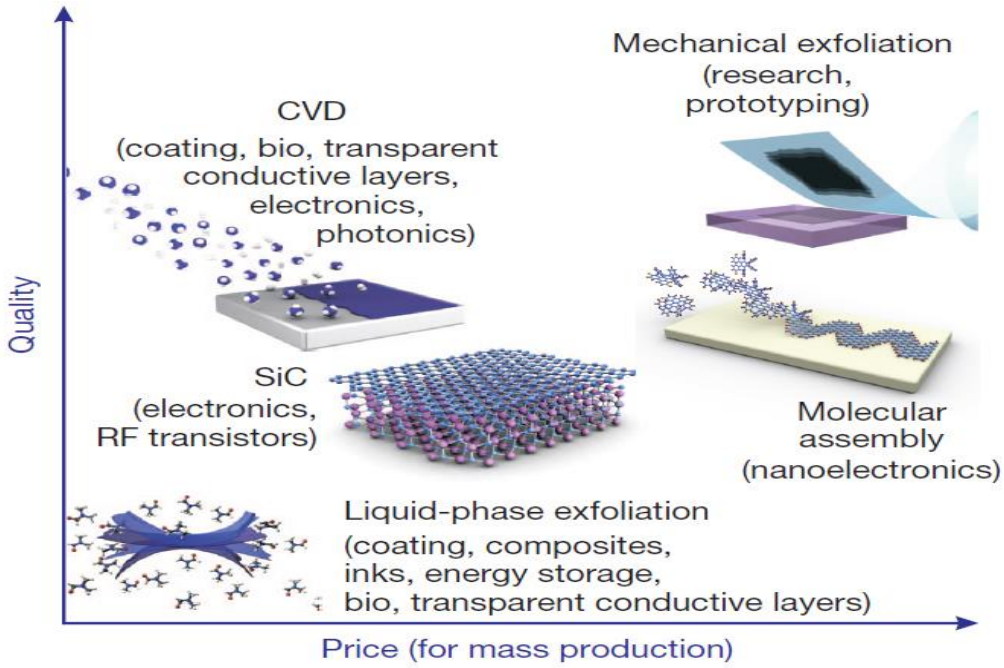

*Figure 1.7: Several methods of mass-production of graphene, which allow a wide choice in terms of size, quality and price for any particular application.(Taken from ref. [**59**].)*

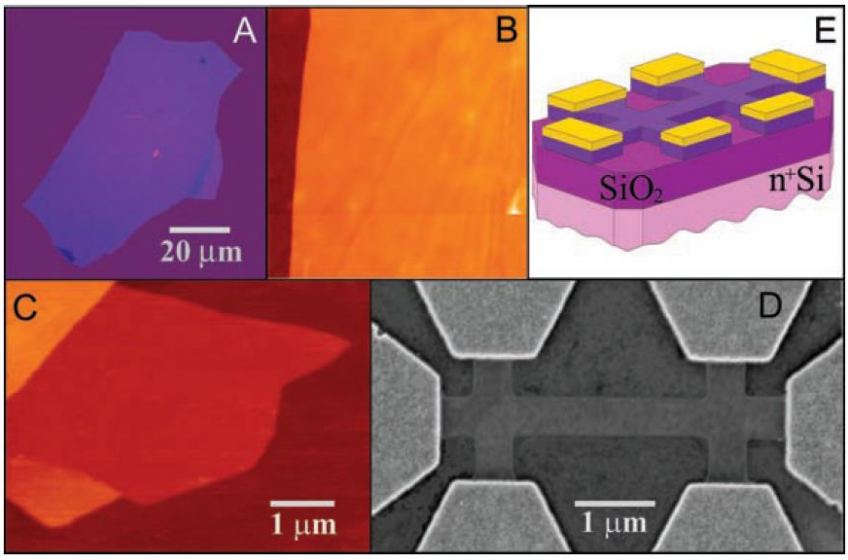

*Figure 1.8: Graphene films. (A) Photograph (in normal white light) of a relatively large multilayer graphene flake with thickness around 3 nm on top of an oxidized Si wafer. (B) Atomic force microscope (AFM) image of 2 μm by 2 μm area of this flake near its edge. Colors: dark brown, SiO_2 surface; orange, 3 nm height above the SiO_2 surface. (C) AFM image of single-layer graphene. Colors: dark brown, SiO_2 surface; brown-red (central area), 0.8 nm height; yellow-brown (bottom left), 1.2 nm; orange (top left), 2.5 nm. Notice the folded part of the film near the bottom, which exhibits a differential height around of 0.4 nm. (D) Scanning electron microscope image of one of the experimental devices prepared from FLG. (E) Schematic view of the device in (D).(Taken from ref. [**1**]).*

1.3. Graphene: preparation techniques

Up to date, graphene and its systems with varying number of layers, dimensions, shapes and quality can be synthesized by different techniques (see Figure 1.7). These techniques include exfoliation of graphite, chemical vapor deposition, arc-discharge method, epitaxial growth on electrically insulating surfaces such as SiC, chemical reduction of graphite oxide and graphite intercalation compounds and others. Generally, these preparation techniques can be distinguished into two major classes. First, the top-down approaches that start from graphite and in many ways try to extract few layer graphene and ultimately monolayers. Secondly, the bottom-up approaches that the graphene can be grown directly on a substrate surface. Techniques of the first and second classes are called, respectively, exfoliation and synthesis methods. Here, I will briefly present some of the most important preparation techniques. For more details on these techniques and the others can be found in [**52**], [**90**] , [**59**] and references therein.

1.3.1. Mechanical Exfoliation

The first single layer of graphene was prepared using the micromechanical exfoliation or, simply, what so-called Scotch tape method from highly ordered pyrolytic graphite (HOPG) in 2004 by Novoselov and Geim [1]. In this technique an adhesive tape was used to repeatedly to peel off flakes of multilayered HOPG layer-by-layer until the multilayer is cleaved into various flakes of few layer graphene and ultimately single layers. After this, the tape is pressed on a Si/SiO2 substrate in order to attach the graphene samples.

Afterwards, thick flakes are, mostly, removed using ultrasound cleaning propanol while the thin ones ($d < 10\ nm$) are, strongly deposited to the substrate due to van der Waals interaction [**1**]. These few layer graphene are identified by the contrast difference in an optical microscope. Finally, in order to confirm the optical microscope observation, more accurate characterization techniques such as atomic force microscopy (AFM), scanning electron microscope (SEM) and Raman spectroscopy can be used as shown in Figure 1.8. This technique can generate few and single layer graphene samples with dimension up to$10\ \mu m$. Besides its historical importance and simple concept, this technique is still extremely valuable especially in fundamental research due to the excellent sample quality with almost no defects that cannot be produced by any recent

technique. However, this method is limited to small size production and cannot be used for industrial applications that require a large- scale production of graphene [**59**].

1.3.2. Chemical Vapor Deposition

In the chemical vapor deposition (CVD) technique, single layer of graphene is prepared, more conveniently, by decomposing a variety of hydrocarbons such as methane, ethylene, acetylene and benzene on films or sheets of different transition metal substrates such as Ni, Cu, Co and Ru. This transition metal can be used as both catalyst and substrate to grow the graphene layer and the number of layers can be varied with the hydrocarbon and reaction parameters. Using CVD method, large-area uniform polycrystalline graphene films on copper foils and films have been produced showing great promise for many industrial applications(see Figure 1.9 (a)) [**91**] . The independent of growth time for graphene monolayer is confirmed by Raman spectroscopy and SEM imaging. The production of square meters of graphene has already been achieved, in spite of the fact that the whole process typically needs transfer from the copper support to a dielectric surface or other substrate of interest [**59**], [**92**].

It has been demonstrated, recently, that, the CVD on copper with a similar process but modified growth conditions can be used as technique to produce uniform bilayer graphene [**93**]. Despite the cons of this method like, the grain boundaries, inclusions of thicker layers and the presence of defects, such produced films can readily be used in transparent conductive coating applications including touch screens.

Several issues associated with the doping level, gaining control of the grain size, number of layers, and the ripples need to be resolved. Finally, in order to minimize the damage to graphene, the transfer process should be also optimized. Using plasma-enhanced CVD or other methods, the future aim would be the improvement of graphene growth on arbitrary surfaces and/or at low temperature with a minimal number of defects.

1.1. Applications of Graphene

The Fascinating properties of graphene make this material extremely appealing for different applications. In the past few years, graphene offers and promises a lot of different applications, such as nano-electronics, optical devices, sensors, water desalination, bio applications, metrology

composites, coating, batteries, flexible transparent electrodes, spintronic energy and hydrogen storage, [**52**], [**53**], [**54**], [**25**], [**55**], [**56**], [**57**], [**58**], [**59**] , [**60**] and references there in. I will mention, in the next sections, some areas for existing and future applications.

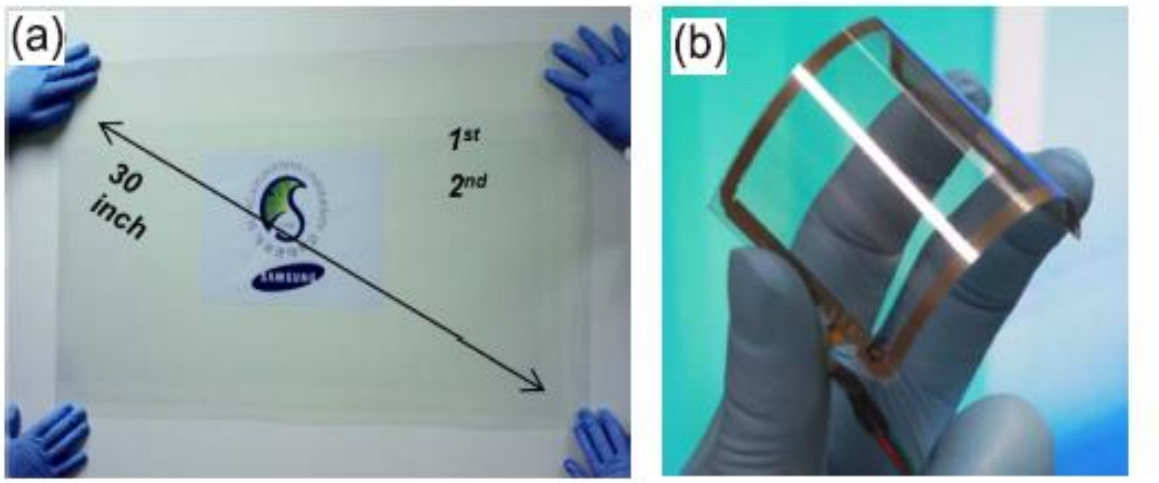

*Figure 1.9 : (a) A large continuous display based on few-layer graphene deposited on a polymer substrate, fabricated by Samsung company (Taken from Ref. [**91**]). (b) A flexible graphene screen.*

1.1.1. Flexible transparent electrodes

Transparent conducting (TCs) materials are widely used as transparent electrodes in several optoelectronic and photovoltaic applications. These applications include liquid crystal displays (LCD), (organic) light-emitting diodes ((O) LEDs) and solar cells devices. Generally, the recent technology used Indium Tin Oxide (ITO) like an electrode in such applications. However, the ITO suffers from the scarcity, high cost of indium (In) and the brittle nature of ITO that greatly restrict its application.

This situation led to the search of an alternating non-toxic and abundant TCO material with optical, electrical and mechanical properties comparable or better to those of the current ITO materials. Due to its high chemical and mechanical stability, unique mechanical flexibility, excellent optical transparency in the visual spectrum, atomic layer thickness and the low sheet resistivity (see Figure 1.10), Graphene based on TCs has been suggested, recently, as an ideal

alternative material for flexible transparent electrodes in various optoelectronic devices [**59**], [**60**].

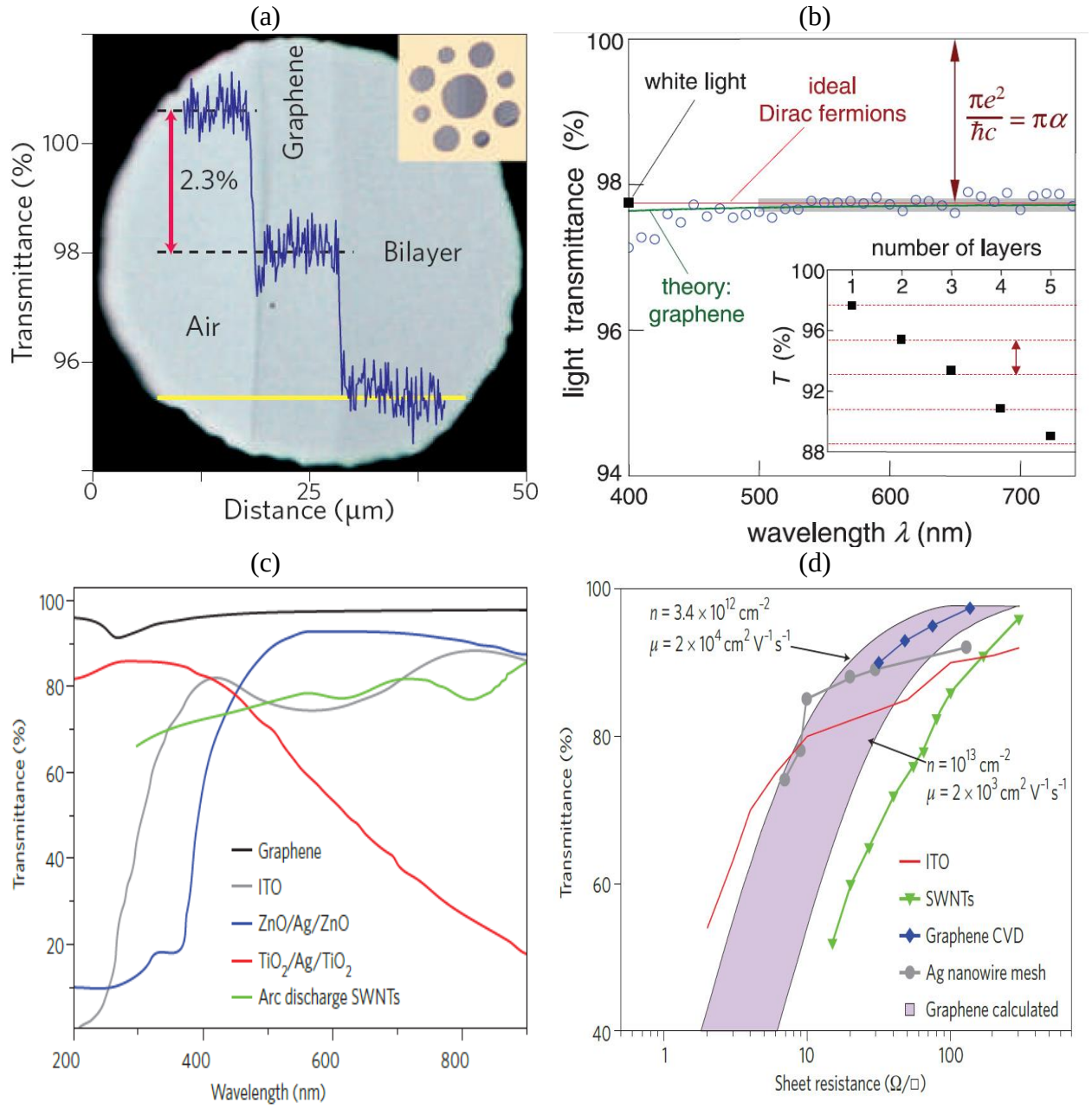

*Figure 1.10: (a) Transmittance for an increasing number of layers. Inset, sample design for the experiment, showing a thick metal support structure with several apertures, on top of which graphene flakes are placed. (b) Transmittance spectrum of single-layer graphene (open circles). (Inset) Transmittance of white light as a function of the number of graphene layers (squares). The dashed lines correspond to an intensity reduction by πα with each added layer. (c) Transmittance for different transparent conductors in the visual spectrum.(d)Transmittance versus sheet resistance for different transparent conductors.(a and b are taken from ref. [**15**] while c and dare taken from ref., [**60**])*

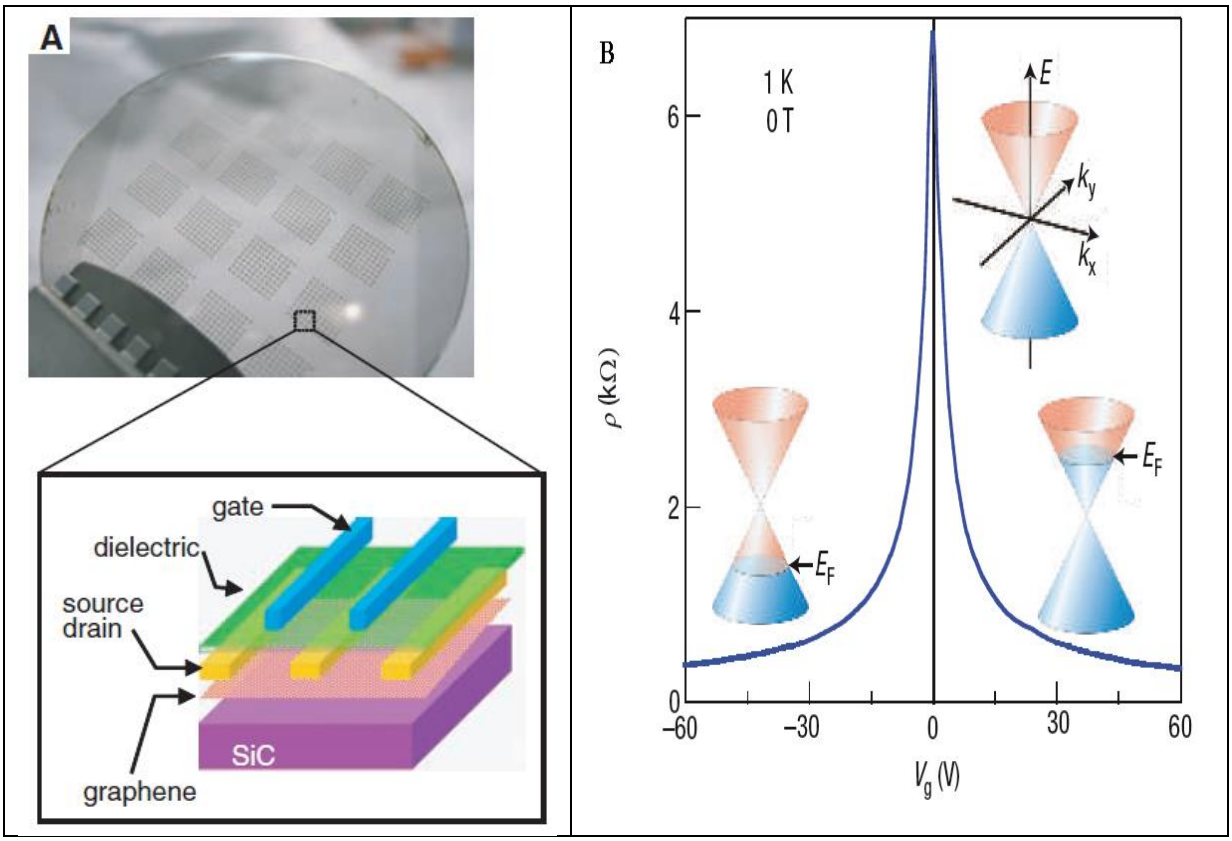

*Figure 1.11: (A) Image of devices fabricated on a 2-inch graphene wafer and schematic cross-sectional view of a top-gated graphene FET.(Taken from ref. [**25**]) (B) Ambipolar electric field effect in single layer graphene on a 300 nm SiO_2 substrate. The insets show the conical low-energy spectrum with different positions of the Fermi-energy, E_F , corresponding to negative, zero, and positive gate voltages, Vg, respectively. The rapid decrease in resistivity on adding charge carriers indicates their high mobility and does not noticeably change with increasing temperature to 300 K. (Taken from ref. [**2**].)*

Moreover, the applicability of thin bendable and rollable graphene-based devices, like flexible screens [**91**] (see Figure 1.9 (b)) have already been demonstrated, due to the high fracture strain of graphene which is found ten times higher [**14**] than those of usual ITO materials. Furthermore, the pure organic graphene-based OLEDs can be also fabricated in even large sizes.

On another side, due to the increasing of global energy demand nowadays, most efforts are concentrated, now, on the renewable energy, especially the solar energy and the improvement of the solar cells efficiency. A solar cell, generally, consists of a layer that absorbs sunlight. This absorber layer is sandwiched between two electrodes which are typically made of ITO. The power conversion efficiency of graphene as an absorber layer is insufficient for these practical purposes .This results from the low intrinsic optical absorption of graphene in the visual spectrum

[**15**] . Instead, graphene can be used as a transparent electrode in either quantum dots or dye-sensitized solar cells, [**60**] , [**94**].

Another new class of solar cells that used graphene as an electrode has been also proposed and demonstrated, recently [**95**]. In these new solar cells, fullerene and carbon nanotubes are used, as absorbers layer, to absorb sunlight and generate electrons and holes. The entire device is based on carbon which is stable in a wide range of temperatures.

1.1.2. Graphene-based transistors

Two principal graphene electronic devices are digital logic and high-frequency transistors. For the first type of transistors, the opening of band gap energy in graphene is essential. Therefore, several methods are devoted, recently, to open the graphene band gap energy like single electron transistor formation [**96**], [**97**], nanoribbons [**98**], [**99**], bilayer [**100**], [**101**], [**102**] and chemically modified graphene [**103**], [**104**].

Most of these methods, except for chemical modified graphene, are unable to open a band gap of more than 360 meV, corresponding to a limited transistor on/off ratio around 10^3 [**59**].In fact, this value is much less than the required threshold value that equals to 10^6. However, new vertical transistor design [**105**] with on/off ratios of $> 10^6$ is introduced in order to overcome the problem of the low on/off ratio.

A low on/off ratio is less important for high frequency applications, so graphene has been considered as a potential candidate for high-frequency transistor or analog applications, such as amplifiers and transmitters [**25**]. The exceptional carriers mobility of about 4×10^4 $cm^2/(V.s)$, in air, at room temperature [**106**] which is essential for achieving high-speed and high-performance transistors, the high trans-conductance which is a crucial parameter for an amplifiers performance, the stability, the large contact region, the possibility to change the amount and type of charge carriers (see Figure 1.11 (b)) and the ultimate thinness make graphene devices an excellent and promising candidate for fast analog nano electronics. After the graphene discovery, notable efforts have been made to fabricate a graphene- based Field Effect Transistor (FET) [**25**], [**26**]. The realization of such device has been carried out, successfully, by researchers at IBM, USA [**25**] (see Figure 1.11 (a)). They demonstrated that the frequency performance of the graphene device already exceeds the cut-off frequency of state-of-the-art silicon transistors for

the same gate length. Indeed, this cut-off frequency is an important parameter in the radio frequency (RF) field .It is defined as the frequency at which the current gain for the device is reduced to one, and is thus the limiting frequency at which a signal will be carried through. In the last few years, a cut-off frequency value with 300 GHz was also found experimentally [**107**], while this value was predicted to be extended to 1 THz, theoretically, [**108**] . One of the future goals, is the possibility of making devices with extremely thin channels which allow graphene based FET to be scaled to higher speeds and shorter channel lengths without encountering the adverse short-channel effects which restrict the performance of existing devices [**26**], [**59**].

1.1.3. Spintronics

In spintronic devices, information can be processed using electron spins beside its charge, and the strong research interest in it originates from the fact that it promises to be faster, smaller and more adaptable than existing electronic devices [**109**]. Furthermore, the seeking of a high-density, high-speed, and low power memory technology that retains its data even when the power is interrupted is one of the great challenges of semiconductor devices industry. Many of technological memories have been fabricated and each one has its concept, cons and pros. These memories include static random access memory (SRAM), dynamic random access memory (DRAM), nonvolatile data memory (NVM),Ferroelectric random access memory (FeRAM), magneto-resistive random access memory (MRAM) and resistance-switching random access memory (RRAM), [**52**].

For spintronic applications, graphene is found to be a promising material due to its electron spin can maintain its direction for a long time , then, information can be stored and coherent quantum manipulation should be realizable over long times. Recently, there is a great interest if nonvolatile memory can also be realized in carbon so that logic and memory devices can be integrated on a same carbon-based platform. Several potential applications of spintronic will include MRAM [**40**], spin field-effect transistor (spin-FET) [**38**], spin-light emitting diode (spin-LED) [**39**], and so on.

1.1.4. Graphene for sensors and metrology

As a 2D material graphene has a large surface area, an excellent surface to mass ratio and graphene screens charges close to it very well making graphene extremely sensitive to the environment for feeling the proximity of molecules. Interactions of various gas molecules with

graphene affect its electronic properties in a measurable way due to graphene low-electronic noise characteristic [**110**], [**111**] .The effect of a single gas molecule bonded to the graphene surface was experimentally measured by looking at the changes in the planer Hall resistance . The measured accuracy makes graphene a potential candidate for the use in sensor applications [**112**] and opens the gate to the manufacturing of commercial sensitive gas sensors. It should be mentioned that, the quantum Hall effect (QHE) is a quantization of resistance has been observed only at liquid helium temperatures, but in graphene, the QHE can be measured even at room temperature. Therefore, the QHE resistance in graphene which is universal and accurate [**113**], [**114**] are available and used to a broader metrological facilities [**59**] , [**115**].

1.1.5. Energy storage

Another possible application is using graphene in the energy storage applications [**59**]. This not includes only Lithium-ion batteries but also hydrogen storage and super-capacitors. In Lithium-ion batteries, graphene can be added to the cathode in order to overcome its poor electrical conductivity first, and may also give rise to new core-shell or sandwich-type nano composite structures. As result of the high thermal conductivity of graphene, the significant amount of heat generated within the battery can be also removed. Besides that, the oxygen-containing functional groups can be used to increase the interlayer spacing between the graphene sheets for maximizing the available surface for Li insertion [**116**].

Graphene is an ideal candidate for super-capacitor application, [**59**], [**117**] .This is related to some interesting properties such as, high electrical conductivity, large surface area, good resistance to oxidative processes, high temperature stability and an accessible and defined pore structure. Further improvement of these devices performance can be achieved in the future by modifying the surface by forming graphene/ metal oxide composites and by introducing the attachment of functional groups.

Computational Methods

2. Computational Methods

2.1. Introduction

Due to the continuous advances in computer technology nowadays, the computational modeling and simulation could be considered as a third stream together with pure theory and experiment to scientific investigation. They provide a modeling of physical phenomenon from a broad range of perspectives, from the electronic structure (*ab* initio/ first-principles) methods to the macroscopic end as shown in Figure 2.1.

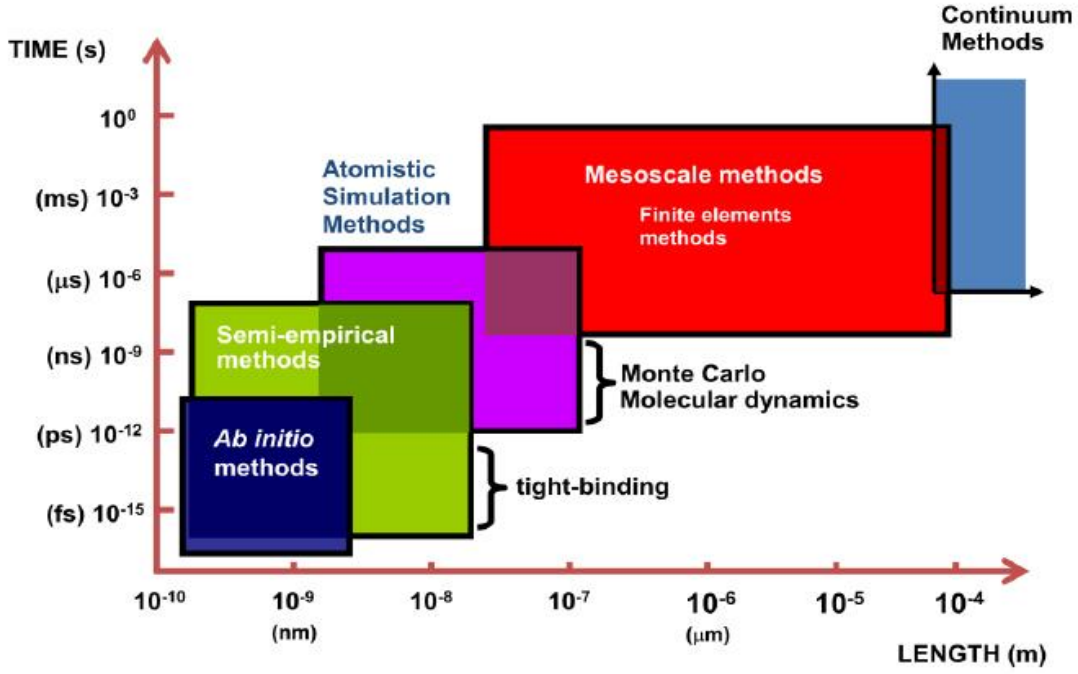

Figure 2.1: The multi-scale modeling methods from ab initio to continuum methods.

In the present-days, the computational modeling tools of different structures of materials and their properties, in different scales, can be very useful and valuable for developing materials and their applications. As they offer acceptable accuracy in prediction of materials properties, they are widely used in the development of new materials and for interpretation of experimental results.

Besides this, they push theories and experiments beyond the limits of manageable mathematics and feasible experiments such as, calculating properties of materials under extreme conditions

that are difficult to do experimentally (temperature, pressure, etc.), calculating properties of complex systems (a solid crystal is already an unmanageable system for a microscopic mathematical model), calculating properties in some cases are easier and fast, testing of theories vs. experimental observation and making suggestion of experiments for saving both money and time as well as for validation of the theory .

The possibility to predict novel materials like, Nano-systems and to calculate their basic physical and chemical properties is quite remarkable with falling back on the elementary interactions and the most accurate electronic structure methods for their simulation. The predictive power of modern electronic structure methods and other modeling tools, like, Monte Carlo simulations, turns out to be the product of decades of intense research, driven by at least two equally important developments:

First of all, the powerful numerical algorithms, which form key elements of computational physics tools including modern electronic structure codes. Some of these algorithms are the most popular and come in the top ten algorithms of the 20th century [**118**], [**119**] as listed in Table 2.1.

	Algorithm	**year**	**Author(s)**
1	Monte Carlo method	1946	J.V. Neumann, S.Ulam, N. Metropolis
2	Simplex method for linear programming	1947	G. Danzing
3	Krylov subspace iteration method	1950	M. Hestenes, E. Stiefel, C. Lanczos
4	Decompositional approach to matrix Computations	1951	A. Householder
5	Fortran optimizing compiler	1957	J. Backus
6	QR algorithm	1961	J.G.F. Francis
7	Quicksort	1962	T. Hoare
8	Fast Fourier transform	1965	J. Cooley, J. Tuckey
9	Integer relation detection algorithm	1977	H. Ferguson, R. Forcade
10	Fast multiple algorithm	1987	L. Greengard, V. Rokhlin

Table 2.1: Top ten algorithms of the 20th century [**118**], [**119**].

The second important factor there is a dramatic increase in the hardware capacities of modern computing systems, due to a continuous down-scaling of microelectronic devices. The

importance of this increasing is directly connected to the matrix representation of the system problem under investigation. But, the down-scaling of microelectronic devices associated with this increasing involves technological challenges [**120**] such as Moore's law, which predicts an exponential growth of computing power when microelectronic devices smaller than the sub-lithographic range must be produced.

In fact, such law can be extended [**121**] over various technologies (electromechanical: 1900– 1935, relays: 1934– 1940, vacuum tubes: 1940– 1960, transistors: 1960– 1970, integrated circuits: since 1970), is, schematically, illustrated in Figure 2.2.

In spite of these challenges, new similar shifts in fabrication technologies and distributed computing will extend Moore's law even into the future [**121**][**7],** and these developments will provide increasing powerful computational platforms for future electronic structure methods and other modeling tools.

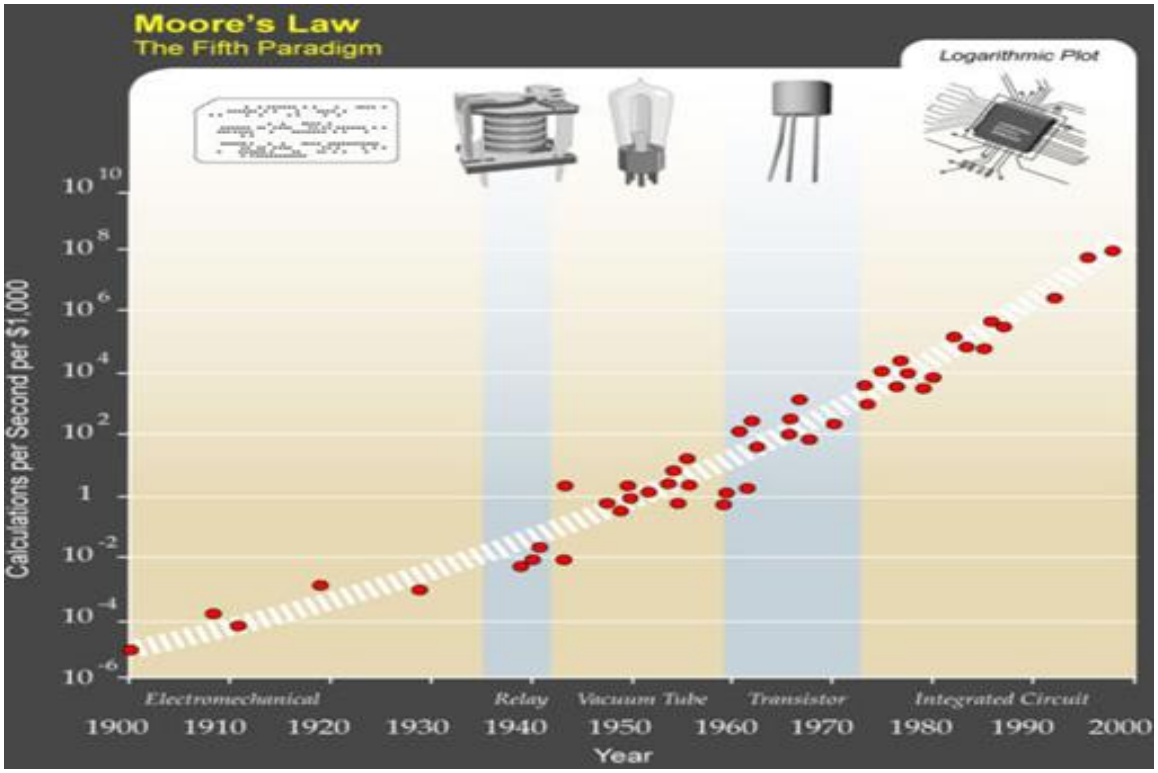

*Figure 2.2: An extension of Moore's law from integrated circuits to earlier transistors, vacuum tubes, relays and electromechanical computers [**121**].*

Moreover, it is interesting to note that in 1998 it was the first time that a Nobel Prize in chemistry or physics was awarded for the development of a numerical method (or more precisely,

a class of numerical methods) rather than a distinct scientific discovery. Acutely, the Nobel Prize in chemistry was awarded, , in the field of electronic structure approaches, jointly to Walter Kohn for his work developing the foundations of the density functional theory DFT and John Pople for his groundbreaking work on developing a quantum chemistry computer code for calculating the electronic structure of atoms and molecules. This awarded reflects the strong connections between DFT and wave-function-based methods and their importance together within material science.

Electronic structure methods are distinct from other forms of modeling because they are first-principles in nature. These methods of calculations contain no external parameters other than a most basic description of the system. However, the other modeling methods require their inputs from experiment or from lower-scale methods that can be difficult to obtain in some cases.

The important factor for the progress of Electronic structure methods are theoretical and conceptional breakthroughs in applying the variational principle. Nowadays acceptable accuracy may routinely be achieved for system sizes that imply hundreds of atoms and electrons, and these developments turned out to be so useful for our current understanding of molecular and solid systems.

In this chapter, the many-body problem is described firstly, followed by introducing approximations that motivated by physical considerations the theoretical frameworks that are used nowadays, for electronic structure calculations in the field of chemistry and condensed matter, are introduced. The basics of the density functional theory (DFT), as powerful quantum mechanical approach for ground state calculations, are explained. This is followed by practical DFT calculations including, the methods and approximations that are used in this thesis to calculate the electronic structure of $2D$ materials. Finally, a brief knowledge on the theoretical basis of Monte Carlo simulation as atomistic method is given.

2.2. The Exact Many body Hamiltonian of a solid

All solids, in nature, consist of heavy, positively charged atomic nuclei (ions) and lighter, negatively charged electrons. The physical and chemical solid properties are associated with the type of its atoms and the positions of both ions and interacting electrons. Since these interactions are happening at the atomic level, the Hamiltonian model for such system is inherently quantum Mechanical.

So, for an arbitrary solid composed of N electrons and M atomic nuclei, the exact non-relativistic many body Hamiltonian [**122**] can be written as:

$$\mathcal{H} = -\sum_i \frac{\hbar^2 \nabla_i^2}{2m_e} - \sum_I \frac{\hbar^2 \nabla_I^2}{2M_1} + \frac{1}{2}\sum_{i\neq j} \frac{e^2}{|r_i - r_j|} + \frac{1}{2}\sum_{I\neq J} \frac{Z_I Z_J e^2}{|R_I - R_J|} - \sum_{i,I} \frac{Z_I e^2}{|r_i - R_I|} \qquad [2.1]$$

Where, $\hbar$ is Planck's constant divided by 2π, e and m_e denote the charge and the mass of a stationary electron , M_I and Z_I indicate respectively the mass and the charge (atomic number) of the nucleus (ion) and R_I and r_i stand for the positions of the nuclei and the electrons respectively.

In this expression, the first and the second terms correspond to the kinetic energies of the electrons and (T_e) the nuclei (T_n) while the reminder terms indicate, respectively, the Coulomb interactions of electron-electron (internal potentialV_{int}), nucleus-electron (external potential V_{ext}) and nucleus-nucleus (V_{nn}). So the Hamiltonian describing the solid simply reads as,

$$\mathcal{H} = T_e + T_n + V_{int} + V_{nn} + V_{ext} \qquad [2.2]$$

And the corresponding time independent Schrödinger equation with this Hamiltonian is given by:

$$\mathcal{H}\Psi(\{R_I; r_i\}) = E\Psi(\{R_I; r_i\}) \qquad [2.3]$$

Here E and ψ are the energy and the many body wave function of the system. By solving exactly the last equation all the macroscopic properties of the solid, in principle, would be

determined. However, this kind of solution is a very hard task or even impossible for most cases. Indeed, this difficulty of solution is related, essentially, to the Coulomb many body terms V_{int} and V_{nn}. So, some approximations for this problem are required. In fact, there are several approximations, depending on some physical considerations, that aimed to solve this problem. Some of them will be briefly explained later in the next sections. In the following, the so-called Hartree atomic units will be used, so $h = e = me = 1$ and the energy is expressed in hartree ($1\ hartree = 27.21138\ eV$) and lengths in bohr ($1\ bohr = 0.529177$Å).

2.3. Born-Oppenheimer approximation

The first approximation was introduced by Born-Oppenheimer in 1927 [**123**]. In this approach the many body wave function Ψ of the coupled nuclei -electrons system can be separated as result of the huge difference in motion between the nuclei and the electrons i.e. they move on different time scales.

Its validity is based on the fact that the mass of the nuclei, except in the case of the lightest elements, are generally, four to five orders of magnitude, much larger than the mass of the electrons. Therefore, they have much slower dynamics than the electrons, and their kinetic energy T_n, which is inversely proportional to the mass of the nucleus M_I, is relatively small and can be then ignored.

Consequently, the nuclei can be considered as "frozen" at fixed positions R_I and the nucleus-nucleus Coulomb interaction term V_{nn} (the fourth term in the Hamiltonian) becomes just a classical constant and the total Hamiltonian then simplifies to:

$$\mathcal{H} \simeq T_e + V_{int} + V_{ext} + E_n \simeq H + E_n \qquad [2.4]$$

Under this assumption, the many body wave function Ψ can be then expressed as a product of the electron wave function and the nuclear wave function:

$$\Psi(r_i, R_I) = \psi(r_i, R_I)\psi_n(R_I) \qquad [2.5]$$

This involves that the many electron wave function ψ depends explicitly on the electronic degrees of freedom r_i while it depends upon the nuclear positions R_I as parameters but not as variables. So, the electronic Hamiltonian and the corresponding Schrodinger equation are given by:

$$H = T_e + V_{int} + V_{ext} \quad [2.6]$$

$$H\psi(r_1, r_2, \dots) = E_e\psi(r_1, r_2, \dots) \quad [2.7]$$

The total energy E_t is then the sum of E_e and the constant nucleus-nucleus Coulomb interaction energy E_n that comes from the constant potential energy V_{nn}

$$E_t = \langle H \rangle + E_n = E_e + E_n \quad [2.8]$$

It is important to note, from the electronic Hamiltonian equation (2.6), that the specific information of the system is completely determined by the third term V_{ext} (i.e. the number of electrons N, and the charges Z_I and positions R_I of the nuclei). However, the first two terms can be considered universal, due to the fact they are entirely independent on the kind of the system. Additionally, Born-Oppenheimer approximation is also called adiabatic because it separates the lattice vibrations problem from the electronic one.

2.4. Wave Function Approaches

Electronic structure methods, which are the numerical solutions of the equation (2.7), are distinct from other forms of modeling because they are first-principles in nature. These methods of calculations contain no external parameters other than a most basic description of the system. The fundamental classification of these calculations of matter can be made according to the quantity that is being calculated. In fact, several methods are developed, that aim either to compute the electron wave function or the electron density. There are many methods where the

object of the calculation is to compute the full electron wave function. These methods are the subject of the following sections

2.4.1. Hartree approximation

Hartree proposed the simplest approximation to solve the many-electron problem [**124**]. With this approach the electrons are considered as non-interacting particles (*i.e* independent particle model) and each electron then has its own individual wave function. Consequently, the Schrodinger equation (2.7) can be written as a one-electron equation and the many-electron wave function can be expressed as a product of all one-electron wave functions:

$$\psi(r_1, r_2, \dots r_N) = \prod_{i=1}^{N} \psi_i(r_i) \qquad [2.9]$$

According to the variational principle in quantum mechanics which states that for any "trail" wave function ϕ the minimal approximate energy E corresponding to this wave function is given by:

$$E[\phi] = \frac{\langle \phi | H | \phi \rangle}{\langle \phi | \phi \rangle} \geq E_0 \qquad [2.10]$$

Where E_0 is the ground state energy solution of the Schrodinger equation, When E[ϕ] =E_0 then ϕ is the ground state wave function.

By applying this principle with the wave function in Hartree form and the Hamiltonian equation (2.7) the Hartree equation can be written as:

$$\left[-\sum_{\mathrm{i}} \frac{\nabla_{\mathrm{i}}^2}{2} - \sum_{I} \frac{Z_I}{|r_i - R_I|} + \sum_{j \neq i} \int \psi_j^*(r_j) \frac{1}{|r_i - r_j|} \psi_j(r_j) \right] \psi_i(r_i) = \epsilon_i \psi_i^*(r_i) \qquad [2.11]$$

Due to this approximation each independent electron i, moves in an effective potential, representing the attractive Coulomb interaction term of the nuclei and the average effect of the repulsive Coulomb interactions of the other electrons that can be given by the integration over their densities. For this reason, this approximation is called a mean field approach in which the complicated many-body problem, due to the Coulomb many body term V_{ee}, is replaced by n simpler problems in a mean field potential.

Since the effective potential for each wave function depends on the solution of all other wave functions, so this problem (2.11) is, in principle, self-consistent with N simultaneous integro-differential equations and then its solution can be achieved iteratively.

2.4.2. Hartree-Fock approximation

In Hartree approach, the electron spins and their fermionic nature are excluded in Hartree wave function and then the Pauli principle is not satisfied as well. In fact, this many-electron wave function, for electron as Fermi particles, must be antisymmetric by exchange of electrons:

$$\psi(r_1, r_2, \dots, r_j, \dots, r_k, \dots, r_n) = -\psi(r_1, r_2, \dots, r_k, \dots, r_j, \dots, r_n) \qquad [2.12]$$

In order to incorporate the fermionic nature of electrons into the many-electron wave function $\psi(\{ri\})$ and to guarantee its antisymmetry, Fock [**125**], assumed that this many-electron wave function should be, approximately, expressed by a single Slater determinant [**126**] , instead of the product, like Hartree approach, as follows:

$$\psi(r_1\sigma_1 \dots r_N\sigma_N) = \frac{1}{\sqrt{N!}} \begin{vmatrix} \phi_1(r_1\sigma_1) & \phi_2(r_1\sigma_1) & \cdots & \phi_N(r_1\sigma_1) \\ \cdot & \cdot & & \cdot \\ \cdot & \cdot & & \cdot \\ \phi_1(r_N\sigma_N) & \phi_2(r_N\sigma_N) & \dots & \phi_N(r_N\sigma_N) \end{vmatrix} \qquad [2.13]$$

Where, N is the total number of electrons and the coefficient$(1/\sqrt{N!})$, is simply a normalization factor. In this determinant, each column and each line correspond, respectively, to a certain one-electron state, and a certain position in space. The interchanging of two electrons

is equivalent to the interchanging of the corresponding two lines or columns in the determinant, which changes its sign (the wave function is antisymmetric). Moreover, this wave function representation ensures that the Pauli principle is satisfied, i.e. if two lines or columns are identical (two electrons have the same quantum state) then the determinant vanishes.

The corresponding Hartree-Fock equation is, also, derived from the variational principle by looking for the minimum of the many-electron Schrödinger equation (2.7) with this single Slater determinant. This equation can be written as:

$$\left[-\sum_i \frac{\nabla_i^2}{2} - \sum_I \frac{Z_I}{|r_i - R_I|} + \sum_j \int \phi_j^*(r_j) \frac{1}{|r_i - r_j|} \phi_j(r_j)\right] \phi_i(r_i) - \sum_J \left[\int \phi_j^*(r_j) \frac{1}{|r_i - r_j|} \phi_i(r_j)\right] \phi_j(r_i) = \epsilon_i \phi_i^*(r_i) \quad [2.14]$$

This equation has one extra term compared with the mean field equation of Hartree, the last one, which is called the "exchange" potential term. This term describes the effects of exchange between electrons that is included in Hartree–Fock many-electron wave function.

The solution procedure of these equations is extremely similar to the iterative self-consistent method that outlined in Hartree approach.

2.4.3. Beyond Hartree-Fock approaches

Even though the Hartree–Fock approximation includes the electron spins and provides an exact description of electron exchange, it is entirely ignored the electrons correlation property (i.e. each electron is affected by the motion of every other electron in the system). The energy associated with this approach, consequently, must be different from the exact energy by an energy difference that is called the correlation energy.

Therefore, many approaches which are more sophisticated and accurate than Hartree-Fock method were developed to include such energy. These approaches are often described the electron correlation by mixing the wave function with some configurations in which the electrons are excited or promoted from lower energy to higher energy orbitals.

Furthermore, these methods are divided into groups based on the number of Slater determent that can be used. The first group uses a single Slater determinant as the reference wave function and excitations are made from that wave function. The methods belonging to this group are known as post- Hartree- Fock methods such as the configuration interaction (CI) [**127**], coupled cluster (CC) [**128**], Møller–Plesset perturbation theory (MP) [**129**], and the quadratic configuration interaction (QCI) approach [**130**]. Another group of methods that is used more than one Slater determinant as the reference wave function. Among these methods are N-electron valence state perturbation theory ($NEVPT$) [**131**], multi-configurational self-consistent field ($MCSCF$)and the multi-reference single and double configuration interaction (MRDCI) methods [**132**].

All these methods, which are mentioned above, are potentially very accurate. However, they are currently applied for small system due to their high computational cost that increases rapidly with system size.

2.5. Density Functional Theory

Density functional theory (DFT) is one of the most powerful, popular and successful quantum mechanical tools. It represents another fundamental method of quantum mechanical calculations that solve the many-electron problem (2.7) obtained from Born-Oppenheimer approximation in the previous section. The basic concept of this method is to deal with a formulation of this many-electron problem that involves the total density of electrons instead of using the many-electron wave function in that formulation without any loss of information. In fact, a huge simplification can be made, in this method, by reducing the many-electron problem of N electrons with $3N$ degrees of freedom to 3 degrees of freedom only. It turns out that such a method will be as accurate as beyond Hartree-Fock approaches, but with a low computational cost. Consequently, physical and chemical properties of large molecular and solid systems can be, possibly, calculated and could challenge, quantitatively, the experimental ones.

Before going through this method, it would be useful first to give some basic definitions. Generally, the term functional means a function of a function which is this case the total electron density. This total electron density for a system of N electrons is defined from the wave functions as follows,

$$n(r) = \sum_{i=1}^{N} \int \cdots \int dr_1 \cdots dr_N \psi^*(r_1, \cdots r_N)\delta(r_i - r)\psi(r_1, \cdots, r_N) \quad [2.15]$$

And the integral of this density over all space provides the total number of electrons:

$$\int n(r)dr = N \quad [2.16]$$

This density is also a non-negative function and it has this property:

$$n(r \to \infty) = 0 \quad [2.17]$$

The following sections are devoted to explain, briefly, the original density functional theory of Thomas–Fermi-Dirac, the basic aspects of the modern density functional theory including Hohenberg-Kohn theorems, Kohn-Sham one-electron equations (that put this theory into practice) and the exchange-correlation approaches. The calculation methods, which are used in this thesis and some technical and related details, are discussed later on.

2.5.1. Thomas–Fermi–Dirac approach

The earliest method of density functional theory was proposed in 1927 by Thomas [**133**] and Fermi [**134**]. In their method, the total energy is represented, by terms defining the kinetic energy, the Coulomb interactions of electron-electron (internal potential V_{int}), nucleus-electron (external potentialV_{ext}), as an explicit functional of the total density of electrons.

$$E_{TF}[n] = \frac{3}{10}(3\pi^2)^{(2/3)} \int dr\, n(r)^{(5/3)} + \int dr\, V_{ext}(r)n(r) + \frac{1}{2}\int drdr' \frac{n(r)n(r')}{|r - r'|} \quad [2.18]$$

The original Thomas and Fermi formulation ignored the exchange and correlation between the electrons. However, the missing exchange contribution has been added latter by Dirac in 1930 [**135**] who defined the local exchange approximation term, which is still in use today. The energy functional, for electrons in an external V_{ext}(r) potential, is written using Thomas–Fermi–Dirac approach as:

$$E_{TFD}[n] = E_{TF}[n] \; -\frac{3}{4}\left(\frac{3}{\pi}\right)^{1/3} \int dr \; n(r)^{4/3} \qquad [2.19]$$

The ground state energy and density will be determined, by minimizing the functional E[n], in this equation, for all possible n(r) with the total number of electrons constraint in which the integral of the density over all space provides the total number of electrons.

The electronic density, in this approach, assumed to be, entirely, local at any given point like a density of non-interacting electrons in a homogenous gas. That means that only one or two points of the density are required to get the terms in the equation which makes a very efficient calculation with a low computational cost.

Shortly following, several important improvements on this method are given by Weizsacker [**136**] in 1935, who introduced the effects of inhomogeneous electron gas and Wigner [**137**] in 1938 who formulated an expression for the electrons correlation.

This approach has been applied to equations of state of element [**138**] but it was unable to predict some essential physical and chemical findings such as shell structures of atoms and binding of molecules.

2.5.2. The Hohenberg-Kohn theorems

The modern density functional theory has been, formally, established in 1964, by the two central Hohenberg-Kohn theorems [**139**].The first theorem indicates that the many-electron wave function, as a fundamental and complicated quantity in quantum mechanics, can be replaced, in the many-electron problem, by the ground state electron density without any loss of information. The second one defines a variational principle for an energy functional, which depends on the

ground state electron density, rather than the many-electron wave function. This variational principle is almost the equivalent of the standard variational principle in quantum theory.

The two theorems can be stated as follows:

i. **Theorem I**. For any system of interacting particles in an external potential V_{ext} (r) the potential V_{ext}(r) is determined uniquely, except for a constant, by the ground state density $n_0(r)$.

ii. **Theorem II**. A universal functional for the energy $E[n]$ in terms of the density $n(r)$ can be defined, valid for any external potential V_{ext} (r). For any particular V_{ext} (r), the exact ground state energy of the system is the global minimum value of this functional and the density that minimizes the functional is the exact ground state density $n_0(r)$.

In order to get more explanations and implications from these theorems, it is important to remind that the first two terms in the electronic Hamiltonian (6) are completely universal. However, the third term, the external potential V_{ext}, which is associated with the parameters $\{N,R_I, Z_I\}$, uniquely specifies this Hamiltonian. As result from this unique specification, the many-electrons wave function and the included information for all ground and excited states will be determined.

In fact, the three parameters $\{N, R_I, Z_I\}$, which are required for the unique specification of the Hamiltonian, can be, possibly, deduced from the ground state electron density making the first theorem feasible . Firstly, as noted before, the total number of electrons $\{ N \}$ can be provided by integrating the density over all space. Secondly, at the positions of the nuclei $\{R_I\}$ the density has maxima which are closely to the charge $\{Z_I\}$ of these nuclei [**140**]

Therefore, the first theorem implies that the ground state electron density uniquely determines this external potential V_{ext} and as an immediate consequence from this theorem is that any property of the system can be completely, specified as a unique functional (i.e. a function of a function which is the electron density in this case) of the exact ground state electron density.

In this way, the ground state energy functional associated with the electronic Hamiltonian can be written as follows:

$$E_{\mathrm{HK}}[n] = T_e[n] + E_{int}[n] + E_{ext}[n] = F_{HK}[n] + \int n(r)V_{ext}(r)dr \qquad [2.20]$$

$$F_{HK}[n] = T_e[n] + E_{int}[n] \qquad [2.21]$$

Where $E_{HK}[\mathrm{n}]$ denotes the Hohenberg-Kohn functional which is universal for any many-electron system and contains the functionals of the kinetic energy and the electron-electron interaction terms.

However, the major problem now is only how to find such ground state density. The second theorem tackles this problem effectively. This theorem indicates that the $E_{HK}[n]$ reaches its global minimum value for the corresponding exact ground state electron density associated withV_{ext}. This theorem is nothing more than the variational principle:

$$E_{HK}[n] = \left(F_{HK}[n] + \int n(r)V_{ext}(r)dr\right) \geq E_0 \qquad [2.22]$$

It should be noted that the densities which correspond to the ground state densities of Hamiltonians with some external potentials V_{ext} are called "V-representable" densities. Actually, an elementary and very popular proof was given by Hohenberg and Kohn [**139**], requires a non-degenerate ground state and the V-representability of the density for the first and the second theorem respectively. However, these requirements can be removed in the formulation of Levy and Lieb who gave a profound and complete proof in which the exact energy functional is defined for all densities called "N-representable" that can be derived from wave functions with N electrons [**141**] [**142**].

It should also be mentioned that the Hohenberg- Kohn formulation works at$T = 0\ K$. An extension and generalization have been made by Mermin in 1965, [**143**] on this formulation to finite temperature canonical and grand canonical ensembles. However, such extension has not

been widely used due to the difficulty of constructing good approximate functionals for the entropy. Other popular and powerful extensions of Hohenberg- Kohn formulation are spin and time-dependent density functional theory.

More specifically, in the case of a spin-polarized system with a fixed quantization axis the system may then have a net magnetization along this axis. In this case, up- and down-spin densities are defined or, equivalently the total density is instead expressed as the sum of the spin-up and spin-down densities

$$n(r) = n_{\uparrow}(r) + n_{\downarrow}(r) \qquad [2.23]$$

While the magnetization is the difference between these densities and given by

$$m(r) = n_{\uparrow}(r) - n_{\downarrow}(r) \qquad [2.24]$$

And the polarization is defined as,

$$\xi = \frac{n_{\uparrow}(r) - n_{\downarrow}(r)}{n_{\uparrow}(r) + n_{\downarrow}(r)} \qquad [2.25]$$

Moreover, although the Hohenberg-Kohn theorems indicate that the electron density can rigorously be considered the central quantity of the many-electron problem, they are pure theorems of existence and say nothing, practically, about constructing the functionals and finding such exact electron density.

However, these major issues can be treated in light of the ingenious Kohn-Sham anstaz which is the subject of the following section.

2.5.3. Kohn-Sham anstaz

Kohn and Sham [**144**] introduced, In 1965, the notion that the true density for the system of interacting electrons with a particular external potential V_{ext} may be identical with the density for a reference system of non-interacting electrons moving in an effective potential V_{KS} from all other electrons. In other words, the problem of solving the difficult interacting many-electron system (2.7) is mapped to solve an auxiliary system of non-interacting electrons in the effective potential V_{KS} having the same ground state density. In this way, Kohn-Sham approach leads to independent electron equations which can be solved exactly by numerical means. Actually, the calculations are performed on the auxiliary system of N non-interacting electrons with an exact kinetic energy T_{KS} and an effective local potential V_{KS}described by the Hamiltonian:

$$H_{KS} = T_{KS} + V_{KS} \qquad [2.26]$$

$$T_{KS} = -\frac{1}{2}\sum_{i}^{N}\langle\phi_i|\nabla^2|\phi_i\rangle \qquad [2.27]$$

For this system the classical Coulomb interaction term of the electronic density interacting with itself can be defined by Hartree energy E_H as:

$$E_H[n] = \frac{1}{2}\int drdr'\,\frac{n(r)n(r')}{|r-r'|} \qquad [2.28]$$

By applying the first Hohenberg–Kohn theorem to this system, there exists a unique energy functional:

$$E_{KS}[n] = T_{KS}[n] + \int V_{kS}(r)\, n_{KS}(r)dr \qquad [2.29]$$

Where the ground state electron density $n_{KS}(r)$of this system, which is identical with the interacting one n(r), can be expressed as:

$$n_{KS}(r) = \sum_{i}^{N} |\phi_i(r)|^2 = n(r) \qquad [2.30]$$

The N occupied orbitals satisfy the Schrodinger-like equations are given by the N lowest energy solutions of:

$$\left[\frac{-\nabla^2}{2} + V_{KS}(r)\right]\phi_i(r) = E_i\phi_i(r), \qquad E_1 \leq E_2 \leq \cdots, \qquad [2.31]$$

These equations are called the Kohn-Sham equations and the ground state wave function is just a Slater determinant of the N orbitals, the so-called Kohn–Sham orbitals. The main problem now is to determine the form $V_{\text{KS}}(r)$ that must take in order that the ground state electron density (2.30) is fulfilled.

For the system of N interacting electrons in an external potentialV_{ext}, Kohn and Sham introduced the following approach to rewrite the Hohenberg–Kohn ground state energy functional of the interacting many-electron problem as:

$$E_{\text{KS}}[n] = T_{KS}[n] + \int drV_{ext}(r)n(r) + E_H[n] + E_{XC}[n] \qquad [2.32]$$

Where this anstaz incorporates all the difficult many-electron terms into an exchange-correlation functional of the density as:

$$E_{XC}[n] = (T_e[n] - T_{KS}[n] + (E_{int}[n] - E_H[n]) \qquad [2.33]$$

These last equations show that $E_{XC}[n]$ must be a functional, since the right-hand sides of these equations are functionals. In fact, this universal functional $E_{XC}[n]$ contains everything that is

unknown about the real system. It represents the difference of the kinetic and Coulomb interaction energy terms between the interacting and non-interacting systems.

According to the second Hohenberg–Kohn theorem, the density $n(r)$ that minimizes the functionals is the ground-state density. Thus by taking the variation of the equations (2.29) and (2.30) with respect to the electron density, using the method of Lagrange multipliers to keep the number of electrons constant, and equating them to obtain the form of the local potential,

$$\frac{\delta T_{KS}[n(r)]}{\delta n(r)} + V_{KS}(r) = \frac{\delta T_{KS}[n(r)]}{\delta n(r)} + \int \frac{n(r')}{|r-r'|} dr' + V_{ext}(r) + \frac{\delta E_{xc}[n(r)]}{\delta n(r)} \qquad [2.34]$$

$$V_{KS}(r) = \int \frac{n(r')}{|r-r'|} dr' + V_{ext}(r) + \frac{\delta E_{xc}[n(r)]}{\delta n(r)} = V_H[n] + V_{ext}(r) + V_{xc}[n] \qquad [2.35]$$

Where $V_H(r)$ and $V_{xc}(r)$ are Hartree and the exchange-correlation potentials, respectively.

The relationship between Hartree potential and the electron density is given by the equation of Poisson as follows,

$$\nabla^2 V_H[n] = -4\pi n(r) \qquad [2.36]$$

Finally, the resulting Kohn-Sham one-electron equations are rewritten as:

$$\left(-\frac{\nabla^2}{2} + V_{ext} + V_H + V_{xc}\right)\phi_i(r) = E_i\phi_i(r) \qquad [2.37]$$

This section will be closed by highlighting a few points about the Kohn–Sham anstaz. Firstly, it provides an explicit algorithm to calculate the ground state energy and density of the interacting system. Secondly, it is formally exact, supposing that the exact exchange-correlation potential V_{XC} is provided. Additionally, the solution of the interacting N-electron problem is given in terms

of non -interacting electrons in an external potential V_{KS} which is an extremely useful simplification.

More precisely, it should be emphasized that one of the great merits defining the Kohn-Sham anstaz is the local form by construction of the effective potentialV_{KS}. This means that V_{KS} is the same for every orbital like Hartree approximation which is in contrast with the Hartree-Fock approach, in which the potential is orbital-dependent due to the non-local exchange term. This makes Kohn-Sham equations much simpler to solve than the Hartree–Fock ones which is of great practical importance.

Consequently, It is relatively easy to solve for Kohn–Sham orbitals (a Slater determinant of N orbitals) even for a big system with a few hundreds electrons. In analogy with Hartree approach, the solutions of the Kohn-Sham equations, (2.37), have to be found self-consistently, the only difference being the presence of the exchange-correlation potential term.

In fact, an initial trial electron density can be chosen, for example, as a superposition or perturbation of atomic densities to find a trial formV_{KS}. The Kohn-Sham equations can now be solved and the orbitals $\phi_i(r)$ then give the electron density according to (2.30) above to find the next iteration for$n(r)$. When this cycle has been repeated a sufficient number of times that no further changes occur (or the difference between two successive densities is no larger than a predefined criterion), then a solution for $n(r)$ has been found and self-consistency is reached. This self-consistent cycle of solution is summarized in the Figure 2.3. The solution not only satisfies the Schrodinger-like equation for the non-interacting electrons, but also is the ground state density and energy for the interacting system.

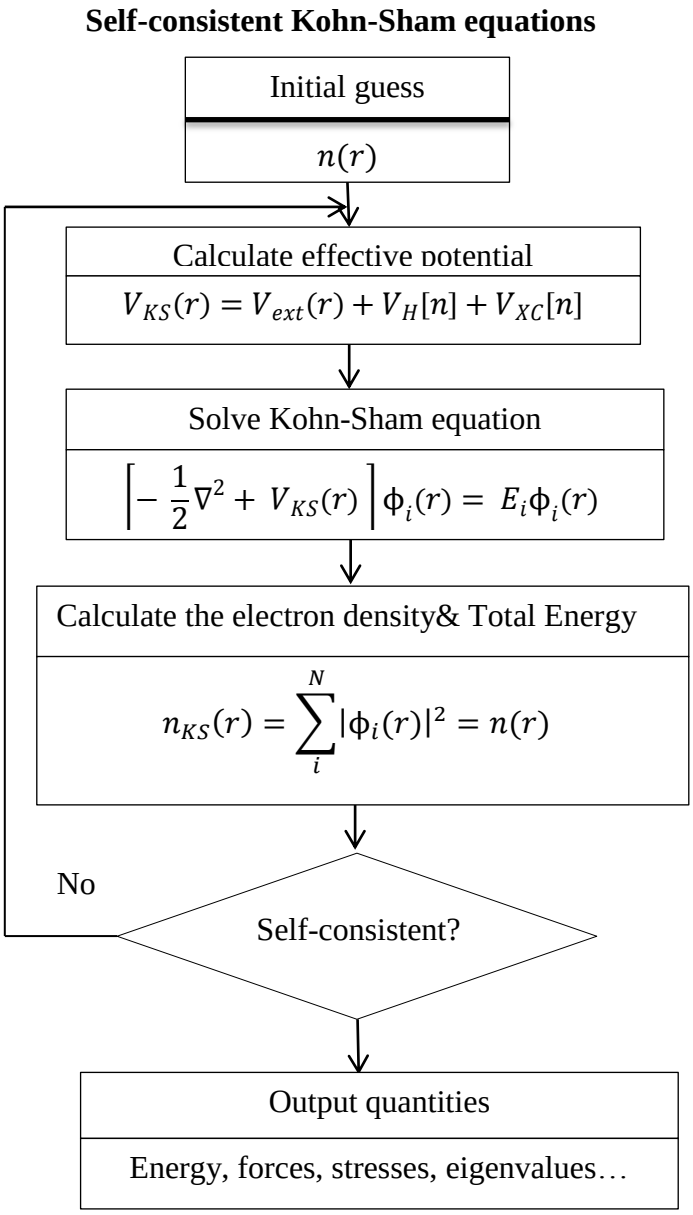

Figure 2.3: Schematic representation of the Self-consistent loop for solution of Kohn-Sham equations.

An additional advantage of this approach is the simultaneous introduction of useful tools for physical interpretation including the electronic charge density, the density of states and the electronic band structure of the system.

Finally, it is worth noting that, for a non-spin-polarized system, each of Kohn–Sham orbitals contains two electrons while in the case of a spin-polarized system each of these orbitals contains only one electron.

2.5.4. The exchange-correlation energy

Although the Kohn–Sham anstaz is formally exact and provides an exact expression for the total energy, unfortunately it introduces the central problem ofDFT, the unknown form of the universal exchange-correlation functionalV_{XC}. From a practical viewpoint, approaches of this functional are unavoidable to solve the Kohn-Sham equations. Therefore, the ground state density and energy will be found with an accuracy limited only by these approximations. In fact, many approximations have been devised to get an explicit form for this functional like the local density approximation (LDA) and the generalized gradient approximation(GGA) . These two are the most widely used approximations in solid state physics. In this section, the approximate expressions for exchange-correlation functional including LDA and GGA are briefly present

2.5.4.1. The Local Density Approximation

The first and simplest approximation for the exchange-correlation energy functional is the Local Density Approximation LDA. In fact, the mean idea behind this approximation is revealed from a homogeneous electron gas. In this LDA, it is assumed that the local exchange-correlation energy per electron depends on the local density, and this energy equals to the exchange-correlation energy per electron of a uniform electron gas having same density, in a neutralizing positive background (jellium background). The total exchange-correlation energy E_{XC} can be then given by summing the contributions of each point in space. Therefore, the exchange-correlation energy E_{XC} is written in the following form:

$$E_{XC}^{LDA}[n] = \int n(r) E_{XC}(n(r))\, dr \qquad [2.38]$$

In this equation, $E_{XC}(n(r))$ stands for the exchange-correlation energy per electron of a homogeneous electron gas of density n(r). This quantity $E_{XC}(n(r))$ can be further separated into exchange and correlation contributions:

$$E_{XC}\big(n(r)\big) = E_X\big(n(r)\big) + E_C\big(n(r)\big) \quad [2.39]$$

The exchange part, $E_X(n(r))$, represents the exchange energy of an electron in a homogeneous electron gas of a particular density and is given by [**135**], [**145**]:

$$E_X(n(r)) = -\frac{3}{4}\sqrt[3]{\frac{3n(r)}{\pi}} \quad [2.40]$$

Since the correlation part $E_C(n(r))$ has no explicit expression like$E_X(n(r))$, several approaches have been proposed. In 1980, Ceperly and Alder used accurate quantum Monte-Carlo simulations of the uniform electron gas in order to find a numerical solution for $E_C(n(r))$ [**146**] as well Perdew and Wang who presented, in 1992, another accurate approximation for $E_C(n(r))$ [**147**].

The LDA is more accurate for systems having slowly varying densities [**144**], as the assumed density is locally a constant. Although, it is a simple approximation, the results of this approximation are surprisingly good.

The accuracy of this simple approximation almost leads to a correct picture of binding trends, structural parameters, vibrational energies, phonon spectra, bond lengths and other properties across the periodic table. Most of these properties are predicted correctly, or with a systematic deviation. However this approximation underestimates the band gap (a famous example of this underestimation is the band gap of bulk Ge, which is predicted to be metallic), and also overestimates the binding energy of solids and molecules which leads usually, to an underestimation of the bond lengths [**148**].

This approximation can be extended to treat magnetic cases, by taking into account the spin-polarization of the material as noted above, and it is then called the Local Spin-Density Approximation ($LSDA$),

$$E_{XC}^{LSDA}[n_\uparrow, n_\downarrow] = \int n(r) E_{XC}(n_\uparrow(r), n_\downarrow(r)) dr \quad [2.41]$$

In this thesis, the LDA version of Perdew and Wang [**147**], which is presently known to be the most accurate LDA approaches, is applied in some of our works.

2.5.1.2. The Generalized Gradient Approximation

In real materials the density varies in space, so a logical improvement of LDA approximation would be to include also extra information of this rate of change in the functional. This can be achieved by adding gradient terms. This approach is called the gradient-expansion approximation. In this class of approximation, a power series of gradient corrections with specific order can be systematically calculated and added to the LDA. The LDA can be then regarded as the zeroth-order approximation of these exchange-correlation functionals. Among others, the generalized gradient approximation (GGA) for the exchange-correlation energy functional improves, generally, upon the local density description of atoms, molecules, and solids. It goes beyond LDA by including not only the information about the density at a specific point ($n(r)$), but also by introducing the density in the local vicinity through the dependence on the gradient ($\nabla n(r)$). Consequently, the non-homogeneity of the true electron density is taken into account within this approximation and the exchange-correlation energy functional is then given as,

$$E_{XC}^{GGA}[n] = \int n(r) E_{XC}(n(r), \nabla n(r)) dr \qquad [2.42]$$

The current generalized gradient approximations ($GGAs$) seem to provide reliable results for all main types of chemical bonds binding energies, etc. than LDA and are popular in computational physics and chemistry. However, they, practically, have also some weakness. Several studies have been carried out to compare the disadvantages or advantages of GGA versus LDA methods see Refs. ([**149**], [**150**] , [**151**]).

In analogy with the local spin-density approximation($LSDA$), this approximation can be also extended to treat spin-polarization cases as,

$$E_{XC}^{GGA}[n_\uparrow, n_\downarrow] = \int n(r) E_{XC}(n_\uparrow(r), n_\downarrow(r), \nabla n_\uparrow(r). \nabla n_\downarrow(r)) dr \qquad [2,43]$$

There are various forms of GGA functionals that are used in many different calculations. In fact, these forms can be roughly divided in two groups. It is possible either to use parameters that are fitted to experimental data like the Becke exchange [**152**] and Lee-Yang-Parr (LYP) correlation [**153**] ($BLYP$) or to construct aGGA, free of empirical parameters and starting from

physical principles, such as the Perdew-Burke-Ernzerhof $(PBE) - GGA$ form [**149**]. This (PBE) version of GGA has been used in some of our works.

2.5.5. Electronic structure of solids: Practical calculations

In real crystalline solids there are a lot of ions and electrons. A regular three dimensional $(3D)$ solid contains almost 10^{24} electrons and ions per cm^3 whereas for Graphene two dimensional materials $(2D)$ there are roughly 10^{16} electrons and ions per cm^2. In order to apply DFT to these real crystals, the Kohn-Sham equations should be, in principle, solved for all these particles present in the system. This task is computationally an impossible. Therefore, to solve this problem, the periodicity of the crystal must be used. According to the periodic symmetry of crystal, the calculation problem can be significantly, reduced to only those electrons and ions that are contained only in the unit cell, which is the smallest repeat unit in dimensions of space. This unit cell consists of atoms, whose arrangement defines the symmetry of the crystal, and it is characterized by lattice parameters. By solving the Kohn-Sham Hamiltonian for the atoms in this unit cell, the electron eigenstates for solid can be calculated, consequently.

According to the Bloch theory, the electrons move in a periodic potential rather than a free space. This potential is generated by the periodicity of the solid and is invariant by translation. Therefore, the effective potential, V_{KS} , in the Kohn-Sham equation will be now periodic for all lattice vectors R of the crystal and can be written as:

$$V_{\mathrm{KS}}(r) = V_{\mathrm{KS}}(r + R) \qquad [2.44]$$

Bloch's theorem states that the eigenstates Φ of a one-electron Hamiltonian has the form of a plane wave times a lattice-periodic function $u_{nk}(r)$ as follows:

$$\phi_{nk}(r) = e^{ik.r} u_{nk}(r) \qquad [2.45]$$

Here, k denotes the wave vector that is chosen in the first Brillouin zone due to the translational symmetry, n stands for the band index which labels different solutions for a given k. For all R in the crystal the lattice-periodic function is written as

$$u_{nk}(r + R) = u_{nk}(r) \qquad [2.46]$$

Another equivalent form of Bloch's theorem is also given by

$$\phi_{nk}(r+R) = e^{ik.R}\phi_{nk}(r) \quad [2.47]$$

The energy values are periodic also in the reciprocal space, so if $E_n(K)$ is an energy eigenvalue, then $E_n(k+G)$ is also an eigenvalue for all vectors G of the reciprocal lattice.

In case of large systems, the spectrum of k-points is quasi continuous therefore, an integration over k is required to calculate properties such as the density or energy of the system. According to Bloch's theorem the problem of infinitely many-electrons has been converted to a problem of infinitely many k-points inside the first Brillouin zone (due to the symmetry). As the wave functions of closely located k-points are nearly identical, a small region can be sampled by one single k-point. It is sufficient, generally, to solve the Kohn-Sham equations in a unit cell, using only a finite discrete number of k-points, and the electronic part of the total energy can be then calculated to a good approximation. This leads to bands of eigenvalues and energy gaps where no eigenstates can be there. By taking the symmetry of the system into account, the number of k-points can be further decreased by restricting the k-points to the so-called irreducible Brillouin zone. The required number of k-points that is needed to get a good description of a system not depends only on the type and size of such system, but also particularly on the studied property. For example in isolators case only a few k-points are required as all bands are filled, while for metals more points are needed for bands that cross the Fermi level. Therefore, the convergence of any calculation should be checked with respect to the k-point grid.

Different schemes are developed in order to sample appropriately the Brillouin zone with a set of k-points that give the best estimate of the full integral such as the most widely scheme proposed by Monkhorst and Pack in 1976, [**154**] .

2.5.6. Equilibrium Position of Atoms: The Force Theorem

Another practical and important task is the equilibrium position of atoms in the material, so in order to determine the equilibrium geometry of a system, it is necessary to calculate the forces on the nuclei in this system. The particular set of equilibrium position that minimizes the total energy (2.8) is found when all forces are vanishing. Therefore the derivative of the total energy with respect to the ionic positions must be calculated and this should be zero for the equilibrium position:

$$F_I = -\frac{\partial E_t}{\partial R_I} = 0 \qquad for\ I = 1, \dots, M \qquad [2.48]$$

These forces can be calculated by applying the force theorem stated by Hellmann [**155**]and Feynman [**156**]: an evaluation of the forces from (8) and (6) gives:

$$-\frac{\partial E_t}{\partial R_I} = -\left\langle \frac{\partial \psi}{\partial R_I} \middle| H \middle| \psi \right\rangle - \left\langle \psi \middle| \frac{\partial H}{\partial R_I} \middle| \psi \right\rangle - \left\langle \psi \middle| H \middle| \frac{\partial \psi}{\partial R_I} \right\rangle - \frac{\partial E_n}{\partial R_I} \qquad [2.49]$$

According to the variation principle, the first and the third term on the right vanish and the only non-zero terms come from the explicit dependence of the nuclear positions this equation can be written as,

$$F_I = \frac{\partial E_t}{\partial R_I} = -\left\langle \psi \middle| \frac{\partial H}{\partial R_I} \middle| \psi \right\rangle - \frac{\partial E_n}{\partial R_I} \qquad [2.50]$$

Form this equation and the equation (2.6), the force is independent on the pure electronic terms and it is, only, given upon the following terms,

$$F_I = -\int n(r) \frac{\partial V_{ext}(r)}{\partial R_I} dr - \frac{\partial E_n}{\partial R_I} \qquad [2.51]$$

From this expression, it is clear that, the forces on the nuclei only depend on the ground state electron density and the positions of the other nuclei and can be then calculated if the electron density is known.

2.5.7. Electronic structure of solids: Basic Methods and Practical calculations

There are several methods for calculating the electronic structure in material. All these methods can be, essentially, categorized in three basic types. There are no fundamental

disagreements: all agree when applied carefully and taken to convergence. Indeed, each one leads to instructive, complementary ways to understand electronic structure and each can be developed into a general framework for accurate calculations. Furthermore, each one has its advantages and pitfalls.

The common point of these methods is the solution of Kohn-Sham equations in self consistent way. However, their specificities are given in the representation of the potential, electronics density and, especially, the mono electronic Kohn-Sham orbitals. Some of these calculation methods are schematized on Figure 2.4.

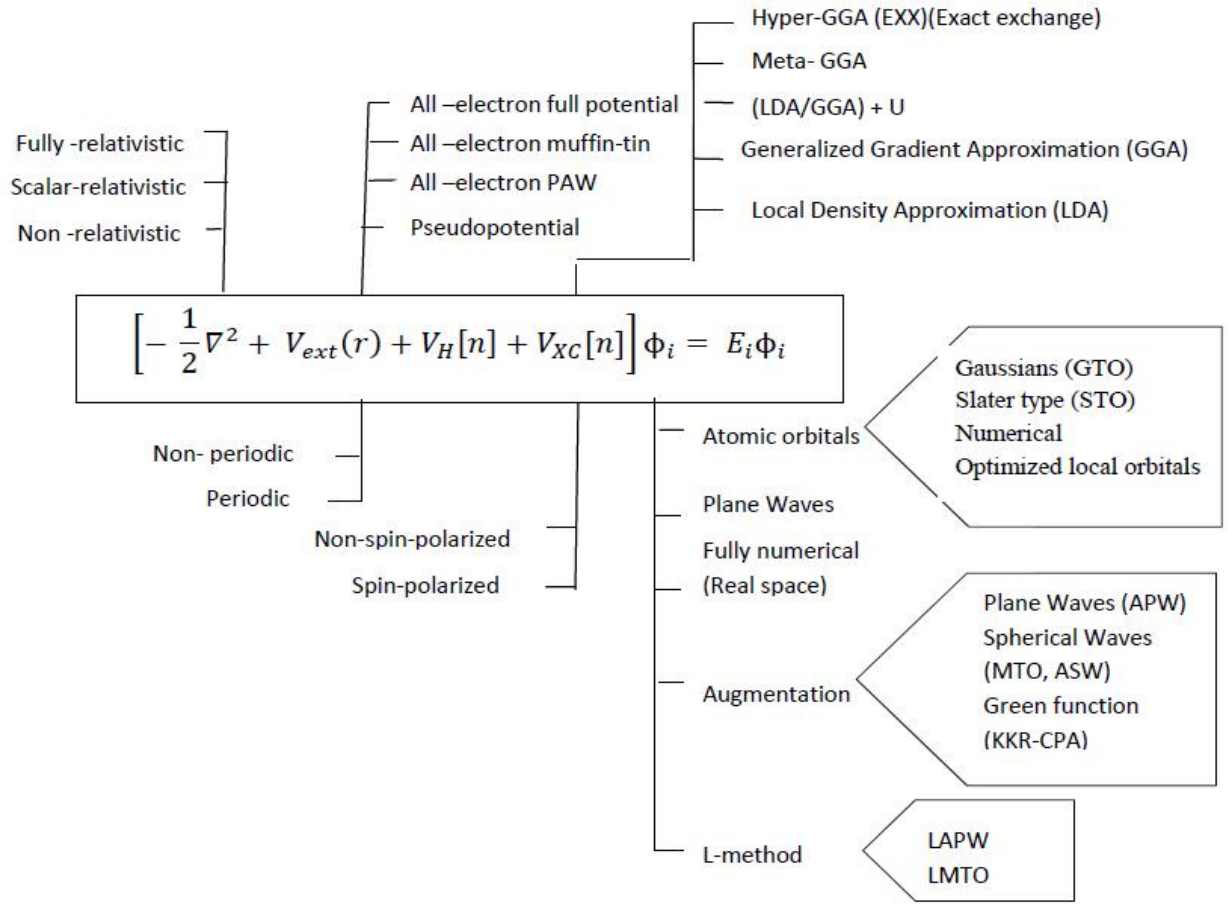

Figure 2.4: Schematic representation of the different calculation methods based on DFT.

Generally speaking, the three groups of methods [**122**] and their characteristics are:

1- Plane wave and grid approaches provide general methods for solution of differential equations, including the Schrodinger and Poisson equations. Plane waves are especially appropriate for periodic crystals where they provide intuitive understanding, a simple derivation of the Bloch theorem as well as simple algorithms for practical calculations.

Since plane waves are eigenfunctions of the Schrodinger equation with constant potential, they are the natural basis for description of bands in the nearly-free-electron approximation which provides important insight into band structures of many materials including sp-bonded metals, semiconductors, etc. Methods based upon grids in real space [**157**] are most appropriate for finite systems and are prevalent in many fields of science and engineering. Moreover, real-space grids are an intrinsic part of efficient plane wave calculations and there is a growing development of real-space methods, including multi-grids, finite elements, wavelets, etc. Modern electronic structure algorithms use both plane waves and grids with fast Fourier transforms. In order to allow calculations to be done with a feasible number of plane waves, pseudopotentials, which are first introduced and used in solid by Hellmann [**158**], [**159**] in 1934, are often intertwined with plane wave methods.

The basic ideas can be understood in terms of empirical pseudopotentials which provide a compact description of bands in terms of a few Fourier components of the potentials. Due to the simplicity of plane waves, they are often the basis of choice for development of new methods, such as Car-Parrinello quantum molecular dynamics simulations [**160**], efficient iterative methods which have made it feasible to apply plane waves to large systems [**161**].

At first sight, plane waves and grids are very different, but in fact each is an effective way of representing smooth functions. They are appropriate for smooth functions, namely pseudopotentials or related operators. "Norm-conserving" [**162**], [**163**] potentials provide accurate solutions with pseudofunctions that are orthonormal solutions of ordinary differential equations.

Furthermore, there are two approaches have brought the orthonormal plane waves (OPW) approach [**164**], [**165**], [**166**], [**167**] [**168**] into the framework of total energy functionals: ultrasoft pseudopotentials [**169**], [**170**] and projector augmented wave (PAW) formulation [**171**], [**172**], [**173**]. With "ultrasoft" pseudopotentials the problem is cast in terms of localized spherical functions and smooth wave functions that obey a generalized eigenvalue equation with an OPW-type Hamiltonian. The PAW formulation completes the transformation by expressing the wave functions as a sum of smooth functions plus core functions, just as in the OPW approach. Unlike pseudopotentials, the PAW method keeps the entire set of all-electron core functions and the

smooth parts of the valence functions. Matrix elements involving core functions are treated using muffin-tin spheres as in augmented methods. Nevertheless, the ultrasoft and PAW methods maintain the advantage of pseudopotentials that forces can be calculated easily and they have made it feasible to apply plane waves to difficult cases such as materials containing transition metals.

2- Localized atomic(-like) orbitals or what so-called linear combination of atomic-like orbitals ($LCAO$) methods provide a basis that captures the essence of the atomic-like features of solids and molecules. In particular, local orbitals provide an illuminating derivation of the original derivation of Bloch theorem [**174**] in 1928. In his work, Bloch considered only the simplest s-symmetry function, while a basis of different atomic orbital was considered by Jones, Mott, and Skinner [**175**] . Moreover, the localized description of electronic structure widely used in chemistry, in recently developed "order- N" methods, and in constructing useful models.

The two principal approaches with localized bases are the semiempirical tight-binding and full calculations methods. The semiempirical tight-binding associated with Slater and Koster, [**176**]which is particularly simple and instructive since one needs only the matrix elements of the overlap and Hamiltonian. Tables of tight-binding matrix elements can be used to determine electronic states, total energies, and forces with very fast, simple calculations.

Full calculations methods such as Gaussians, Slater-type orbitals, and numerical radial atomic-like orbitals [**132**], [**177**], [**178**], [**179**]can vary from quick to highly refined with many basis orbitals per atom. Even in the latter case, the calculations can be much smaller than with plane waves or grids. However, compared to general bases like plane waves and grids, it is harder to reach convergence and greater care is needed in constructing basis functions of sufficient quality. Further development and optimization to $LCAO$ has been introduced by Eschrig [**180**]. This optimized $LCAO$ is very accurate and more appropriate to solve the Kohn-Sham problem of solids.

3- Atomic sphere methods are the most general methods for precise solution of the Kohn–Sham equations. The basic idea, in such methods, is to divide the electronic structure problem, providing efficient representation of atomic-like features that are rapidly

varying near each nucleus and smoothly varying functions between the atoms like plane waves. The original method is the augmented plan wave (APW) of Slater [**181**] in which smooth functions are "augmented" near each nucleus by solving the Schrodinger equation in the sphere at each energy and matching to the outer wave function. Beside the resulting augmented plan wave (APW), there is also the Green function of Korringa, Kohn, and Rostoker (KKR) method [**182**], [**183**]. Both (APW) and (KKR) methods are very powerful, but suffer from the fact that they require solution of non-linear equations. The Green's function KKR method is particularly elegant, providing local information as well as global information such as the Fermi surface. The non-linearity does not present any problem in a Green's function approach; however, it is difficult to extend the KKR approach beyond the muffin-tin potential approximation. Muffin-tin orbitals ($MTOs$) [**184**] are localized, augmented functions that can lead to physically meaningful descriptions of electronic states in terms of a minimal basis, including the concept of "canonical bands," described in terms of structure constants and a very few "potential parameters."

An advance that has made augmented methods much more tractable and useful: the "L" methods that make use of linearization of the equations around reference energies. This allows any of the augmented methods to be written in the familiar form of a secular equation linear in energy involving a Hamiltonian and overlap matrix. The simplification has led to further advances, e.g. the development of full-potential methods, so that $LAPW$ [**185**], [**186**], [**187**], [**188**], [**189**], [**190**] provides the most precise solutions of the Kohn– Sham equations available today. The $LMTO$ approach [**191**], [**192**], [**193**] describes electronic states in terms of a reduced linear Hamiltonian with basic functions that are localized and designed to provide understanding of the electronic states. $LMTO$ involves only a small basis and can be cast in the form of an "ab initio" orthogonal tight-binding Hamiltonian with all matrix elements derived from the fundamental Kohn–Sham Hamiltonian. It is also possible to go beyond linearization and a methodology is provided by the "$NMTO$" generalization to order N [**194**], [**195**].

Here and in what follows, the electronic structure methods that are used to calculate the electronic band structure in this thesis are briefly presented. These are the full-potential local-orbital minimum-basis ($FPLO$) and the full-potential (linearized) augmented plane-wave

((L)APW) + $local\ orbitals$ (lo) method that implemented in$WIEN\ 2K$ code. Such methods are called all-electron methods in which all the electrons are explicitly used in the computation and full-potential, which means there is no shape restriction to the potential, as in pseudopotentials and muffin-tin based methods. Both these all-electron methods are considered among the most accurate schemes for band structure calculations of crystalline solids.

2.5.1.3. FPLO

$FPLO$ code is a full-potential local-orbital minimum-basis scheme [**196**], [**197**], [**198**]. It is based on the optimized $LCAO$ method [**180**], in which the Kohn-Sham orbitals are projected on local atomic orbitals and these orbitals are written in terms of radial functions and spherical harmonics as,

$$\varphi_{s\upsilon}(r-R-s)=\psi_s^{\upsilon}(|r-R-s|)Y_{\upsilon}(r-R-s) \qquad [2.52]$$

Where, R stands for a Bravais vector, s is a site vector in the unit cell, and υ is a multi-index, which is denoted either by the non-relativistic quantum numbers as, $\upsilon=(\mathrm{n},\mathrm{l},m_l)$ or by the relativistic ones as, $\upsilon=(\mathrm{n},\kappa,\mu)$. These two notations correspond to the non-relativistic , and the relativistic cases, respectively.

The periodic boundary conditions, grant that the Bloch functions $\phi_{\mathrm{kn}}$are eigenfunctions of the Kohn-Sham Hamiltonian,

$$\phi_{\mathrm{kn}}=\sum_{R,s,\upsilon}C_{s\upsilon}^{kn}\varphi_{s\upsilon}(r-R-s)e^{ik(R+s)} \qquad [2.53]$$

Now, these Bloch functions are used in the self-consistent Kohn- Sham ansatz which leads to a matrix equation with an eigenvalue problem. It should be emphasized that, in the case of too small basis, completeness of the basis is achieved by adding more states to the basis. Moreover, the core states are assumed to be orthogonal to each other, so the overlap between core states of distinct sites is neglected. However, semi-core, and valence states may have a non-zero overlap. Due to this distinction between core, semi-core, and valence states, the diagonalization effort is, effectively, reduced. Recalling that, the matrix diagonalization scales as the cube of the matrix size. Consequently, this method can achieve high accuracy relies on a relatively small number of

basis states in comparison with plane-wave based codes, which use a high number of plane waves to get such accuracy.

The essential feature which allows for the use of a minimum basis is that the basis is not fixed in the course of iterations, instead it is adjusted to the actual effective crystal potential in each iteration step and it is even optimized in the course of iterations. In fact, all non-core orbitals are compressed by adding to the crystal potential, spherically, averaged around the site center s, a confining potential,

$$v^{conj} = (r/r_0)^4 \quad with \quad r_0 = (x_0 \; r_{NN}(s) \; / \; 2)^{3/2} \qquad [2.54]$$

Here, $r_{NN}(s)$ is the nearest neighbor distance, and x_0 denotes the parameter which is optimized in every iteration step. The parameters $x_0 r_{NN}(s)$ are determined by minimizing the total energy. There are two main effects of this potential: firstly, the counterproductive long tails of basis orbitals are suppressed and secondly, the orbital resonance energies are pushed up, providing the optimal curvature of the orbitals and avoiding insufficient completeness of the local basis.

The resulting potential and density are expanded in spherical harmonics at each lattice site s, as follows,

$$v(r) = \sum_{R+s,v} v_{sv}\,(|r-R-s|)Y_v(r-R-s) \qquad [2.55]$$

$$n(r) = \sum_{R+s,v} n_{sv}\,(|r-R-s|)Y_v(r-R-s) \qquad [2.56]$$

2.5.1.4. WIEN 2K (FP- LAPW)

$WIEN2k$ code is based the full-potential (linearized) augmented plane-wave ((L)APW) + $local\ orbitals$ (lo) method [**186**] . The $LAPW$ method is a procedure for solving the Kohn-Sham equations of a many-electron system by introducing a basis set which is especially adapted

to the problem [**185**], [**186**], [**187**], [**188**], [**189**], [**190**]. This method is developed in order to overcome the non-linearity problem in Slater's old APW method [**181**] as noted, briefly, before. The $LAPW$ method uses a plane wave basis set which is especially modified to solve the problem. This modification can be achieved by dividing the unit cell into (I) non-overlapping atomic spheres (centered at the atomic sites), also known as the $Muffin-Tin$ spheres, and (II) an interstitial region. This is schematically illustrated in Figure 2.5 with a unit cell containing two types of atoms: A and B. For the two regions, the electron potential $V\ (r)$ is expanded as

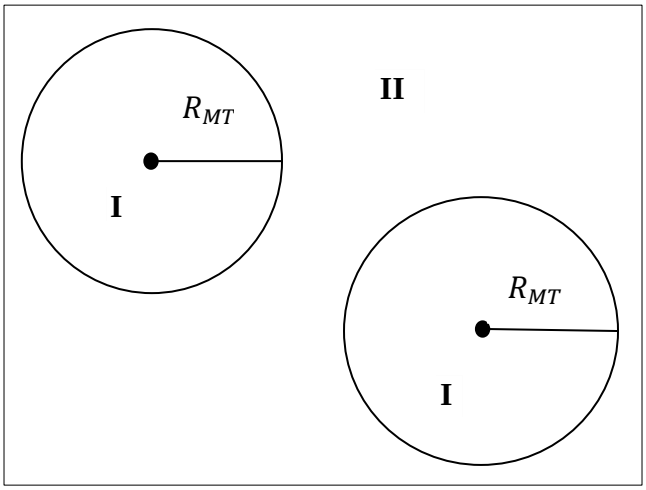

Figure 2.5: Schematic representation of the division of unit cell, with two types of atoms A and B, in Muffin-Tin atomic spheres (I) and an interstitial region (II).

$$V(r) = \begin{cases} \sum_{lm} V_{lm}(r) Y_{lm}(\hat{r}) & (r \in MT) \\ \sum_{G} V_G e^{iG.r} & (r \in I) \end{cases} \qquad [2.57]$$

In the two types of regions, the different basis sets are used:

$$\phi_{kn}^{LAPW}(r) = \begin{cases} \sum_{lm} \left[A_{lm,kn} u_l(r, E_l) + B_{lm,k_n} \dot{u}_l(r, E_l)\right] Y_{lm}(\hat{r}) & (r \in MT) \\ \frac{1}{\sqrt{V}} e^{ik_n . r} & (r \in I) \end{cases} \quad [2.58]$$

Inside the atomic spheres (MT) of radius R, a linear combination of radial functions times spherical harmonics $Y_{lm}(\hat{r})$ is used. $u_l(r, E_l)$ is the regular solution (at the origin) of the radial Schrodinger equation for energy E_l and the spherical part of the potential inside the sphere

$$-\frac{1}{r^2}\frac{d}{dr}\left(r^2 \frac{du_l}{dr}\right) + \left[\frac{l(l+1)}{r^2} V(r) - E_l\right] r u_l = 0 \quad [2.59]$$

E_l is chosen normally at the center of the corresponding band with l-like character. $\dot{u}_l(r, E_l)$ is the energy derivative of u_l (which can be given by expanding the radial wave function in a Taylor series expansion around E_l) evaluated at the same energy E_l. The linear combination of these two functions constitutes the linearization of the radial function. u_l and $\dot{u}_l$can be obtained by numerical integration of the radial Schrodinger equation on a radial mesh inside the sphere. The modified basis functions provide the extra flexibility to cover a large energy region around the linearization energy. The coefficients $A_{lm,kn}$ and B_{lm,k_n} are functions of k_n and determined by requiring that this basis function matches (in value and slope) each plane wave (PW) which is the corresponding basis function of the interstitial region.

In the interstitial region (I) a plane wave expansion is used. Here $k_n = k + G_n$; G_n are the reciprocal lattice vectors, k is the wave vector inside the first Brillouin zone and V is the volume of unit cell.

Therefore, each plane wave is augmented by an atomic-like function in every atomic sphere. The solutions to the Kohn-Sham equations are expanded in this combined basis set of $LAPW's$ according to the linear variation method

$$\phi_k(r) = \sum_n c_n \phi_{k_n}(r) \qquad [2.60]$$

In which the coefficients c_n are determined by the Rayleigh-Ritz variational principle.

For improving the linearization (i.e. to increase the flexibility of the basis) and making possible a consistent treatment of semi-core and valence states in one energy window (to ensure orthogonality) additional (k_n independent) basis functions can be added. They are called "local orbitals (LO)" [**199**] and consist of a linear combination of 2 radial functions at 2 different energies and only one energy derivative (at one of these energies):

$$\phi_{lm}^{LO} = \left[A_{lm} u_l(r, E_{1,l}) + B_{lm} \dot{u}_l(r, E_{1,l}) + C_{lm} u_l(r, E_{2,l})\right] Y_{lm}(\hat{r}) \qquad [2.61]$$

The coefficientsA_{lm}, B_{lm} and C_{lm} are determined by the requirements that ϕ^{LO} should be normalized and has zero value and slope at the sphere boundary.

Another efficient way to linearize the APW method is achieved by the introduction of local orbitals (lo) [**200**]. The basis set of the introduced $APW + lo$ method is also energy independent and still has the same basis size as the original APW method. To allow enough variational flexibility local orbitals are added, which are defined as

$$\phi_{lm}^{LO}(r) = \begin{cases} [A_{lm} u_l(r, E_1) + B_{lm} \dot{u}_l(r, E_1)] Y_{lm}(\hat{r}) & (r \in MT) \\ 0 & (r \in I) \end{cases} \qquad [2.62]$$

This new lo is denoted with lower case to distinguish it from the LO given in (61)

The two coefficients A_{lm} and B_{lm} are determined by normalization and by the condition that the local orbital is zero at the Muffin-Tin boundary. The advantage of the $APW + lo$ method is that it

has a small basis set like the APW method but with the same accuracy compared to the $LAPW$ method.

2.6. Monte Carlo simulation

Monte Carlo simulation is a method that belongs to the atomistic methods which can use empirical or *ab* initio results, together with classical statistical mechanics, to determine thermodynamic and transport properties of systems. In this simulation one attempts to follow the 'time dependence' of a model for which change, or growth, does not proceed in some rigorously predefined way, but rather in a stochastic manner which depends on a sequence of random numbers which is generated during the simulation [**201**] .Monte Carlo methods, which is form the largest and most important class of numerical methods used for solving statistical physics problems in the equilibrium and out-of-equilibrium cases [**202**] . Among the most popular and powerful numerical algorithms, this method based on Metropolis algorithms come in the first top ten algorithms of the 20th century [**118**], [**119**] as listed in Table 2.1. However, the only limitation of this powerful method, as other numerical tools, is related by the computer time and memory.

In the following sections, a brief introduction to the problem of classical statistical physics systems and some properties of phase transitions and the magnetic models is given. . This followed by the basic ideas including, the concept of importance sampling, of Monte Carlo methods is introduced. Finally, the implementation of Monte Carlo methods by the standard local update Metropolis algorithms within Ising model is discussed. This discussion includes also some practical calculations. In fact, this discussion is restricted to the model and algorithm that used in our work.

2.6.1. Introduction

It is well-known that Statistical mechanics is primarily concerned with the calculation of properties of condensed matter systems. It is defined as the branch of physics in which, the microscopic quantities of a physical system can describe correctly the macroscopic phenomena of this system. However, the crucial difficulty associated with these systems is that they are composed of very large number of particles with many different types which makes many

difficult problems when a concrete solution for these interacting systems is sought. In almost all non-trivial cases, analytical methods can only provide approximate answers.

Numerical computer simulations, such as Monte Carlo, are, therefore, an important complementary method on this way to a deeper understanding of complex physical systems such as spin, spin glasses, critical phenomena and order-disorder phase transitions or of biologically motivated problems such as protein folding. Moreover, quantum statistical problems in condensed matter or the broad field of elementary particle physics and quantum gravity are other major cases which, after suitable mappings, also rely on classical simulation techniques [**201**] [**202**] [**203**].

It might be convenient now to remind that, the critical phenomena and magnetic phase transitions field is one the principal subjects of theoretical and experimental physicists of condensed matter [**204**], [**205**], [**206**]. Recently, many efforts have been devoted to study the magnetic properties and phase transitions of magnetic models describing magnetic systems, in connection with elaborating magnetic materials used in technological applications [**207**]. In the absence of exact analytical solutions as results of the mathematical difficulties involved in the theoretical treatment of problems of phase transition, most of these transitions have been interpreted in the context of theories based on some approximations. Therefore, the magnetic properties and phase transitions of such systems have been extensively studied using different techniques including mean-field approximation (MFA) [**205**], [**206**], [**208**], effective-field theory [**209**], finite cluster approximation [**210**], [**211**], renormalization group [**212**], series expansions [**213**] and Monte Carlo simulations [**202**], [**214**]. However, it is no exaggeration to say that Monte Carlo simulations is the most accurate and powerful one among these methods in this field.

On the other side, it should be emphasized that all magnetic systems do not, necessarily, have a phase transition. An existence of a phase transition depends, generally, on very general parameters such as the dimension of the space, the nature of the interaction between the particles and the symmetry of the system. In order to characterize a phase, an order parameter is defined according to the symmetry of the system under study. A good order parameter must be non-zero in one phase, usually above the critical point, and zero elsewhere. In the case of the magnetic system undergoing a phase transition the order parameter is the magnetization [**204**], [**205**], [**206**].

2.6.2. Magnetic Models

Generally, In order to describe and to study a physical system, there are two ways: the first one is to include, as realistically as possible, all the complicated many body interaction and try to obtain a quantitative predication of the behavior by solving Schrödinger's equation numerically. The other way is to write down the simplest possible model that still includes the essential physics and this model can be, hopefully, tractable to analytic or precise numerical solution.

Many magnetic models have been proposed to describe the interactions of the magnetic systems by different Hamiltonians. These models consist, essentially, of two principal elements the lattice and spin model. [**204**], [**206**].

Moreover, it is convenient and conventional to use magnetic language and use the model Hamiltonian in terms of spin variables, although they will turn out to be applicable to many non-magnetic systems.

2.6.1.1. Lattice Models

The lattice model is space where the degrees of freedom live on the sites or/and links of a D-dimensional lattice. For instance, in spins system the spins have to possess some location, or there must be some way, at least, to connect them to each other for deciding which of them interact (usually only nearest neighbor). In fact, this can be done by postulating a regular geometric structure (lattice) consisting of vertices that linked by lines. These lattice are often taken to be simple regular (e.g., honeycomb, square, triangular, cubic) or more complicated regular lattice types (e.g., diamond, body-centered cubic (BCC), face-centered cubic (FCC), hypercubic, etc.) and even random lattices [**203**], [**204**], [**205**], [**206**].

It should be mentioned that, other systems based on the decorated square lattice models have been proposed in the literature [**215**] . A close inspection in such works reveals that the lattices used in these building models appear also in the construction of the root systems of Lie algebras of rank two [**216**], [**217**].

Inspired by the connection between the Lie symmetries and the two dimensional materials with the honeycomb structure, being considered as the most promised research topics in condensed

matter physics, we have proposed a new lattice model based on a double hexagonal structure [**218**],as extension of our works, shown in Figure 2.6 with other $2D$-lattices.

In the regular lattice, each vertex is occupied by a spin which is known as a site. However, in the random lattices not every site has to be occupied by a spin. A line connecting two sites is called a lattice bond.

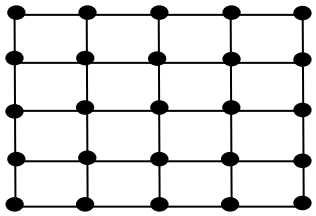

Square Lattice

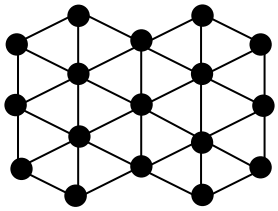

Triangular Lattice

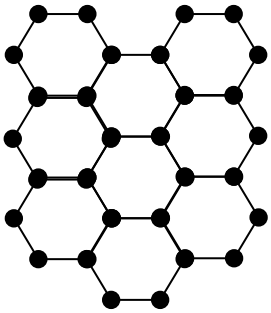

Honeycomb Lattice

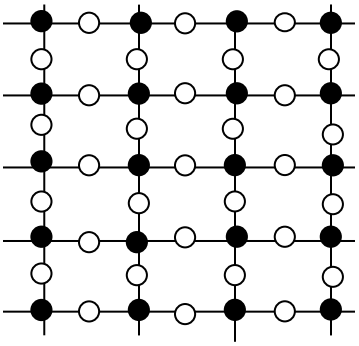

Square decorated lattice

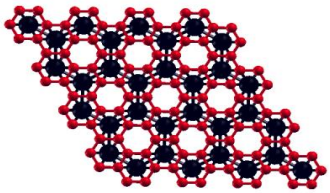

Double hexagonal lattice

Figure 2.6: Different types of $2D$ *lattices.*

Generally, a spin system has a lattice in which all sites are occupied and all lattice bonds are presented as energetic bonds (i.e., the associated bond energy that contributes to the total energy of the spin system). Such a spin lattice is called a pure or non-diluted lattice.

However, there are other cases where not all lattice sites have to be occupied by spins and/or not all lattice bonds are energetic bonds. These two types called a site-diluted lattice and a bond-diluted lattice respectively. It would also be possible to consider both kinds of dilution together.

Furthermore, one of the characteristic properties of the lattice geometry is the number of sites directly linked to a site which is usually the same for all sites. If so, this number is known as the coordination number of the lattice.

The following table, Table 2.2 listed the coordination numbers of different lattice geometries:

D	2	2	2	3	3	3	4
Name	honeycomb	Square	Triangular	Diamond	Cubic	Tetrahedral	Hypercubic
Coordination number	3	4	6	4	6	12	8

Table 2.2**:** The coordination number of some lattices.

Effectively, more complex lattice structures are also studied in statistical physics and they can be found in [**203**], [**204**], [**205**], [**206**], [**219**].

2.6.1.2. Spin Models

Several spin models have been developed which depend essentially on to the degrees of freedom and also on others term of interaction in the Hamiltonian. Spin models may either be classical or quantum mechanical in nature. Precisely, the classical spin models include models with discrete spins such as Ising model [**220**], [**221**] and Potts model [**222**], [**223**] or continuous spins like the two dimensional unit vectors XY model, three dimensional unit vectors of the classical Heisenberg model [**204**], [**206**] and n dimensional unit vectors(n-vector model or O(n) model) [**224**] or arrow configurations along the links of the lattice such as in Baxter's vertex models [**219**]. Here and in what is follows, the Ising model will be only discussed. The first and the simplest spin model was proposed in 1920 by W. Lenz to his student Ising for explaining qualitatively the ferromagnetic- paramagnetic transitions [**220**]. Shortly following, this model has been developed by Ising in 1925 [**221**]. In this model the spins interact according to the following Hamiltonian:

$$\mathcal{H} = -J \sum_{\langle ij \rangle} \sigma_i \sigma_j - h \sum_i \sigma_i \qquad [2.63]$$

Here J is a coupling constant which is positive for a ferromagnetic ($J > 0$), zero for a paramagnetic ($J = 0$) and negative for an anti-ferromagnetic state ($J < 0$), h is an external magnetic field, and the symbol $\langle ij \rangle$indicates that the lattice sum is restricted to run only over all nearest-neighbor pairs with $\sigma_i = \pm 1$. The two-dimensional square lattice Ising model in vanishing field has been solved analytically in 1944 by Onsager [**225**] . However, systems with more than two states higher-spin or with mixed different spins or with a dimensional greater than two have no exact solutions. For these cases, there many approaches that developed to study such systems and determine its magnetic properties such as, the magnetization, susceptibility, specific heat, energy, critical temperature, critical exponents and the phase transitions. Among others, Monte Carlo method provides the most accurate calculations. The basic of this method will be explained briefly in the following sections. A more detailed exposition of the theoretical concepts underlying Monte Carlo algorithm can be found in many textbooks like [**201**], [2], [**203**], [**204**] , [**206**].

2.6.3. The Monte Carlo Method basic concept: Importance Sampling

Generally, The ideal way to calculating the expectation value (Q) of some observable quantity (Q), such as the magnetization in a magnetic model, or the internal energy in a model of a gas, by averaging the quantity of interest over all states of the system in phase space, which is in the canonical ensemble, written as

$$\langle Q \rangle = \sum_{states} Q e^{-\beta \mathcal{H}/\mathrm{Z}} \qquad [2.64]$$

With the summation running over all possible states of the system (the state space may be continuous or discrete). As usual, Z stands for the partition function. $\beta \equiv 1/k_{\mathrm{B}}T$ denotes the inverse temperature fixed by an external heat bath, k_{B} is Boltzmann's constant, H is the Hamiltonian of the system, encoding the details of the interactions which may be short-, medium-, or long-ranged. In general, the degrees of freedom could be continuous or discrete field variables such as a gauge field or the height variable of a crystal surface, continuous or discrete spins.

For an Ising model, with two spin states, on a lattice of N sites the sum is over $2N$ configurations in phase space. This a number which increases very quickly with make the calculation of the

partition function, which is sum a very large number of states, and consequently, the expectation values in (2.64) become very difficult or even more impossible tasks. Unlike, the standard techniques used for the evaluation of integrals, a naive random sampling of the spin configurations $\{\sigma\}$and weighing them appropriately according to (2.64) work out also a very unreliable estimate of the required average. The problem, here, is that the important region in the high-dimensional phase space is relatively narrow and then too seldom hit by random sampling. In fact, only the spin configurations in this relevant region are important in determining the averages .Therefore, it would be useful to restrict the sampling, only, to these important configurations. This solution to the sampling problem is known since long time what so-called the importance sampling [**203**], [**226**].

The mean idea behind the importance sampling is to construct a suitable Markov chain that draws configurations according to their Boltzmann weight as

$$\mathcal{P}^{eq}(\{\sigma_i\}) = \frac{e^{-\beta\mathcal{H}(\{\sigma_i\})}}{\mathrm{Z}} \qquad [2.65]$$

In a Markov chain, stochastic rules are defined for transitions from one state to another under the condition that the probability for the new configuration only depends on the previous state but not on the whole trajectory history in state space, i.e., it is almost local in time. Symbolically this can be given by,

$$\left\{\cdots \xrightarrow{W} \{\sigma_i\} \xrightarrow{W} \{\sigma_i\}' \xrightarrow{W} \{\sigma_i\}'' \xrightarrow{W} \cdots\right\} \qquad [2.66]$$

Here, the transition probability W must satisfy the following conditions:

$$\left\{\begin{array}{l} (i)\ W\left(\{\sigma_i\} \to \{\sigma_i\}'\right) \geq 0\ for\ all\ \{\sigma_i\}, \{\sigma_i\}' \\ (ii)\ \sum_{\{\sigma_i\}'} W(\{\sigma_i\} \to \{\sigma_i\}') = 1\ for\ all\ \{\sigma_i\} \\ (iii)\ \sum_{\{\sigma_i\}} W(\{\sigma_i\} \to \{\sigma_i\}') P^{eq}(\{\sigma_i\}) = P^{eq}(\{\sigma_i\}')\ for\ all\ \{\sigma_i\}' \end{array}\right\} \qquad [2.67]$$

From condition (iii) one can see that the desired Boltzmann distribution P^{eq} is a fixed point of W (i.e. it is an eigenvector of W with unit eigenvalue). A simpler sufficient condition is detailed balance that can be written as,

$$\mathcal{P}^{eq}(\{\sigma_i\})W\ (\{\sigma_i\} \to \{\sigma_i\}') = \mathcal{P}^{eq}(\{\sigma_i\}')W\ (\{\sigma_i\}' \to \{\sigma_i\}) \qquad [2.68]$$

The more general condition (iii) follows, by summing over $\{\sigma_i\}$ in the last equations and using condition (ii). The expectation values can be estimated, after an initial equilibration period, as an arithmetic mean over the Markov chain of length n, for example,

$$E = \langle \mathcal{H} \rangle = \sum_{\{\sigma_i\}} \mathcal{H}(\{\sigma_i\}) p^{eq}\ (\{\sigma_i\}) \approx \frac{1}{n} \sum_{j=i}^{n} \mathcal{H}\big(\{\sigma_i\}_j\big) \qquad [2.69]$$

Here $\{\sigma_i\}_j$ stands for the spin configuration at "time" j.

2.6.4. Metropolis Algorithm

Many different concrete update (or single spin flip) algorithms can satisfy the general Markov chain conditions (i)–(iii). The first and the most flexible update rule is the classic Metropolis algorithm [**227**], which is conceptually much simpler and, as the main merit, quite universally applicable. This algorithm can be applied in practically all cases (discrete/continuous, lattice/off-lattice, short-range/ long-range interactions, etc.) where one can propose an update for a single degree of freedom which is the spin and accepts this proposal with following probability

$$W(\{\sigma_i\}_{old} \to \{\sigma_i\}_{new}) = \begin{cases} 1 & E_{new} < E_{old} \\ e^{-\beta(E_{new} - E_{old})} & E_{new} \geq E_{old} \end{cases} \qquad [70]$$

Here E_{old} and E_{new} stand for the energy of the old and new spin configuration $\{\sigma_i\}_{old}$ and $\{\sigma_i\}_{new}$, respectively, where $\{\sigma_i\}_{new}$ differs locally from $\{\sigma_i\}_{old}$ only by one modified degree of

freedom. With this choice of transition probabilities, the system tends asymptotically (when the Markov chain of states $n \to \infty$) to a steady state in which the probability of a given configuration is $e^{-\beta E\{\sigma\}}$).

To decide whether a proposed update should be accepted or not, if the proposed update lowers the energy, it is always accepted. On the other hand, when the new configuration has a higher energy, the update has still to be accepted with a certain probability. Therefore, one draws a uniformly distributed random number r $[0, 1)$, and if $W \leq r$, the new state is accepted. Otherwise one keeps the old configuration and continues with the next spin.

The practical implementation of the Metropolis algorithm is very simple and it is given as follows,

1- Define a spin-lattice of N sites associated with the lattice size L.
2- Define N variables are: a matrix which takes the values of spin.
3- Apply the periodic boundary conditions.
4- Choose the temperature range and its variation step ΔT.
5- Select the initial Configuration.
6- The initial state at $T + \Delta T$ is the equilibrium state of T.
7- Select a spin, either randomly or sequentially, to be updated. Flip it and calculate the associated change in energy $\Delta E = E_f - E_i$ and its probability W.
8- Select a random number r and accept the update, only, if $\Delta E \leq 0$ or $W \leq r$.
9- If the local update is accepted. The associated changes in energy and magnetization should be computed.
10- Repeat the steps (7-9) until the thermal equilibrium is reached.
11- After the thermal equilibrium, repeat the steps (7-9) n times in order to calculate the measurements and averages.
12- Change the temperature by ΔT and the steps (6-11) until the temperature reaches its extreme.

2.6.5. Measurement

Once the system has reached equilibrium, the most interested quantities should be measured. For the Ising model, the Metropolis algorithm is used to compute the thermodynamic quantities

of interest. Thus, the magnetization, the magnetic susceptibility and the specific heat respectively by:

$$m = \frac{1}{N}\sum_{i=1}^{N} S_i \qquad [2.71]$$

$$\chi = \beta N(\langle m^2\rangle - \langle m\rangle^2) \qquad [2.72]$$

$$C_v = \beta^2(\langle E^2\rangle - \langle E\rangle^2)/N \qquad [2.73]$$

Furthermore, in order to get a good estimation of the critical temperature T_c in our work [**228**] , we use the Metropolis algorithm to compute the Binder cumulant (U) [**229**] for different sizes. This will be used to determine the value of T_c from an indirect way through the curve of the magnetization in terms of the temperature. This quantity is given by:

$$U_4 = 1 - \frac{\langle m^4\rangle}{3\langle m^2\rangle^2} \qquad [2.74]$$

Where N is the total number spin corresponding to the lattice size L.

Finally, it is worth noting that in order to calculate the magnetic properties of real material, the coupling constant J and the other terms, like the magnetic anisotropy Δ, in the Hamiltonian should be determined first either by experimental or theoretical means. In fact, in our works we used the DFT calculations to calculate these terms in the frame of Ising Model with higher-spin than two states [**228**], [**230**] and Heisenberg model [**231**], [**232**]. These calculations can be extend to study magnetic material described by classical Heisenberg model and determine beside its magnetic properties the critical exponents like our work concerning the perovskite $LaMnO_3$ [**231**].

2.6.6. Practical Details and Data Analysis

This section is devoted for highlighting a few remarks on the practical implementation of the Metropolis method and data analysis:

1- Initial Configuration. In principle, the initial configuration should not influence the final configuration. However, the equilibrium may be reached faster if a proper initial configuration is chosen.

2- Select the degrees of freedom. There are several ways for choosing the degrees of freedom to be updated. They may be selected at random or according to a random permutation, which can be updated. However, a simple fixed sequential order is also permissible. In lattice models one might also update first all even and then all odd sites, which is the usual choice in vectorized codes. When the average for all degrees of freedom an update was proposed, a so-called sweep is completed. The quantitative, indeed, performance depends on the choice of the update scheme while qualitative behavior of the update algorithm is not sensitive to these details.

3- Boundary Conditions. Different boundary conditions are used. In periodic boundary conditions the system is periodically repeated in all directions to mimic an infinite system. Alternatively, free boundary conditions use to describe the finite system like Nano-particles. While the semi-finite systems may be described by both boundary conditions like surface, multi-layers system, Nano- wire and Nano-tube.

4- Finite-size effects. Lattices, considered in Monte Carlo simulations, as numerical tools limited by computer memory, must have a finite size (L) whereas the macroscopic properties are usually interested. In order to take the limit of L to ∞, one calculates, usually, an average for several different lattice sizes and then extrapolates the average to infinite L.

5- Random numbers: in Monte Carlo simulations, random numbers are generated by pseudo-random number generators (RNGs), which can produce nearly uniform distributed numbers whose values are very hard or even impossible to predict by using any deterministic rule. The goodness of an RNG is measured by the difficulty to derive the deterministic rule underlying their generation, the absence of correlations and a very long period. It is very important that, an RNG should yield reproducible results for testing

purposes and it should be also portable among different computer platforms. As a recommendation, one should rely only on well-tested and well-documented routines of RNG.

6- Statistical errors. To obtain reliable results, an average must be taken over steps much larger than the number over which the Monte Carlo states are correlated. This becomes more difficult near the critical point because of critical slowing down.

Finally, it has to be mentioned that, there are another two local update (or single spin flip) algorithms, that are also widely used in the present-day, are heat-bath and Glauber algorithms [**233**]. Beside these local update algorithms there is another class of algorithms called non-local update (cluster) algorithms Like wolf [**234**] , Swendsen-Wang [**235**] .Both classes satisfy the general Markov chain conditions (i)–(iii) and each algorithm and class has its disadvantages and advantages.

Physical properties of 2D hexagonal nanostructured materials: A theoretical study

3. Chapter 1: Preliminary view on Single Layer Materials: Models and Methods

3.1. Introduction

Two dimensional materials (2DM) with honeycomb structure have many nice and interesting properties and have been considered as a subject of great interest in lower energy physical models [**1**], [**2**], [**3**], [**4**] [**5**], [**6**], [**236**], [**8**], [**9**] [**10**], [**11**], [**12**] . They become the most promised research topics in condensed matter physics and related areas including high energy physics. A special interest is to investigate the electronic structure of some particular materials composed of atoms appearing in the fourth group of Mendeleev chemistry table [**18**], [**19**]. It has been shown that honeycomb-structured models play crucial role placed in Nano-science. Moreover, it has been suggested that, they could be considered as the most stable material systems used in the semiconductor electronic applications [**5**], [**22**], [**23**].

Many efforts have been devoted to study the physics of such materials using different methods with appropriate approximations. Besides that, some theoretical and analytic developments have been also given supporting the obtained experimental results found in 2DM with success in isolating single layer material. This includes the discovery of the graphene from bulk natural graphite by Novoselov et al [**1**] . The very nice feature of this material is that near the so-called Dirac points the valence and the conduction bands intersect, exhibiting linear energy dispersion [**22**]. This research area has received an intense attention because the graphene behaves like a gapless semiconductor with massless charge carriers. Analytically, the corresponding low energy excitations are described by the Dirac equation dealing with 2 dimensional massless fermions [**23**].

On the other hand, there has been also a great interest in studying the silicene since it involves properties similar to those of the graphene [**5**], [**6**], [**10**]. For this reason, the silicene, which is a monolayer of the silicon atoms forming a 2D honeycomb lattice, can be also viewed as an alternative potential candidate for nanotechnology applications. This material has been synthesized and modeled using different approaches [**78**], [**79**], [**80**], [**81**], [**82**], [**83**], [**84**].

Recently, the electronic properties of two-dimensional hexagonal materials of germanium and numerical calculations on the ground state properties of germanene have been also done using first-principles method [**85**], [**86**], [**87**], [**88**], [**89**]. In particular, it has been found that the buckled germanene is more stable than the planar one involving an electronic structure similar to graphene with linear energy dispersion around the K point [**86**].More recently, the 2D buckled and nearly flat germanene sheets have been, also, fabricated with two different surface substrates [**20**], [**21**].

The main object of this chapter is to provide an examination on the models, and the calculation methods and making contact with the literature

3.2. Computation methods

As mentioned in the introduction, the systems we consider here are described by a single layer of 2D honeycomb structured materials of carbon, silicon and germanium which can be flat or buckled with parameter Δ. The hexagonal crystal structure and the reciprocal lattice with the hexagonal the first Brillouin zone are plotted in (Figure 3.1).

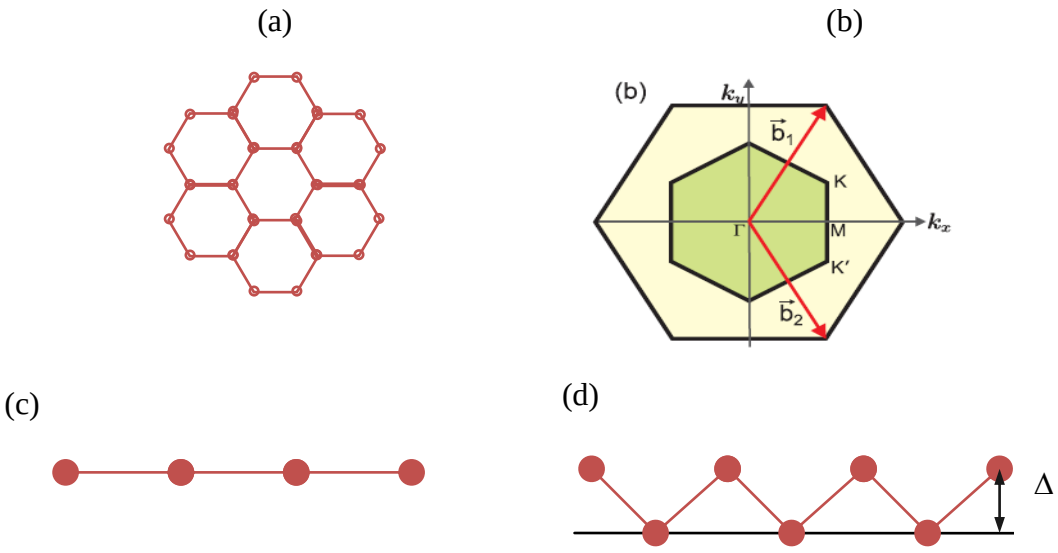

*Figure 3.1: (a) Hexagonal lattice (top view). (b) The reciprocal lattice with the hexagonal first BZ shown in green and the second BZ shown in yellow.(c) Side view of flat geometry. (d) Side view of flat geometry with the parameter*Δ.

Through this study, we have used ab intio calculations based on the all-electron full-potential local-orbital minimum-basis scheme FPLO9.00-34 [**196**], [**197**] . This has been performed to solve the Kohn-Sham equations using the scalar-relativistic scheme. The parameterization of the exchange-correlation energy has been done within the local density Perdew- Wang (PW92) and the generalized gradient approximations Perdew-Burke- Ernzerhof (PBE96) [**147**], [**149**]. To ensure a high accuracy in our performed computations, we have used both self-consistent criteria of the energy and the density together with a precision of 10^{-8} Ha and 10^{-6} respectively. To accurate Brillouin zone integrations we have considered the tetrahedron scheme and the centered 48x48x1 K-point mesh. The valence basis state sets are (1s,2s,2p,3s,3p,3d,), (2s,2p,3s,3p,3d,4s,4p), and (3s, 3p, 3d, 4s, 5s, 4p, 5p, 4d) for the carbon, silicone and the germanium atoms respectively. To avoid the interactions of the monolayer system with their periodic images, a 40 Å is used as a vacuum spacing along z-direction (perpendicular).

3.3. Results and discussions

Before undertaking the calculation corresponding to other effects on the electronic structure, we have first examined the method for a single layer materials and making contact with the literature. For that, we have modeled systems corresponding to a single layer of graphene, silicene and germanene with appropriate approximations. Similar study could be done for all 2DM with hexagonal flat geometries. In order to compute the band structure and density of states, we have first relaxed the planar lattice parameters ($a=b$). In this way, the total energy of the system is computed, using the DFT method, depending on the atoms positions, hence one can minimize the energy functional with respect to the positions. The total energy of two dimensional materials is a function of the lattice parameter 'a' which has been calculated using the force theorem method, as we have mentioned in the computational method, based on FPLO9.00-34 with the LDA and GGA approximations.

For the graphene and the silicene, our results are presented in the (Figure 3.2 (a,b) and Figure 3.3(a,b)) for LDA and GGG approximations respectively**.** Fitting our result with respect to a generic polynomial of the second order, the equilibrium positions corresponding to the minimal energy for each treated case are listed in (Table 3.1). For LDA approximation, the results show

that the lattice equilibrium of the graphene and the silicene correspond to a_{eq}=2.447Å and a_{eq}=3.867Å respectively and a_{eq}=2.469Å and a_{eq}=3.911Å for GGA approximation.

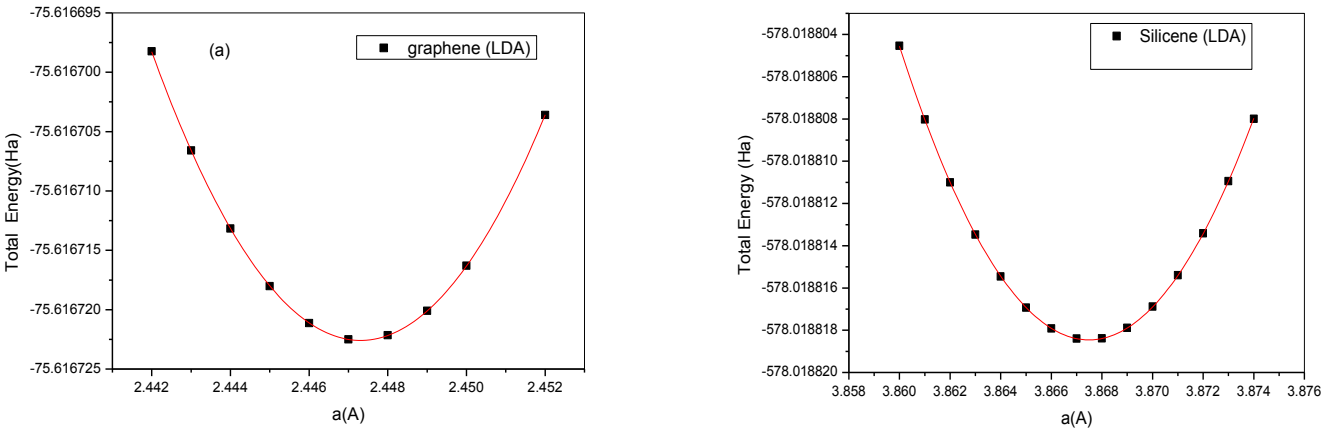

Figure 3.2: (a) Total energy as a function of lattice parameter a for graphene monolayer with LDA approximation. (b) Total energy in terms of lattice parameter a for the case of the silicene monolayer with LDA approximation

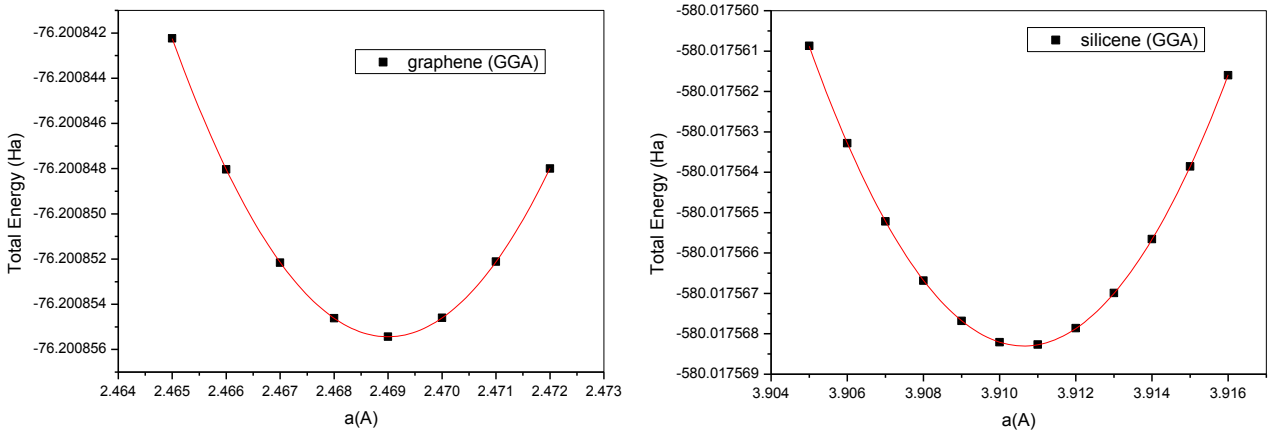

Figure 3.3: (a) Total energy as function of lattice parameter a for graphene monolayer within GGA approximation. (b) Total energy in terms lattice parameter a for the silicene monolayer within GGA approximation.

Approximation	**a_{eq}(Silicene)**	**a_{eq}(Graphene)**
LDA	3.8674Å	2.4473Å
GGA	3.911Å	2.469Å

Table 3.1: Lattice equilibrium positions for the graphene and the silicene corresponding to LDA and GGA approximations.

In the case of the buckled geometries (see Figure 3.1), we have relaxed the planar lattice parameters (a=b) and the parameter Δ controlling the buckled geometries, the results are listed in (Table 3.2). According to all calculations, we found that the buckled geometries of silicon and germanene are most stable than the flat ones. All these obtained values for flat and buckled geometries are comparable to those obtained recently in the literature [**85**], [**86**], [**237**].

	Flat- silicene	Buckled- silicene	Flat- germanene	Buckled- germanene
Δ(Å)	0	0.504	0	0.66
a_{eq}(Å)	3.87	3.82	4.03	3.97

Table 3.2**:** Lattice equilibrium positions of silicene and germanene for flat and buckled monolayers corresponding to LDA approximation

For simplicity reason, we restrict our calculations to LDA approximation. Taking the equilibrium positions obtained from the relaxation method, we have calculated the electronic structure and the band structure for the graphene and the flat silicene and germanene. The results are shown in the (Figure 3.4), (Figure 3.5) and (Figure 3.6). For graphene and silicene systems figures (Figure 3.4) and (Figure 3.5), we find similar results obtained in the literature [**85**], [**86**], [**237**] . In particular, near the so-called Dirac points the system has a linear energy dispersion i.e.

$$E = \pm h v_F k$$

Where k and v_F are momentum and Fermi velocity respectively. Linear dispersion behavior indicates that the charge carriers near Dirac point become like massless fermionic fields

satisfying the relativistic Dirac-like equation. On *K*-points, the usual graphene material is considered as a gapless semi-conductor.

However, for the flat germanene (Figure 3.6), the conduction band and the valence band meet at *K* points which are now situated little higher than the Fermi energy. This result shows that the atomic monolayer of the germanene is a semimetal. This calculation agrees with the result obtained in literature [**85**], [**238**].

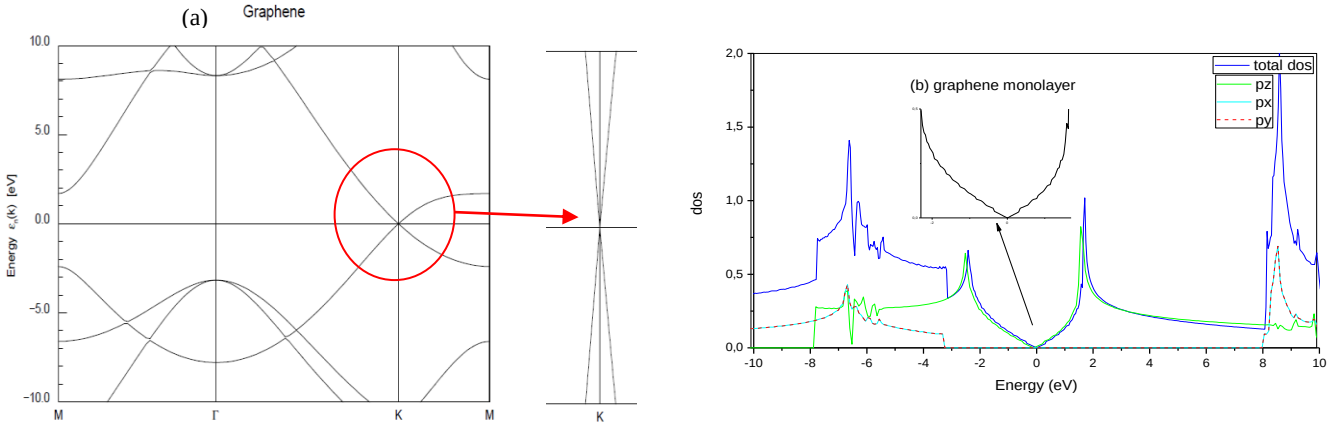

Figure 3.4: (a) Band structure of monolayer of the graphene. (b) Density of states for optimized structures of the graphene associated with electronic orbitals.

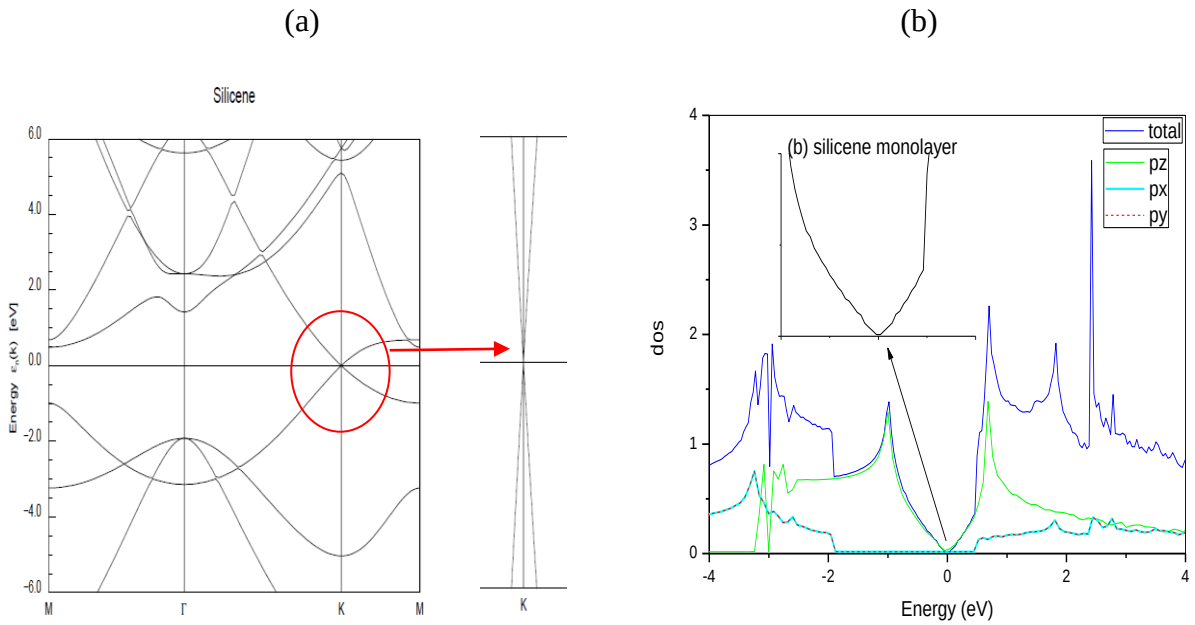

Figure 3.5: (a) Band structure of the silicene. (b) Density of states for optimized structures of the silicene with respect to electronic orbitals.

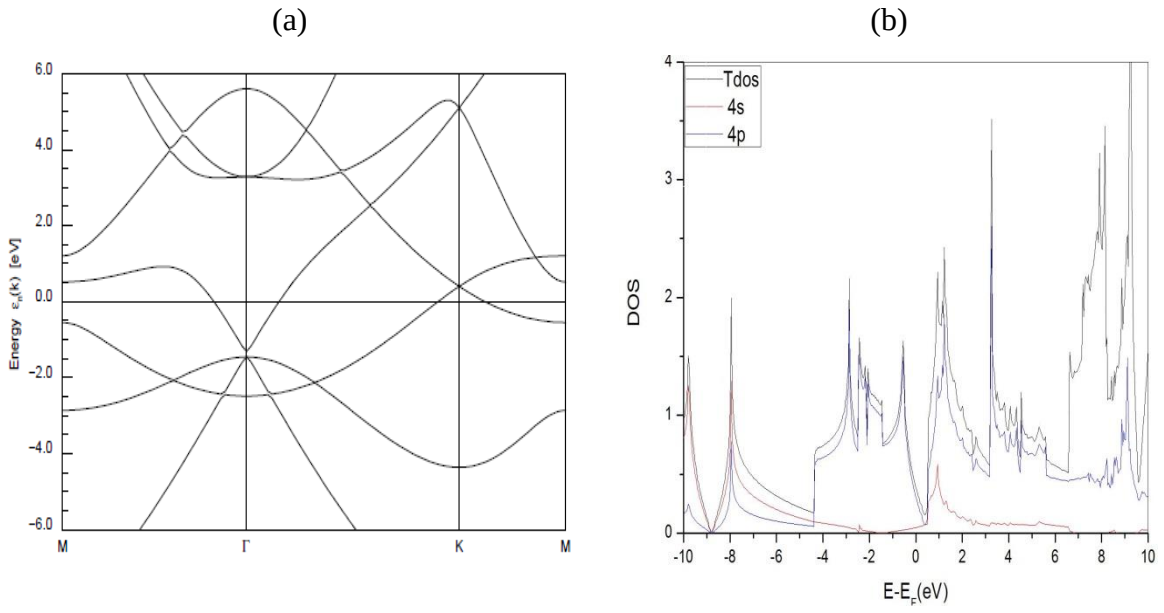

Figure 3.6: (a) Band structure of germanene sheet. (b) Density of states for germanene sheet.

Considering the equilibrium positions for the buckled cases, we have calculated the band structure around K-point for the silicene and germanene. For the buckled geometry, they behave

like graphene. In particular, near the so-called Dirac points each system involves a linear energy dispersion which means a gapless semiconductor with massless charge carriers. The results are shown in the (Figure 3.7(a, b)) and (Figure 3.8 (a, b)) and for planar and buckled geometries respectively showing similar results obtained by other groups [**85**], [**86**], [**237**].

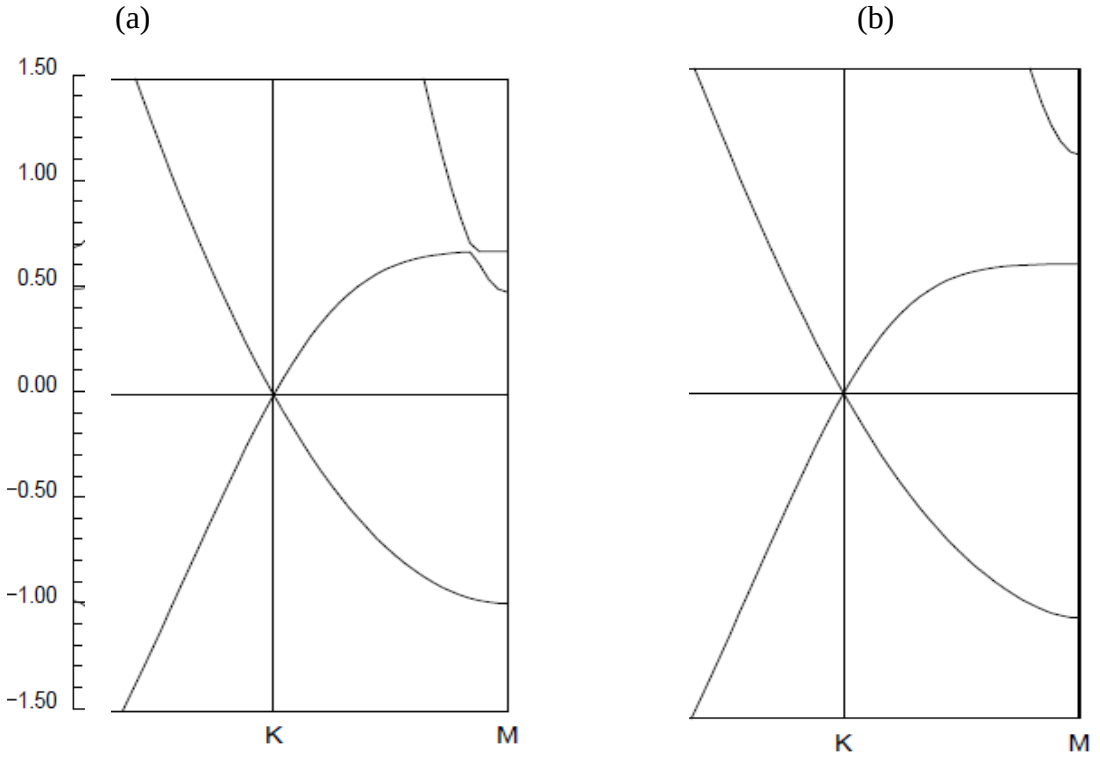

Figure 3.7: Monolayer Band Structure of silicon around K-point: (a) flat geometry and (b) buckled.

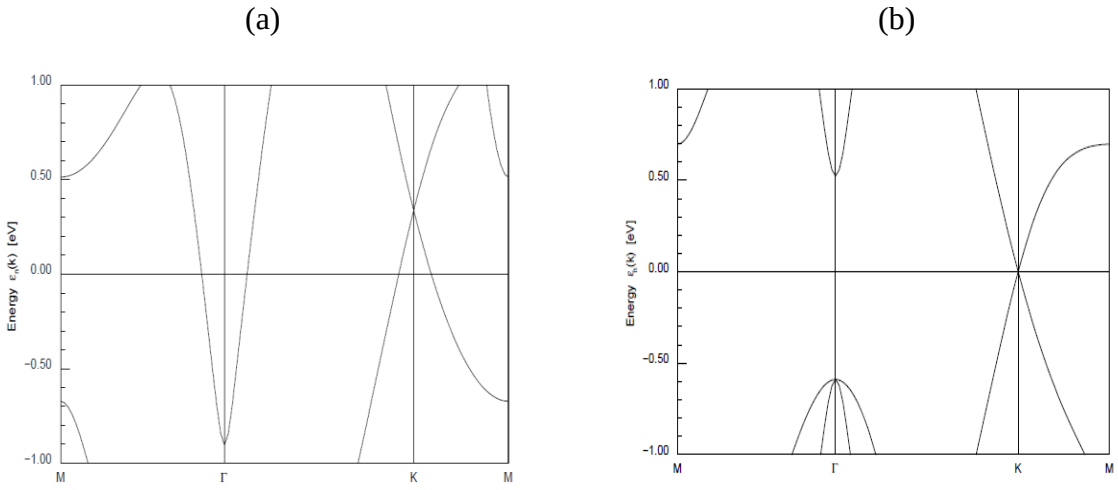

Figure 3.8: Monolayer Band Structure of germanene: (a) flat geometry and (b) buckled

This is a good agreement allowing the validation of our modeling approximations based on FPLO9.00-34 code using the above mentioned parameterizations. Moreover, we observe from these results that, the vanishing of the energy gap is intimately related to the valence p_z orbitals, i.e. $2p_z$, $3p_z$ and $4p_z$ orbitals for graphene, silicene and germanene, respectively, where the electrons move freely. This is due to the fact that such orbitals are not correlated with extra ones.

In order to reduce the high mobility of the electrons living on such orbitals, a new layer moving on the z direction should be introduced to build like bilayer systems. This extra layer may lead to new correlations between the electrons of p_z orbitals placed in the two parallel layers of these materials. At this level one may ask the following question. Do these correlations modify the band structure? This question will be addressed in the following chapter.

3.4. Conclusion

In this chapter we provide an examination on the single layer materials models, and the calculation methods and making contact with the literature. In fact, these models can be flat in all cases or buckled as the case of silicene and germanene only. An examination of the method for these models is very important before undertaking the calculation corresponding to other effects on the electronic structure. For that, we have modeled systems corresponding to a single layer of graphene, silicene and germanene with appropriate approximations using FPLO9.00-34 code. Then, we determine the relaxed lattice parameter and the corresponding density of states and band structures as well. The obtained results show also that, the buckled model is most stable in the case of silicene and germanene. . This calculation agrees with the result obtained in literature. This is a good agreement allowing the validation of our modeling approximations based on FPLO9.00-34 code using the LDA parameterizations

4. Chapter 2: On Distance Variation Effects on Graphene Bilayers

4.1. Introduction

Recently, it has been found that, the systems based on the graphene physics are interesting for the electron-device community see refs. [**24**], [**25**] and references therein. In particular, the systems based on transistors have been extensively investigated and they are considered as an alternative option for the silicon electronic applications. However, in order to use the graphene in semiconductor electronics, such as transistors, the band gap should be opened [**26**] . In this context, the idea of doping a single layer or a bilayer graphene has been explored and it can be considered as a promising topic. In fact, the doping of the graphene could be classified into two categories; the first one is an electrical doping including a gate-controlled doping [**239**], [**240**], [**101**] , metallic cluster-induced doping [**241**], and substrate-induced doping [**242**], [**243**]. The second one is a chemical doping, using chemical routes, such as substitution doping with heteroatom [**244**], [**245**] , or molecular doping [**246**], [**247**], [**248**] . In order to develop further the electronic applications of the graphene materials, the doping procedure provides an appealing way for achieving the band gap engineering [**240**]. It turns out that the graphene bilayer systems have been developed to open small band gap without degrading the electronic properties. They have been synthesized and modeled using different methods and numerical approaches [**101**], [**249**], [**250**], [**251**], [**252**], [**253**], [**254**].

It has been shown that, there are various types of bilayer arrangements; the most symmetric configurations are the direct (AA) and Bernal (AB) stackings which will be reconsidered in the present work. It is recalled that this later configuration appears in the three dimensional geometry, describing the natural graphite [**255**], [**256**] [**257**], [**258**], [**259**], [**260**].

More recently, it has been shown that the rotation produces a new graphene like systems with electronic properties depending on the rotation angles. In particular, this graphene bilayer system can be seen as two decoupled graphene sheets for large rotation angles. However, the small rotated angles lead to interacting system in the (AA) arrangement with non-trivial behaviors including the confined states in p_z orbitals [**261**].

The aim of this chapter is to present our contribution to these activities by considering a new way for discussing the opening of the energy gap using distance variation effects on two

parallel sheets of the graphene placed in various stacking arrangements. The studied system consists of a static graphene single layer interacting with a dynamic one placed at distance *d* along the normal direction *z* in a (AB) stacking arrangement. Using the ab-initio calculations implemented in FPLO9.00-34 code, we first consider the effect of the dynamic layer on the bilayer system by varying the vertical distance *d* starting from a distance around the van der Waals (VdW) bond length. It is shown that the vertical distance variation does not affect the opening of the energy gap and the corresponding bilayers reveal graphene like properties. In particular, the behavior of the band structure at *K* point has been changed from a linear to a parabolic one. It follows that the charge carriers become slightly massive. Moreover, it has been found that such distance variation could be used only to control the lattice size deformation of the studied system.

However, we show that the diagonal distance variation of the graphene bilayers affects the electronic properties that drastically depend on intermediate stacking arrangements between the (AA) and the (AB) configurations. For large vertical distances, we find that the bilayer systems behave like two isolated graphene planes. While, for small vertical distances, the states in the Dirac cones belonging to the two layers interact between them. It has been shown that these interactions lead to the opening of the energy gap of the system.

4.2. Models and method

As mentioned in the introduction, the studied system is based on a static single graphene layer interacting with an extra dynamic one forming a generic arrangement including (AA) and (AB) ones. These arrangements consist of two coupled hexagonal lattices of the graphene, with four carbon atoms in the unit cell, namely A1, B1 on the lower layer and A2, B2 on the upper layer. More precisely, in the AA stacking, all carbon atoms are superposed. In the AB stacking, however, the atoms in the sub-lattice A from the upper layer are faced to those of the lower layer, while, the atoms of the sub-lattice B are faced to the centers of the hexagons of the lower layer. The extra dynamic layer can move either along the vertical or along the horizontal direction. In this way, two models will be considered. The first one corresponds to the vertical displacement controlled by the parameter *d*.

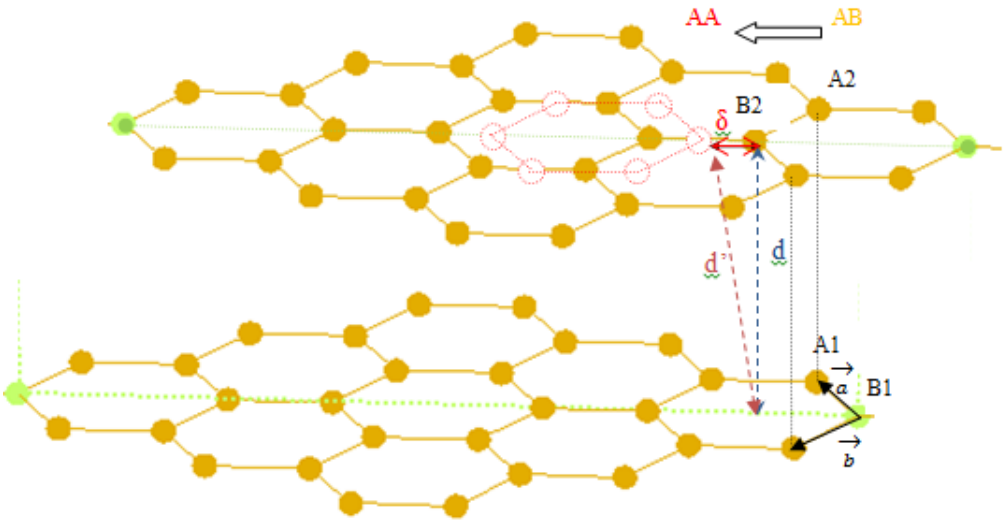

Figure 4.1: Two graphene sheets separated by the distance d along the vertical direction z.

The second model, corresponding to the horizontal motion, is obtained by fixing the vertical distance *d* and pushing horizontally an extra dynamic layer. A priori, there are many possible directions for the horizontal displacement. In this paper, we consider a special direction specified hereafter. The choice of this direction is motivated from the fact that this is the only direction that can produce the (AA) configuration starting from the (AB) geometry, (see Figure 4.1). This operation, which can cover all possible intermediate arrangements between (AB) and (AA) configurations, is controlled by a new parameter δ. A close inspection shows that the displacement of the extra layer follows the planar diagonal direction described by the following algebraic equation:

$$y = x \qquad [4.1]$$

This equation is obtained by considering a basis formed by two vectors a and b of the hexagonal lattice at angle 120 degree. In this way, x and y represent the atomic coordinates such that the atomic coordinates of the upper layer moving according to the above equation will vary with respect to their initial positions in the AB configuration. This can be reached by taking,

$$\Delta x = \Delta y = \frac{1}{2} n \times \delta \qquad [4.2]$$

where δ and n denote the step and the displacement number, respectively.

Inspired from the above equation and the corresponding statement, we will refer to this operation as a diagonal distance variation.

It is worth nothing that this diagonal distance can be related to the vertical distance d by the following relation:

$$\delta = \sqrt{d'^2 - d^2} \qquad [4.3]$$

where, d' can be identified with d in the turning off of the horizontal motion of the extra layer. These distances are illustrated in figure (3.2.1).

In this way, the second model has a two dimensional parameter space. In fact, the calculations will depend on the two parameters d and δ. More precisely, the total energy will be varied as a function of d and δ. The behavior of the energy is described by two dimensional surface. However, to see the effect of the new parameter δ, we consider only one dimensional moduli space obtained by fixing the vertical distance d.

Through this work, we use ab initio calculations based on the all-electron full-potential local-orbital minimum-basis scheme FPLO9.00-34 [**196**], [**197**] . This has been performed to solve the Kohn-Sham equations using the scalar-relativistic scheme. The parameterization of the exchange-correlation energy has been done within the local density approximation (LDA) Perdew- Wang (PW92) [**147**], which can give the equilibrium interlayer distance in the layered compounds better than the generalized gradient approximation (GGA) Perdew-Burke-Ernzerhof(PBE96) [**149**]. Moreover, the LDA seems to be reliable as far as the geometry and the energy differences are concerned [**262**]. Despite the LDA does not describe completely the van der Waals (VdW) interaction between layers in graphite [**263**], the electronic structure calculations obtained respectively by LDA and VdW approximations in the single graphene sheet and the bulk graphite are almost the same [**264**]. This indicates clearly the fact that the weak Van

der Waals interaction is dominated by the covalent one, which determines the shape of the band structure. Based on these results and although the VdW correction is not implemented in FPLO code, our electronic structure calculations based on the LDA could be compared qualitatively with the VdW approximation for the large distances.

To study and compare the different arrangement properties, a high level of numerical accuracy is needed for the developed computations in the present work. To ensure such a high accuracy, we have used both self-consistent criteria of the energy and the density together with precisions of 10^{8}Ha and 10^{-6}, respectively. To perform accurate Brillouin zone integrations; we have considered the tetrahedron scheme and the centered 48x48x1 K-points mesh. The valence basis state sets of the carbon are (1s, 2s, 2p, 3s, 3p, 3d). To avoid the interactions of the bilayer system with their periodic images, a 40 Å is used as a vacuum spacing along z-direction (perpendicular).

The planar parameter lattice "a=b" has been determined for each distance d using the relaxation method for (AB) and for all intermediate stacking arrangements between the (AA) and the (AB) configurations. Each horizontal displacement, in the calculations, equals the tenth of the distance between carbon atoms and the hexagons centers of the lower layer

$$\delta = \frac{2\sqrt{3}}{10}a \qquad [4.4]$$

4.3. Results and discussions

Before studying the effect of the variation of the vertical distance on the energy gap and the total energy of the system, we first recall, from the first chapter that, the observed vanishing of the energy gap is intimately related to pz orbitals where the electrons move freely. This is due to the fact that such orbitals are not correlated with extra ones. In order to reduce the high mobility of the electrons living on pz orbitals, a new layer of graphene is introduced with the varying distance d along the z-direction. This idea is inspired from the fact that the stacking of several layers on top of each other affects the original electronic structure of the materials. This

procedure may lead to new links between the electrons of pz orbitals residing in the two parallel layers of graphene. In particular, it may destroy the linear dispersion of the system.

The aim of the coming parts of this work is devoted to study such effects in (AB) stacking arrangement of the bilayer graphene systems.

4.3.1. Vertical distance variation

To study the effect of the vertical distance on the electronic structure and the total energy, the configuration (AB) corresponding to a vanishing diagonal distance ($\delta = 0$), has been considered. The obtained results of the total energy variation as a function of the vertical distance are shown in the (Figure 4.2). It shows that the total energy minimum associated with the equilibrium distance is $d_{eq}(C) = 3.30$Å. This value is very close to the one found in the bilayer system [**265**], [**266**], [**267**] .

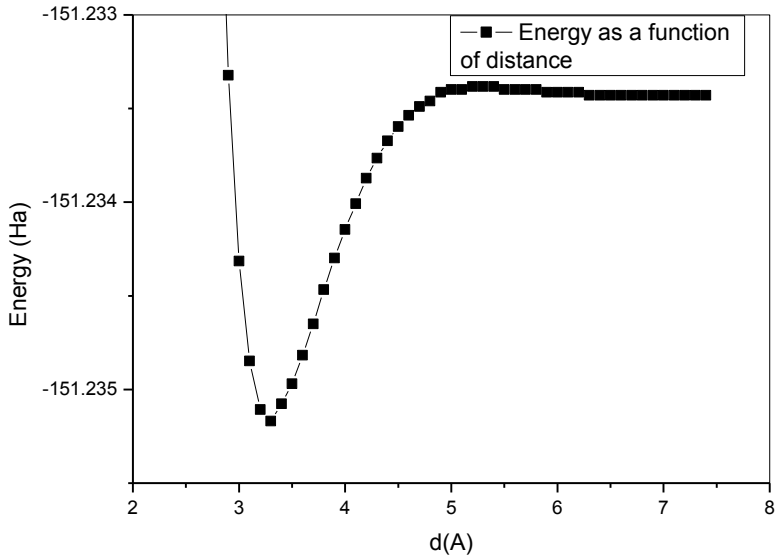

Figure 4.2: Total energy as function of the distance parameter d for AB bilayer system of the graphene with LDA approximation.

The equilibrium position values obtained from relaxation are used in order to calculate the density of states and the band structure which are plotted in (Figure 4.3 (a)). The system involves

also graphene like properties with new behaviors appeared around the Dirac points. Indeed, there are four energy bands, which correspond to the number of atoms in the bilayer system, in which a pair of them meet each other at the point K (the lower energy bands), while the other one (the higher energy bands), has a gap equal to 0.8 eV. This energy gap is associated to the double of the splitting between the lower and higher ones. In fact, the splitting describes the interlayer coupling between the faced atoms. This result is correlated with those obtained experimentally and numerically [**268**], [**269**]. The behavior of the band structure at k point has been converted from a linear to a parabolic one. This shows that the charge carries become slightly massive. These new behaviors are intimately related to the vertical distance variation. To understand that, we analyze the p_z orbital states atoms forming the bilayer-like system. It is recalled that the presence of the p_z orbital states is the responsible for the vanishing of the energy gap in the graphene and in the bilayer with (AB) stacking arrangements as well. A close inspection reveals that in the (AA) arrangement the interactions in p_z orbitals are relevant due to the fact they are faced to each other compared with the (AB) configuration. Besides the new behavior, the existence of the Dirac cone pictures showing zero energy gap is obtained from the p_z orbitals of no faced carbon atoms of the two parallel sheets of the graphene. The opened energy gap at Fermi level is related to the $p_z$orbital of the carbon atoms that are faced to each other. It depends also on the distances between them. These behaviors reach the maximum at 3.8 Å, see (Figure 4.3(b)). This observation drives us to think about an intermediate configuration between the (AA) and (AB) configurations. The study of this intermediate configuration, describing the disorder in the bilayer of the graphene, should be interesting. It may occur during the production of samples and that it can influence quite strongly on the electronic properties. Effectively, such structures have been observed experimentally by STM on graphite surfaces [**27**], [**28**]. It has also been revealed experimentally that the Moiré patterns appear when the graphene plane is the considered cleaved graphite [**29**]. A priory, there are many ways to get such a configuration [**261**]. However, the way we propose here is based on a particular distance variation according to a special direction defined herein below. It turns out that this way allows one to move from (AB) to (AA) as a limit configuration overcoming a symmetric arrangement. This model will be studied in the next subsection.

(a)

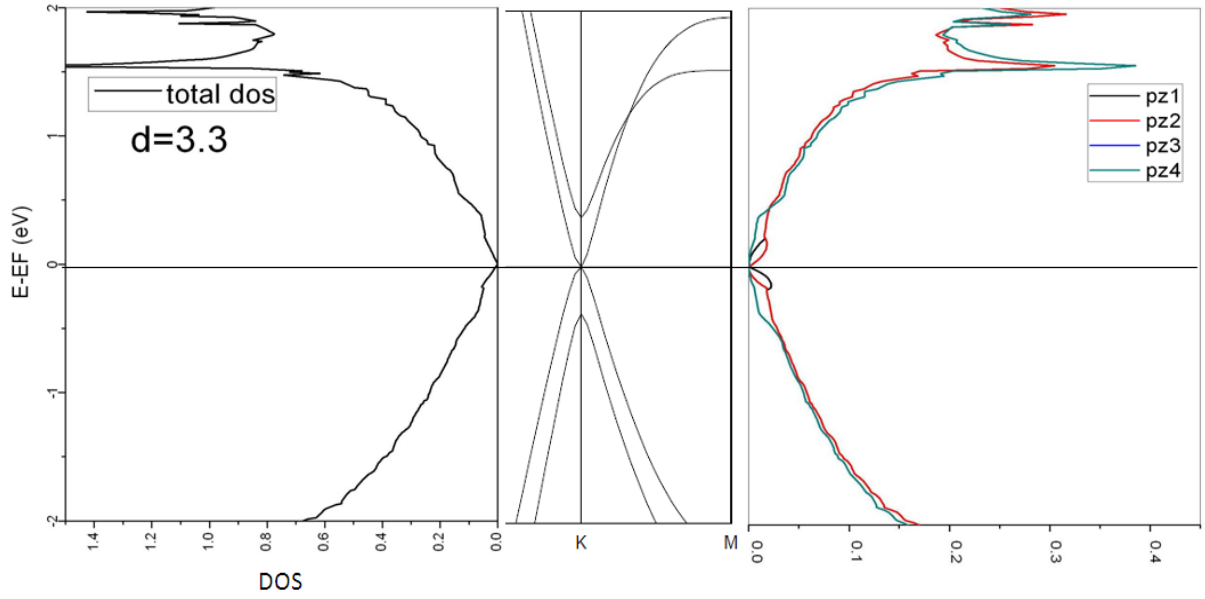

(b)

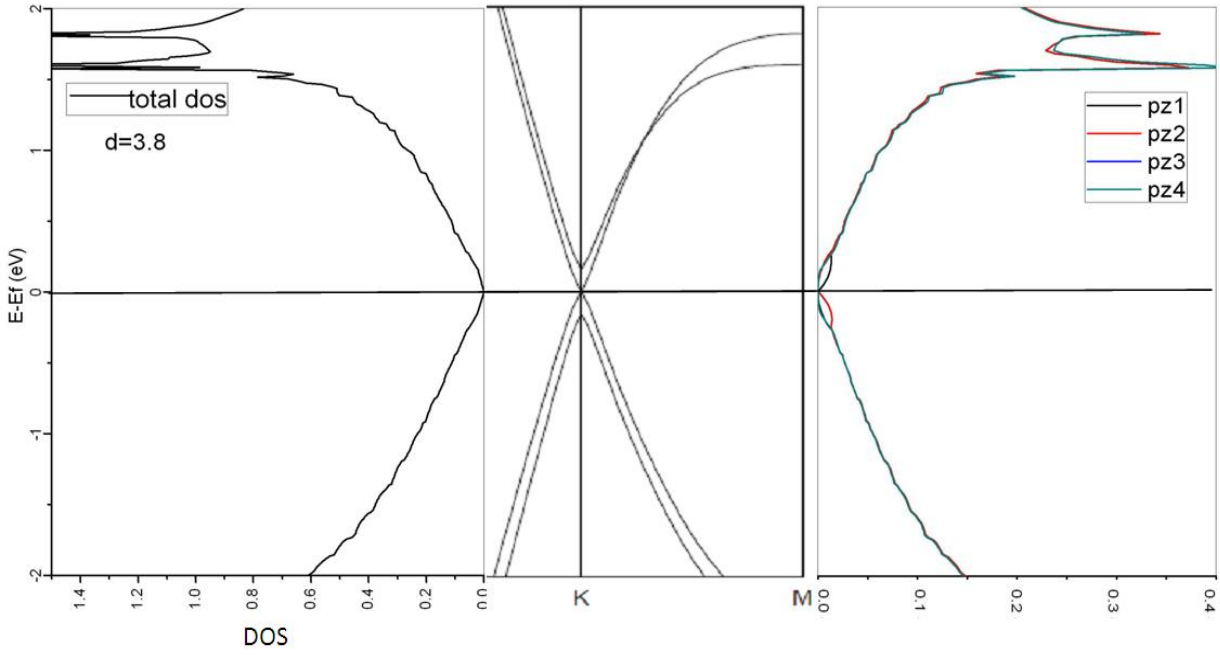

Figure 4.3: For d=3.3 Å and d=3.8 Å distances, (a) and (b) represent respectively the total density, band structure and the local density of pz orbital states of (AB)-bilayer

4.3.2. Diagonal distance variation

To start, we vary the diagonal distance δ with a particular step distance 1/10 between (AB) and (AA) configuration starting from a special vertical distance 3.6 Å corresponding to the equilibrium distance of the (AA) configuration. Then we calculate the total energy and the energy band gap. The results are given in (Figure 4.4 (a,b)). Figure 4.4(a)) shows that the total energy behavior depends on the vertical distance and the diagonal one. More precisely, we have observed two behaviors related to a special distance equal to d =6.9 Å. For vertical distances less than d =6.9 Å, the total energy increases with the diagonal distance δ. However, for distance higher than d =6.9 Å, the diagonal distance variation does not have any effect on the bilayer system. Moreover, at the mid-distance between the (AA) and (AB) configurations, the total energy develops an inflection point where the bridge of the tangent line decreases with the vertical distance d. This bridge vanishes for a particular distance d = 6.9 Å.

All these behaviors can be explained by the total energy difference between the (AB) and the (AA) arrangements. Based on this observation, it is clear that the total energy of the (AB) configuration is always less than the one associated with (AA) configuration which means that the (AB) configuration is the most stable one, while the intermediate ones is less stable than (AB) configurations. Furthermore, this energy difference gives arise an inflection point at the diagonal mid-distance where it involves the interaction competition between the two arrangements. To cheek this feature, the difference between the half total energy of the bilayer (bi) and the monolayer (m) total energy, has been calculated.

$$\Delta E = \frac{1}{2} E_{tot}(bi) - E_{tot}(m) \qquad [4.5]$$

The energy variation calculation shows the existence of a critical distance d_{cr} where the energy difference $\Delta E \approx 0$. It has been observed that this distance is identified with a special distance mentioned above (d = 6.9 Å). It indicates the absence of the interactions between the two parallel layers. For distances less than d_{cr}, ΔE has non null values indicating the appearance of the interactions between two parallel layers.

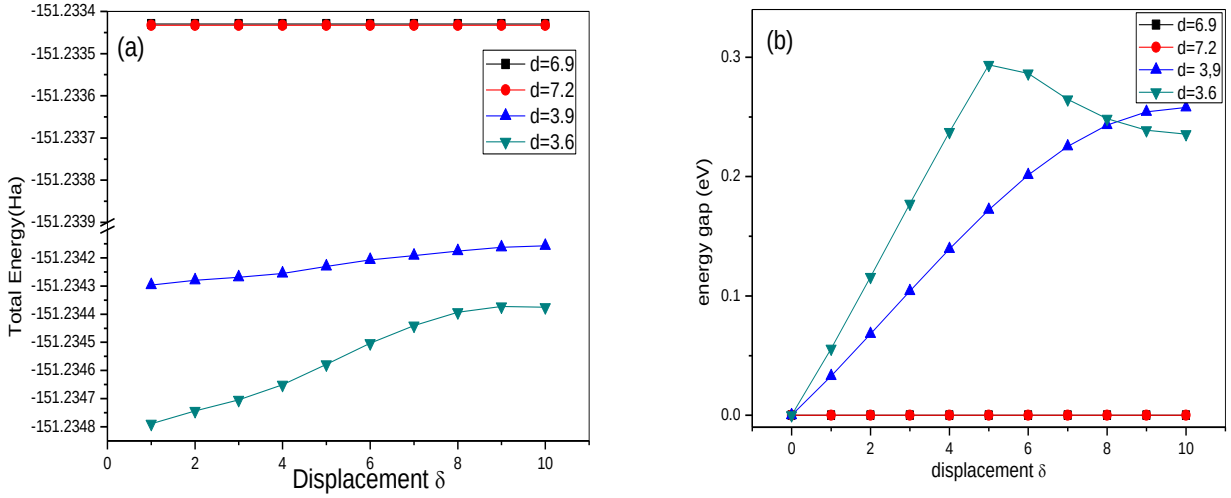

Figure 4.4: a) Total energy as function of the diagonal distance variation. b) The energy gap as function of the diagonal distance.

Using similar techniques, the band gap energy as function of diagonal distances has been calculated. The result is shown in (Figure 4.4 (b)). We note that the band gap energy have three behaviors, depending on the vertical distance. The first one is located between 3.6 Å and 3.9 Å in which the band gap opens for non-vanishing δ displacement. This band gap reaches the maximum in the intermediate configuration. The second one corresponds to the distance between 3.9 Å and the critical distance $d_{\mathrm{cr}} = 6.9A°$. In this region, the band gap increases progressively with δ displacement of the dynamic layer. The last one is associated with distances greater than d_{cr}in which the band gap vanished.

To understand the origin of such behaviors, the density of states and the band structure around k point, have been computed. The results are given in the (Figure 4.5). It shows that the variation of the diagonal distance has an influence on the electrons states living on p_z orbitals in the (AB) arrangement. In particular, when the diagonal distance is augmented, the graphene behavior disappears at K point corresponding to non-faced $p_z$orbitals. This effect leads to an opening energy gap. This is due to the fact that the dynamic layer undergoing a diagonal variation can turn on the p_z orbital interactions of non-faced carbon atoms of the (AB) arrangement.

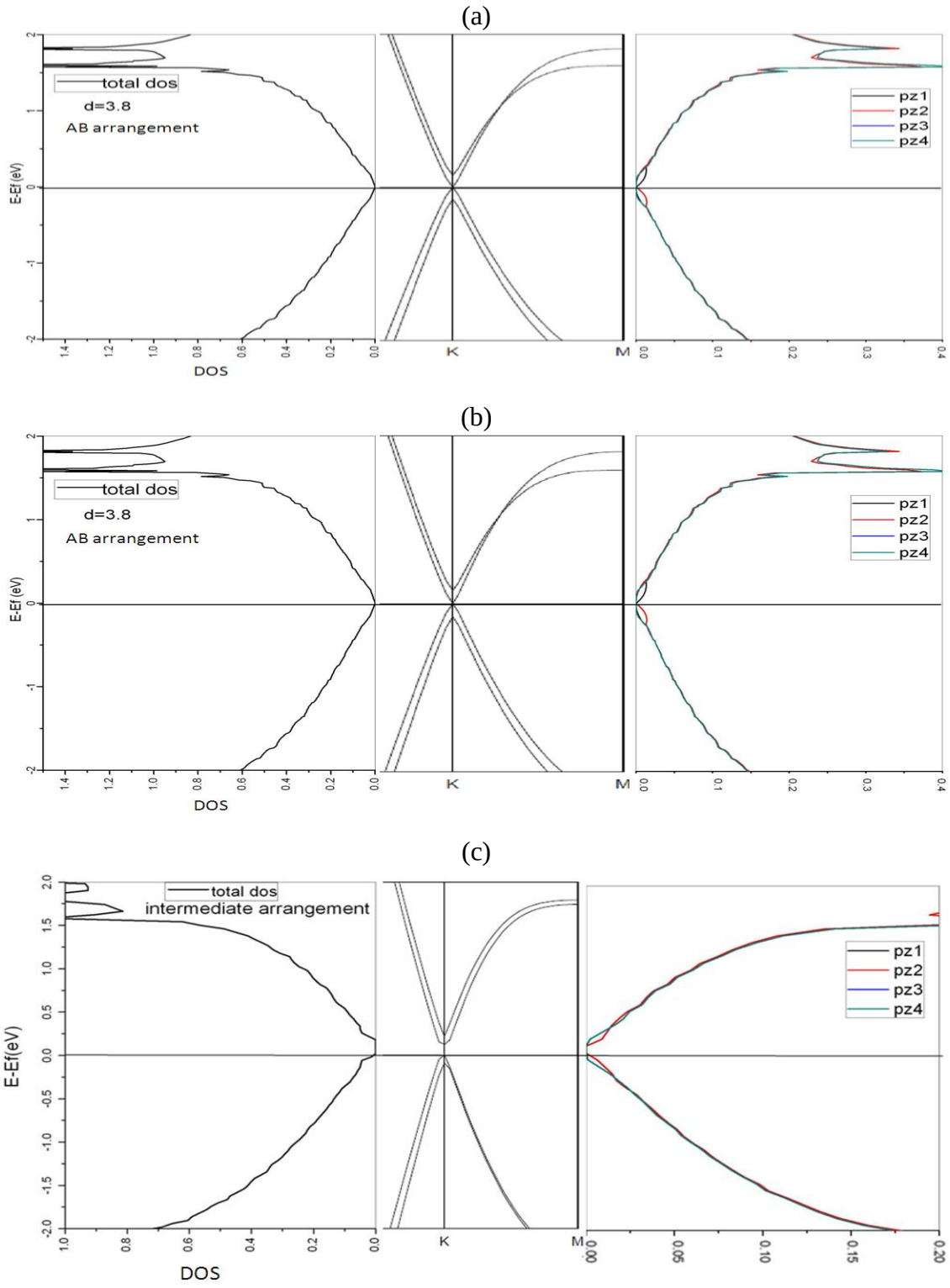

Figure 4.5: Total density, band structure and local density of states p_z for different diagonal distances of graphene bilayer from (AB) to (AA) arrangement at distance d=3.8 Å.

Indeed, the distance of bands at K can be understood by looking at the environment of the B2 atom. Initially, it is not faced to the $B1$ atom. Up to the translation of the upper layer, the B2 atom moves away from the center of the hexagon of the lower layer and the interaction with the atom B1 is growing due to the increasing of the orbital overlap with the displacement. Based on the Tomanek and Louie model presented in [**270**], there is an interaction that tends to separate the bonding and anti-bonding bands at K point. The separation energy of the bonding and the anti-bonding bands also increase to become relevant when we get to the AA configuration. The interaction can be easily seen from the computed total energy of the system see Figure 4.5 (a)) in which the contribution of attractive and repulsive interactions are reflected on the behavior of the band gap energy.

4.4. Conclusion

In this chapter, we have studied the electronic structure of the two parallel sheets of graphene using ab-initio calculations implemented in FPLO9.00-34 code. The studied systems are based on a static single layer interacting with an additional layer placed at distance d along the normal direction z forming with the first one a (AB) stacking arrangement. Indeed, we have first discussed the effect of the dynamic layer on the bilayer system by varying the vertical distance d starting from a distance around the van der Waals bond length. In particular, we have shown that the variation of the vertical distance does not modify the energy gap. In particular, the behavior of the band structure at K point has been changed from a linear to a parabolic one. This means that the charge carries become slightly massive. Moreover, we have found that such a distance variation can be used only to control the lattice size deformation.

However, we have shown that a diagonal distance variation of the graphene bilayer affects the electronic properties that drastically depend on intermediate stacking arrangements between the (AA) and the (AB) configurations. It has been shown that bilayer system behaves like two isolated graphene planes for large vertical distances. For small vertical distances, states in the Dirac cones belonging to the two layers interact between them. These interactions lead to the opening of the energy gap.

5. Chapter 3: Interdistance Effects on Silicene and Germanene Like-bilayers

5.1. Introduction

As we have mentioned the previous chapter, the results of single layer studies of 2DM with honeycomb structure have been extended to multi-layers systems. Special emphasis is put on bilayer like systems relying on inter-interactions between two parallel layers [**265**] . In such systems, the electronic and transport properties can be modified radically according to layer stacking arrangements [**257**]. It turns out that there are various types of layer arrangements where the most symmetric configurations are the direct (AA) and Bernal (AB) stacking. The latter appears in three dimensional geometries describing the graphite natural configurations, which have received quite important deeper studies [**271**]. However, the (AA) stacking arrangement has been also synthesized and observed in few layer configurations including the bilayer hexagonal systems [**258**], [**259**], [**260**], [**101**].

More recently, many efforts have been devoted to the study of the opening energy gaps in both single and multilayers of 2D honeycomb-structured materials using different approaches. In particular**,** methods based on exciton interactions [**272**], the application of the magnetic field [**22**] [**23**], and curved geometries [**22**] have been well developed using various numerical calculation codes [**273**], [**274**], [**275**]. More precisely, the opening of the band gap in the graphene and the silicene has been investigated using first principle calculations by the help of quantum chemistry methods. In this context, the low-bucked structure in the silicene has been studied by turning on spin orbit interactions in the quantum spin Hall effect physics [**276**], [**277**], [**83**]. It is worth noting that experiments have also shown, recently, that the band gap can be opened up in a bilayer system by applying an electric field [**278**].

On other hand, opening of the energy band in both single and bilayers of graphene and silicene has been discussed using different approaches and simulation technical ways. In pervious works [**279**], [**280**], we have reported our first-principles study on graphene and silicene using *ab* intio calculations based on the all-electron full-potential local-orbital minimum-basis scheme FPLO9.00-34 for both the direct (AA) and Bernal (AB) stacking arrangements. It has been shown that the opening of energy gap depends on the inter-distance between two parallel layers and the

stacking configurations. However, bilayers of germanene remain an open issue and deserve to be studied.

It is recalled that the vanishing of the energy gap is intimately related to p_z orbitals where the electrons can move freely. This is due to the fact that such orbitals are not interacting with extra ones. In order to reduce the high mobility of the electrons living on such orbitals, a new layer moving on the z direction should be introduced to build like bilayer systems. This extra layer may lead to new correlations between the electrons of p_z orbitals placed in the two parallel layers of the silicene. At this level one may ask the following question. Do these correlations modify the band structure? This question will be addressed in the following subsection.

In this chapter, we use Ab-initio calculations to discuss the band gap energy variation based on the effect of the inter-distance between two parallel layers of silicene or germanium separated by distance *d*. In particular, we consider a dynamic monolayer of the silicone located at distance *d* along the normal direction *z* forming with a static one a (AA) stacking arrangement. The present work can be considered as an extension to our preliminary works on graphene. Here, we treat the planar and buckled geometries in (AA) arrangements, see figure 1. These buckled geometries involve two kinds of the configurations. The first one is associated with the usual (AA) configuration that keeps the same vertical distance between the two layers atoms, while the remaining one is obtained by reversing one the layer of the silicene. For both configurations, the starting distance is taking around the Van der Waals length. We show that the band gap can be opened by simply varying the distance, starting from a distance around the bond length of Van der Waals, between two parallel silicene for flat and buckled configurations. However, such behaviors have been not found in flat germanene geometry .Furthermore, we study the stability between the buckled and the flat configuration in the bilayer systems.

5.2. Building models and method

Before presenting the computation method, we first build the model. In fact, the systems we consider here are described by a static single layer of the silicone or germanium interacting with an extra dynamic layer. The latter is located at a distance *d* along the normal direction z forming with the first one a (AA) stacking arrangement as plotted in (Figure 5.1).The main object of this

work is to see the effect of this extra layer of silicone or germanium by varying the distance d starting from a distance around the van der Waals bond length. Here, we have performed *ab* intio calculations based on the all-electron full-potential local-orbital minimum-basis scheme FPLO9.00-34 [**196**], [**197**]. This has been used to solve the Kohn-Sham equations using the scalar-relativistic scheme. The parameterization of the exchange-correlation energy has been done within the local density approximation (PW92) [**147**]. This choice of approximation is motivated in the previous chapter. To ensure a high accuracy in the performed computations, we have used both self-consistent criterions of the energy and the density together with a precision of 10^{-8}Ha and 10^{-6} respectively. To accurate the Brillouin zone integrations, we have used the tetrahedron scheme and the centered 48x48x1 K-point mesh. The valence basis state sets for silicone and germanium are $(2s, 2p, 3s, 3p, 3d, 4s, 4p)$ and $(3s, 3p, 3d, 4s, 5s, 4p, 5p, 4d)$, respectively.

The lattice equilibrium parameters "$a = b$" and the buckled parameter Δ has been determined from the relaxation method in the previous chapter.

5.3. Results and discussions

In this section, we discuss the distance variation effect on silicene and germanene like-bilayers with various geometries. For each material, we start, firstly, with the flat case, and then we move to investigate the buckled geometries. A comparative between the studied geometries will be given and discussed.

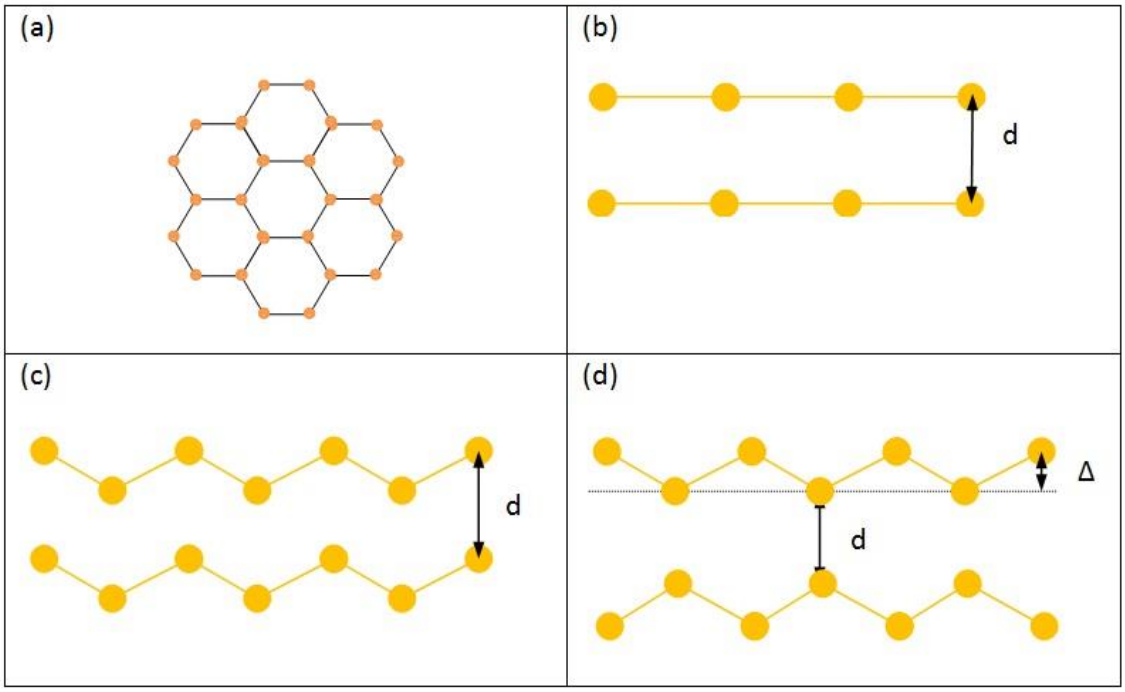

Figure 5.1: (a) hexagonal structure of silicene and germanene. (b) Two parallel flat separated by distance d (c) buckled AA1 (d) buckled AA2 geometry.

5.3.1. Bilayers of silicene

In this subsection, we study the inter-effect of two layers system by changing the distance *d* between two parallel layers for planar and buckled geometries with the (AA) arrangement. For the buckled geometry, we distinguish two sorts of configurations. The first one corresponds to the usual (AA) configuration that keeps the same vertical distance between bilayer atoms, while the second one is obtained by reversing one buckled layer of the silicene. In the usual (AA) geometry, the buckled Si atoms of the top layer are faced with the buckled atoms living in the bottom layer (referred AA1). While in the reversed one, the buckled Si atoms of the top layer are faced to flat atoms of the bottom layers (referred AA2).

Varying the distance *d*, we have calculated the total energy in both configurations. These results are plotted in Figure 5.2 left (a,b and c)) for buckled AA1, AA2 and flat geometries respectively. From these figures, we have found the equilibrium distance positions corresponding to the minimal energy for flat and two buckled geometries. The obtained results are listed in the (Table 5.1). From this table, we observe that we have two minima energies for flat geometry at

the inter layers distances 4.2 Å and 2.4 Å which correspond to the Van der Waals and covalent bond length respectively. However, it is shown clearly that, among these two minima the most stable minimum is related to the covalent distance 2.4 Å which is in a good agreement with the value reported in [**281**] .It follows that the minimal energy corresponding the minimal distance for two buckled geometries is less than the one associated with flat configuration. More precisely, the calculation indicates that the first buckled geometry is the most stable one. Now, we move to study the distance variation effect on the behavior of the opened energy gap and the electronic structure for the three possible configurations mentioned before. As we mentioned above, we can distinguish two zones that are related to the inter layer distance for the Van der Waals and covalent bond length. In fact, we focus, essentially, on the distance variation effect starting from the Van der Waals bond length. This choice is motivated from the fact that this bond is the weak one appearing in the two separated two layers system.

geometries	Equilibrium distance (Å)		Energy (Ha)	
Buckled AA1	d_{min} =2.62		E_{min} =-1156.06276	
Buckled AA2	d_{min} =3		E_{min} =-1156.06249	
Flat	d_{min1} = 2.4	d_{min} = 4.2	E_{min1}= -1156.06155	E_{min2} =-1156.04003

Table 5.1: Equilibrium distance positions corresponding to the minimal energy for each configuration.

The present calculations show that the band energy gap can be opened up due to the influence of the variation of the distance *d* for the flat and buckled geometries. This result, which has been obtained from the distance corresponding to a maximal gap, is shown in Figure 5.2 right (a,b and c)).

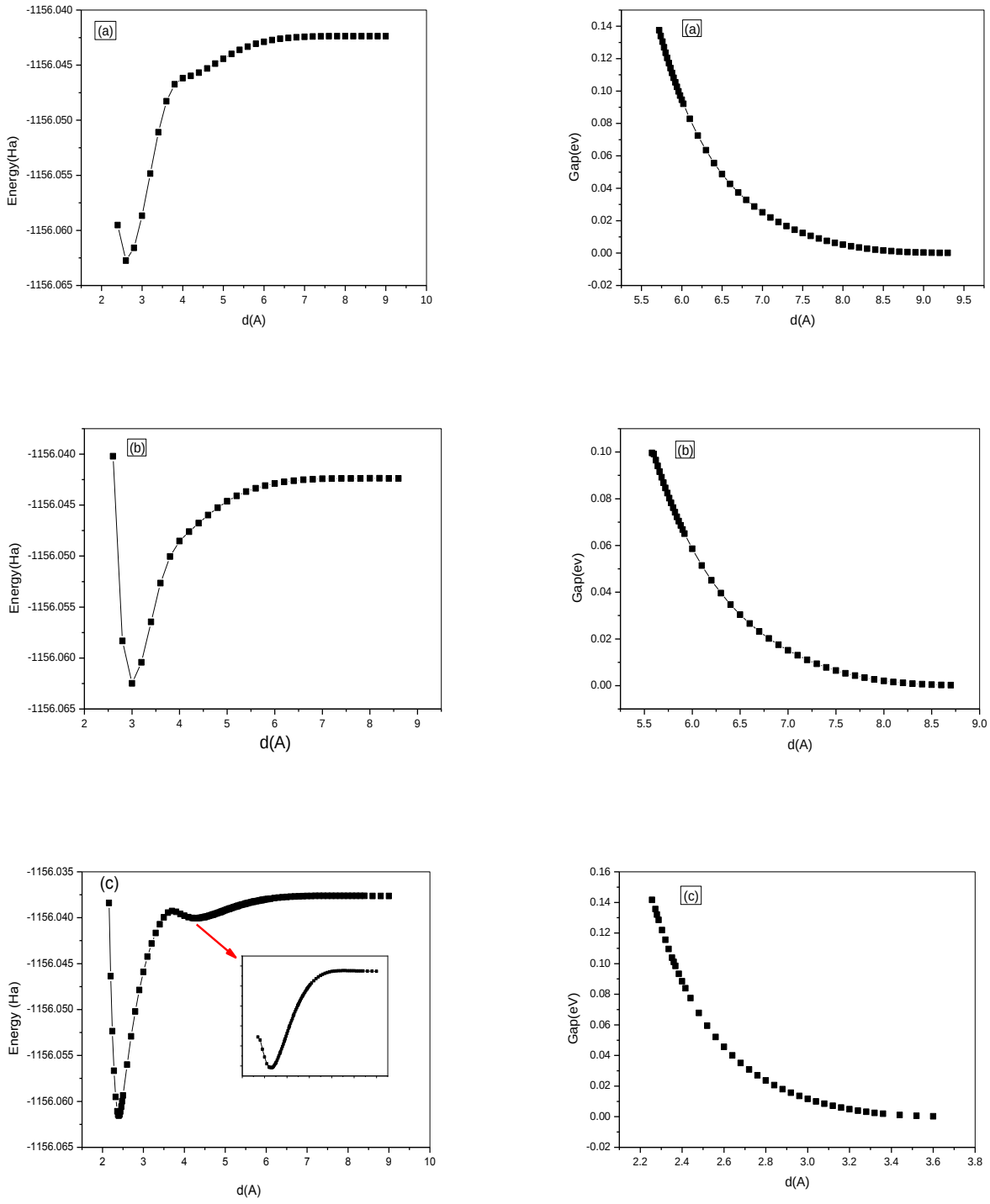

Figure 5.2: Total energy (left) and band gap energy (right) as function of distance d: (a) AA1 geometry, (b) AA2 geometry and (c) Flat geometry.

In particular, we see that the bad gap varies exponentially with the distance *d*. It has been also observed that the obtained values of the band energy of AA1 and flat geometries are bigger than the ones obtained in the case of the AA2 geometry. This difference of the energy gap values between the two configurations is due the interaction between two the silicene layers. This can be understood in terms of the distance between two opposite atoms, of the two layers, in both configurations. Indeed, for the AA1 configuration, the opposite atoms have the same distance allowing the maximum gap simultaneously. However, for theAA2 configuration, the opposite atoms do not have the same distance so the system cannot reach the maximum gap at the same distance.

To understand the origin of such an opening energy gap variation, we have calculated the band structure around K-point at the maximal gap distance for each geometry. The corresponding results are depicted in the Figure 5.3 (a,b and c)) for flat AA, buckled AA1 and AA2 respectively.

The distance variation shifts the p_z orbital states to the valence band for small distance. For large distances, however, the system behaves like single layer of the silicene. It has been seen that the p_x and p_y orbitals are not changed. It is known that the electrons located at the valence band contribute to the local cohesion between neighboring atoms and they form localized states. Based on this observation, the variation of the distance has an influence on states of the p_z orbital electrons. Taking small values of *d*, the p_z states get stable situations forming a consistent bilayer system. This can be supported from the computed total energy depending on the distance *d*.

This stabilization can be understood in terms of an electronic structure transition in p_z orbitals. It is a transition from delocalized to localized states allowing the opening of the energy gap. One possible explanation of this behavior can be given in terms of the coupling interaction between two parallel material planes caused by varying the inter-bilayer distance.

In the end of this work, we would like to make contact with many works dealing with the graphene like bilayers. Concerning the opening of energy gap, the buckled silicene like –bilayers share similar behaviors appearing in the case of the graphene only for the distance greater than Van der Waals bond length. The results obtained in this work may support the buckled silicene to be a potential candidate for the Nano science applications.

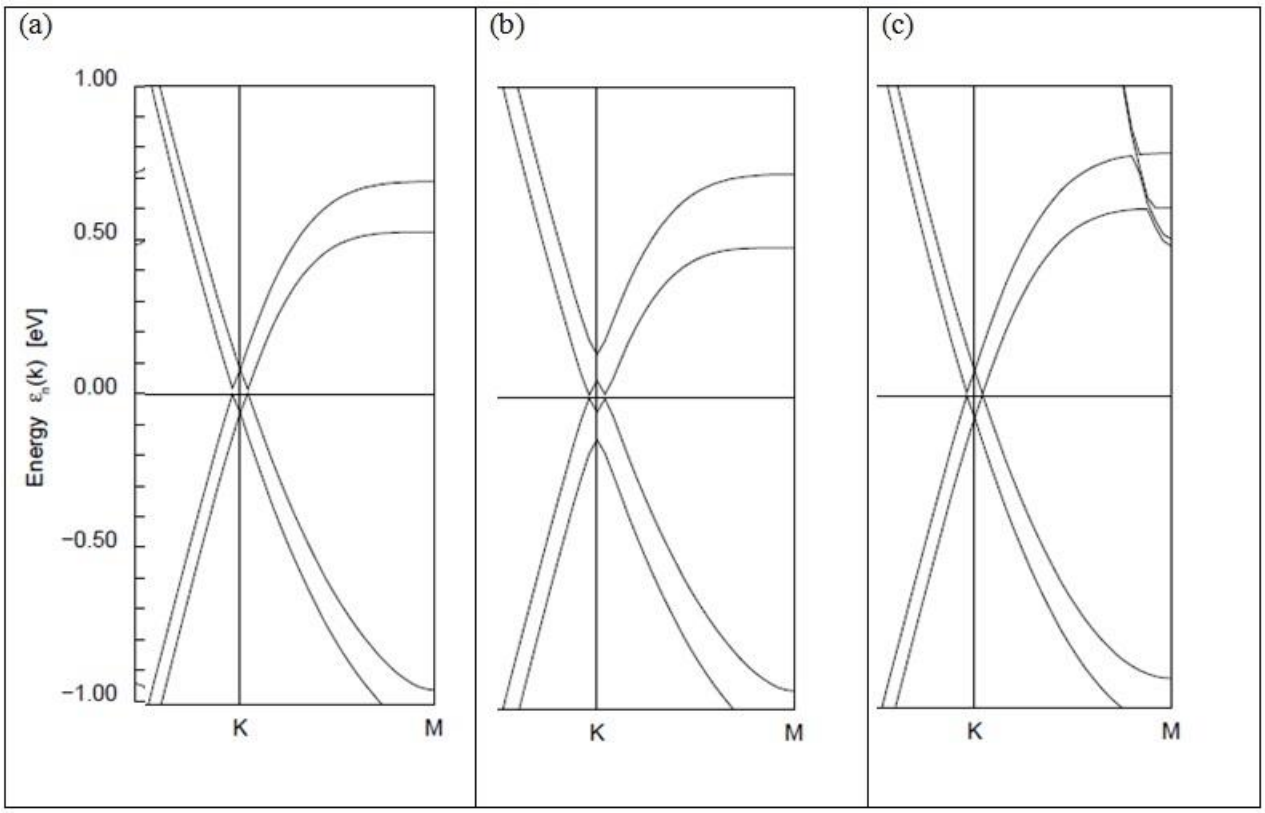

Figure 5.3: Bilayer Band Structure of silicon around K-point: (a) for AA1 geometry, (b) AA2 geometry and (c) Flat geometry associated with the maximal gap.

5.3.2. Bilayers of germanene

In this subsection, we study the effect of inter-bilayer interaction by changing the distance *d* between two parallel layers for planar and buckled geometries with the (AA) arrangement. For buckled geometry, we distinguish two sorts of configurations. The first one corresponds to the usual (AA) configuration that keeps the same vertical distance between two layer atoms, while the second one is obtained by reversing one buckled layer of germanene. In the usual (AA) geometry, the buckled Ge atoms of the top layer are faced with buckled atoms living in the bottom layer (referred AA1). While in the reversed one, the buckled Ge atoms of the top layer are faced to flat atoms of the bottom layers (referred AA2).

(a)

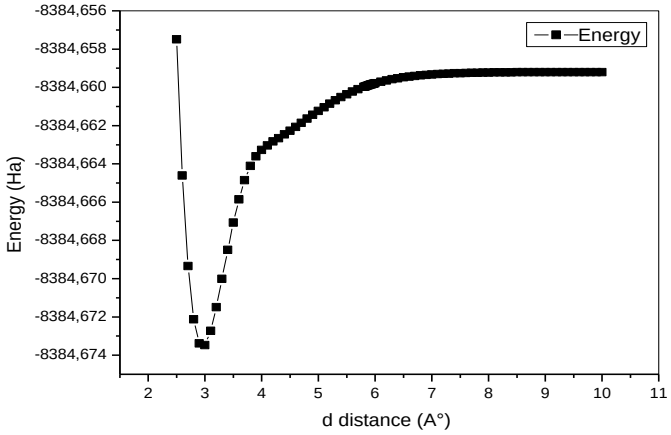

(b) (c)

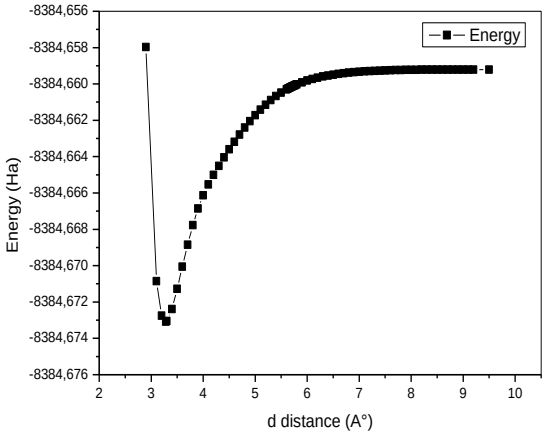

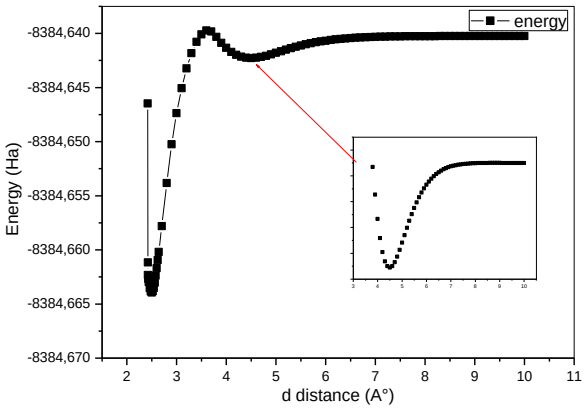

Figure 5.4:: Energy as function of distance d: (a) AA1 geometry, (b) AA2 geometry and (c) Flat geometry.

Varying the distance *d*, we have calculated the total energy in both configurations. These results are plotted in Figure 5.4 (a, b and c)) for buckled AA1, AA2 and flat geometries respectively. From these figures, we have found the equilibrium distance positions corresponding to the minimal energy for flat and two buckled geometries. Our results are presented in the Table 5.2. From this table, we observe that we have two minima energies for flat geometry for the distances 4.5 Å and 2.5 Å that correspond to the Van der Waals and covalent bond length respectively. In fact, it is shown clearly that, among these two minima the most stable minimum

is related to the covalent distance 2.5 Å while the meta stable one is associated with Van der Waals distance 4.5 Å which is very close with the value reported in [**282**] It follows that the minimal energy corresponding the minimal distance for two buckled geometries is less than the one associated with flat configuration. More precisely, the calculation indicates that the first buckled geometry is the most stable one.

geometries	Equilibrium distance (Å)		Energy (Ha)	
Buckled AA1	d_{min} =3.0		E_{min} =-8384.67347	
Buckled AA2	d_{min} =3.28		E_{min} =-8384.67308	
Flat	d_{min1} = 2.5	d_{min2}= 4.5	E_{min1}= -8384.66395	E_{min2} =-8384.64227

Table 5.2: Equilibrium distance positions corresponding to the minimal energy for each configuration.

Now we move to study the distance variation effect on the behavior of the opened energy gap and the electronic structure for the three possible configurations mentioned before.

It is recalled that, we can distinguish two zones that are related to the inter layer distance for the Van der Waals and covalent bond length. In fact, we focus, essentially, on the distance variation effect starting from the Van der Waals bond length. This choice is motivated from the fact that this bond is the weak one appearing in the two separated two layers system.

Our calculations show that the distance variation does not affect the band energy gap of flat configuration keeping the same behaviors arising in monolayer case. However, for buckled geometries we observe that the band energy gap can be opened up due to the influence of the variation of the distance *d*. This result, which has been obtained from distance corresponding to maximal gap, is shown in Figure 5.5 (a, b)). In particular, we see that the band gap varies exponentially with the distance *d* for both buckled configurations. It has been also observed that the obtained values of band energy of AA1 are bigger than the one obtained for AA2. Such a difference of the energy gap values between the two configurations is due the interaction between two germanene layers. This can be understood in terms of the distance between two opposite atoms, of the two layers, in both configurations. Indeed, for AA1 configuration, the opposite atoms have the same distance allowing the maximum gap simultaneously. However, for AA2

configuration, the opposite atoms do not have the same distance so the system cannot reach the maximum gap at the same distance.

(a) (b)

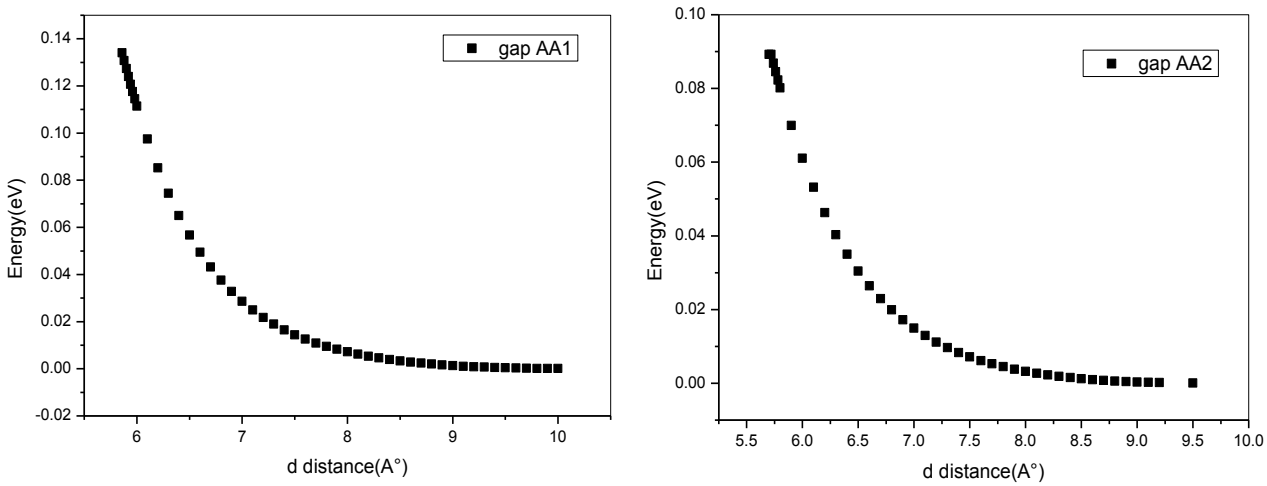

Figure 5.5: band gap energy as function of distance: (a) for AA1 geometry and (b) AA2 geometry.

To understand the origin of such an opening energy gap variation, we have calculated the density of states. The corresponding results are depicted in the Figure 5.6 (a, b, c, d, e, f)) and Figure 5.7 (a, b, c, d, e, f)) for buckled AA1 and AA2, respectively.

The distance variation shifts the p_z orbital states to the valence band for small distance. However, for large distance the system behaves like one sheet of germanene. It has been seen that the p_x and p_y orbitals are not changed. It is known that the electrons located at the valence band contribute to the local cohesion between neighboring atoms and they form localized states. Based on this observation, the variation of the distance has an influence on states of the p_z orbital electrons. Taking small values of *d*, the p_z states get stable situations forming a consistent bilayer system. This can be supported from the computed total energy depending on the distance *d*.

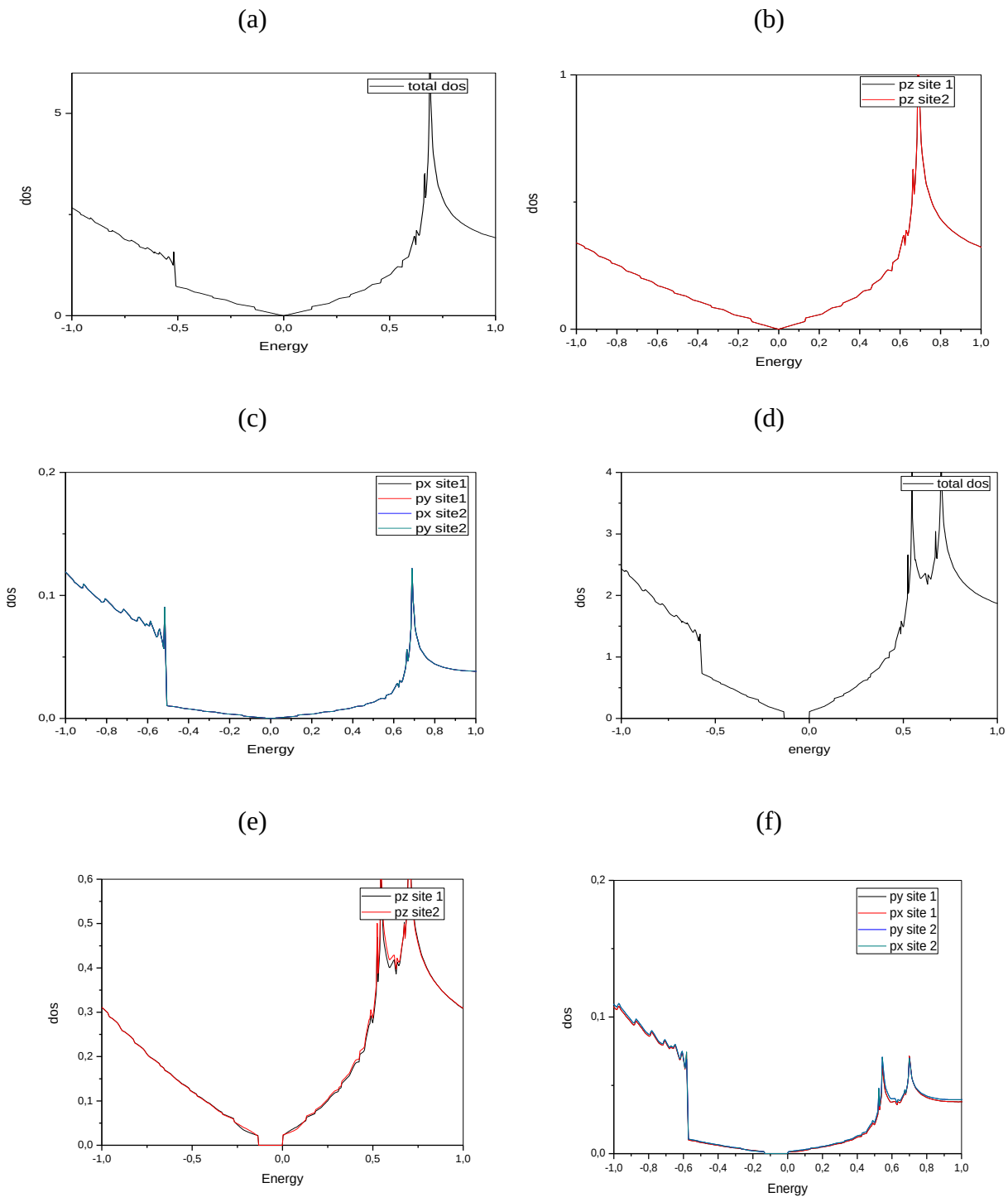

Figure 5.6: Total and partial electronic structure of AA1: (a, b, c) for distance far away from d=9 Å and (d ,e, f) correspond to the distance d=5.86 Å associated with the maximal gap.

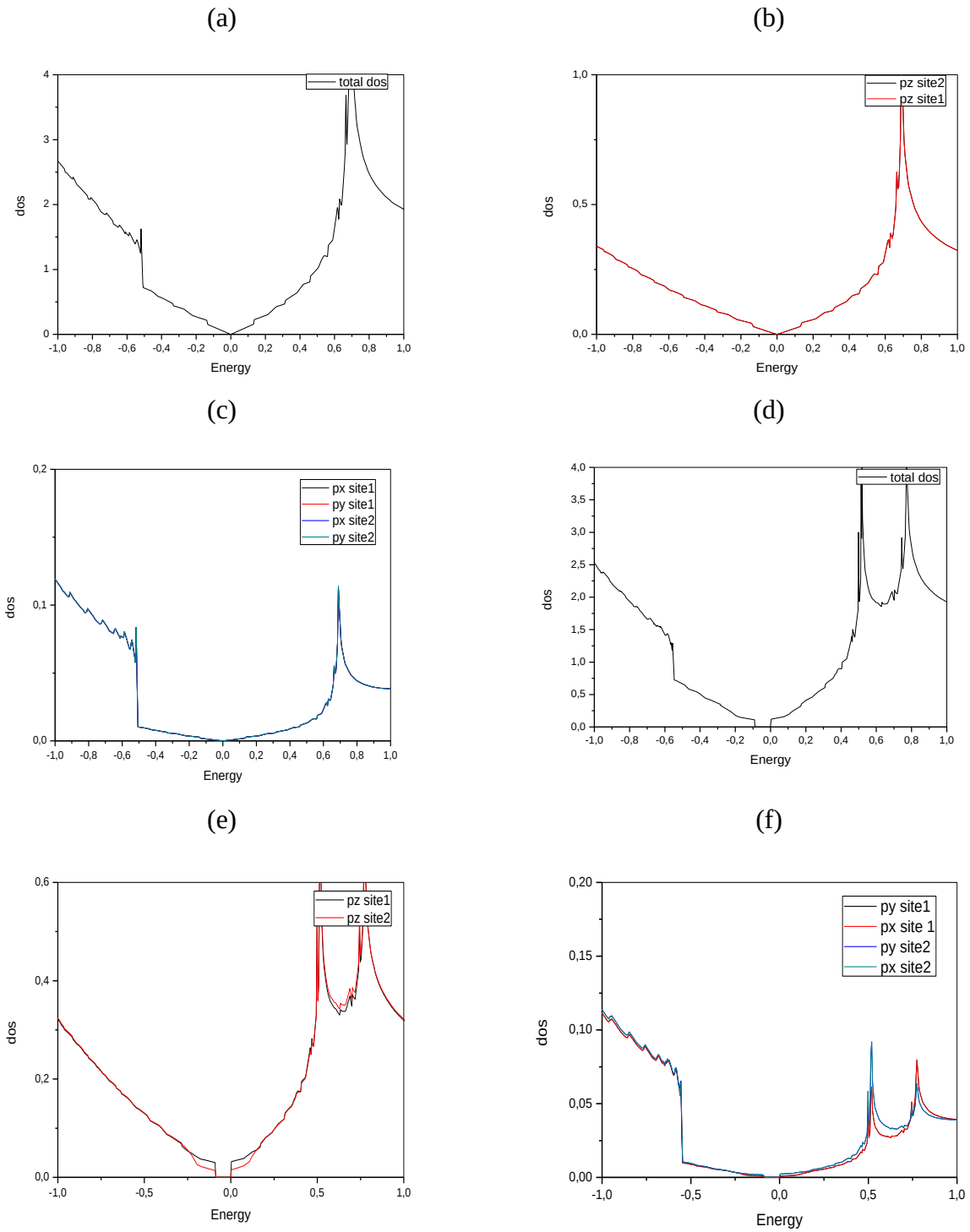

Figure 5.7: Total and partial electronic structure of AA2: (a, b, c) for distance far away from d=9 Å and (d, e, f) correspond to the distance d=5.7 Å associated with the maximal gap.

This stabilization can be understood in terms of an electronic structure transition in p_z orbitals. It is a transition from delocalized to localized states allowing the opening of the energy

gap. One possible explanation of this behavior can be given in terms of the coupling interaction between two parallel material planes caused by varying the inter-bilayer distance.

In the end of this work, we would like to make contact with the pervious works dealing the silicene and graphene like bilayers [**279**], [**280**]. Compared with such materials, buckled germanene bilayers share similar behaviors concerning the opening of energy gap. However, the flat geometry in germanene does not bring any modification in energy gap contrast to graphene case. The results obtained in this work may allow the buckled germanene to be a possible candidate for Nano science applications.

5.1. Conclusion

In this chapter, we have discussed the electronic band structure of two parallel planes of silicene and germanene having hexagonal geometries using first-principles calculations based on FPLO9.00-34 code. For each material, we have reported an explicit computational study of a static single layer in the presence of an extra dynamic one. The latter one is located at distance *d* along the normal direction z forming with the first one a (AA1) and reversed (AA2) stacking arrangements. It has been shown that band gap can be opened by simply varying the distance between two parallel layers of silicone only for the distance greater than Van der Waals bond length. But, in the germanene case, the flat geometry does not respond to such a distance variation. However the band gap can be opened by simply varying the distance between two parallel layers of germanene for two different buckled geometries. The existence of the energy gap behavior is due to the transition from delocalized to localized states in p_z orbitals. We believe that our results present the first systematical study on germanene and silicene like bilayers.

6. Chapter 4: Adsorption of Fe, Co and Ni on the Graphene with a Double Hexagonal Symmetry: Electronic and Magnetic properties

6.1. Introduction

Recently, many efforts have been devoted to study the interaction of the metal adatoms in the graphene-like models [**30**], [**31**], [**32**], [**33**], [**34**]. This interaction can be used for many potential applications including the building of the Nano-magnetic materials. In particular, the interaction of the magnetic atoms with the graphene like materials can produce half-metallic systems which have been considered as interesting tools for the spintronic device applications [**35**], [**36**], [**37**]. It has been shown, experimentally and theoretically, that the adsorbed metals on the graphene sheets exhibit various geometrical properties like the continuous coatings or the discrete clusters [**283**], [**284**], [**285**]. These structures can be explored to show interesting physical phenomena. Several works, including the experimental and the theoretical ones, have been focused on the investigation of such models [**285**], [**42**], [**286**], [**287**], [**288**], [**289**].

The goal of this chapter is to show our contribution to these activities by studying the electronic and the magnetic properties of the iron, cobalt and nickel adsorption on the graphene geometry using DFT calculations. To start, it is worth noting that an unexpected superstructure has been found in the silicene and the epitaxial graphene [**41**], [**290**]. In both systems, the hexagonal symmetry develops an unexpected hexagonal superstructure. For instance, an experimental work on the silicone material by low temperature STM and scanning tunneling spectroscopy (STS) has been explored leading to a $(\sqrt{3}\times\sqrt{3})R30°$ structure on silicene sheet, in contrast to the (1×1) usual structure. For this new structure, it has been revealed that the electronic property measured by STS is in good agreement with theoretical result opening a new window for silicene applications. Moreover, it has been obtained a quasi-particle interference (QPI) patterns suggesting intervalley and intravalley scattering of charge carriers [17].The same hexagonal symmetry has been dealt with in the study of the epitaxial graphene doped with the oxygen using various method including Low Energy Electron Microscopy, microprobe Low Energy Electron Diffraction and microprobe Angle Resolved Photoemission. In particular, the

$(\sqrt{3}\times\sqrt{3})R30°$ structure has been also obtained on a different localization of the material suggesting that the oxygen can intercalate between the interface and the first graphene layers without producing the covalent bounds with the graphene layers [**290**].Moreover, it has been found that the rock-salt-type films exhibit an anomalous wurtzite-type stacking near the surface [**291**] and form a $(\sqrt{3}\times\sqrt{3})R30°$ superstructure in their low-temperature ground state [**292**].

Motivated by all these activities and the fact that, in 3d transition metals, the atoms prefer the hollow H sites leading to a stable configuration [**32**], [**293**], we consider a hexagonal geometry involving a $\sqrt{3}\times\sqrt{3}\ R30°$ superstructure in the presence of the usual one (1×1). We will refer to this structure as double hexagonal structure which will be based on a special Lie algebra.

It has been observed that the double hexagonal symmetry forces the systems to behave like metals. In fact, a similar feature has been obtained in the case of the silicene and the iron, cobalt and nickel adatom on the graphene material [**294**], [**8**], [**230**] , [**228**]. In particular, in our previous work [**230**] , some properties of the iron adatom system, based on a double hexagonal structure inspired from Lie symmetries proposed in ref [**294**], [**8**], have been investigated. More precisely, we have computed the Curie temperature and the magnetic moments, the energy adsorption, the geometry and the density of states [**230**] . Among others, the model reveals higher spin polarizations. However, it involves a lower Curie temperature value. Shortly following, we extend our previous work by implementing new adatoms sharing some properties of the iron atoms but they produce higher critical temperatures. Precisely, we consider the Co and Ni atoms. More precisely, it has been found that the Co adatom induces the ferromagnetic behaviors with high Curie temperature value in the presence of a strong spin polarization around 79% [**228**]. However, the system based on the Ni adatom does not exhibit ferromagnetic properties [**228**]. For simplicity reason, we refer to such models as the Fe-graphene, Co-graphene and the Ni-graphene, respectively. For the first systems, we reveal that the responsible mechanism for such a behavior is the interaction between Co or Fe adatoms. A priori, there are two interaction types. The first one corresponds to the direct interaction between the adatoms while the second one is associated with the indirect interaction via the carbon atoms. These interactions will be discussed later one. The Curie temperature is also estimated using the Monte Carlo simulation in the case of cobalt adatom.

Roughly speaking, the new material geometries, up some details, involve a similar feature as the one obtained recently in the flat silicone and graphene [**294**], [**8**], [**230**] , [**228**]. The material is built using the G_2 symmetry with a double hexagonal appearing in the Lie algebra classification [**216**], [**295**]. In this atomic configuration, it appears a double hexagonal structure of the unequal side length at angle 30° in two parallel plans. This geometry allows us to engineer two parallel superstructures associated with the (1×1) and $(\sqrt{3}\times\sqrt{3})\,R30°$separated by an optimal length distance Δ, specified later on. The small hexagon, corresponding to the (1×1) structure, corresponds to the pure graphene. The planar projection of the big hexagon, associated with the $(\sqrt{3}\times\sqrt{3})\,R30°$ structure, will be formed either by the Co atoms or the Ni atoms depending on the model in question. The principal unit cell contains now twelve atoms on the two parallel sheets. To model the structure presented in Figure 6.1, the adsorbed elements should be placed at sites hollow (H) on the graphene with a 25% concentration in a homogeneous manner corresponding to a coverage of 0.666 monolayer (ML) placed at H sites. Firstly, it has been realized that the choice of the H adsorption sites on the graphene is the most stable for the adsorbed transition metals (TM) [**32**], [**293**], [**296**], [**297**], [**298**], [**299**]. Secondly, the interatomic distance between the Co or Ni atoms that placed in the two centers of adjacent hexagonal carbon rings is around d_{TM} $(TM = Fe\ or\ Co\ or\ Ni)$ $= 2.4699$ Å. This value is less than 1% being smaller than the distance between the nearest neighbors in their pure hexagonal structure [**300**]. Furthermore, we find that these nanostructures are thermodynamic stables by calculating theirs binding energies as we will mention later. This allows one to predict the corresponding structure and its modeling. We believe that this method provides a good way to discuss its effect on the electronic and the magnetic properties.

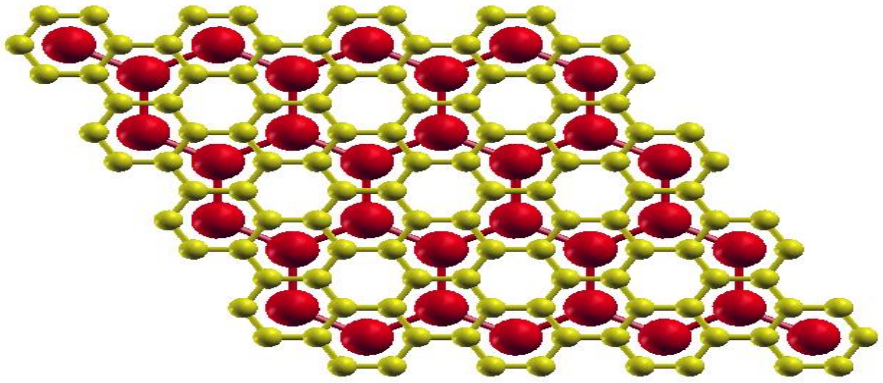

Figure 6.1: Double hexagonal structure of carbon (yellow) and TM (red) atoms.

6.2. Computational Method

Using the WIEN2K code [**301**], based on density functional theory (DFT) method, we study the magnetic properties of such TM adatom adsorption on the grapheme using the parameterization of the exchange-correlation energy within the generalized gradient approximation [**149**]. The radii of the muffin tin atomic spheres of Fe, Co, Ni and C atoms are $1.90, 1.80, 1.80$ and 1.27 Bohr respectively. The cutoff parameter $R_{\mathrm{MT}}\ K_{\mathrm{MAX}}$ is set to 7.0 where $\mathrm{R_{MT}}$ denotes the smallest muffin tin radius of the atoms. K_{MAX} is the maximum value of the reciprocal lattice vectors used in the plane wave expansion. A mesh of $(11, 11, 1)$ k-points in the irreducible part of the first Brillouin zone has been used in our calculation. To ensure a high accuracy in the performed computations, we have used self-consistent criteria of the energy and the force together with a precision of $10^6 Ry$ and $1.0\ mRy/Bohr$ respectively.

6.3. Relaxation method

Before studying the magnetic properties of the studied systems, we first determine the optimal vertical distances respect to the flat geometry of the graphene using the relaxation method for the magnetic configurations, (the ferromagnetic (FM) and the antiferromagnetic (AFM)), corresponding to the Fe, Co and Ni adsorbed atoms. These optimal distances will be used later for calculating the thermodynamic stability, the density of states and the magnetic properties of the most stable state. In all calculation, we use the lattice parameter of the pure graphene due to the fact that the C-C bonds are stronger than the bonds of the carbon atoms with the metals [**302**].

Having fixed the lattice parameter of the pure graphene to $a_c = 2.47A°$, the obtained equilibrium values of Δ are 1.90 and 1.84 for FM and AFM respectively for the Fe adatoms. For the Co adatoms these values are 1.88 and 1.74 for FM and AFM respectively. Moreover, we have found that the same value1.76 for FM and AFM in the case of Ni adatoms. These values are bigger compared to the one obtained from the single the Fe, Co and the Ni adatoms adsorption on the graphene. [**293**], [**298**] This shows a good agreement with the results obtained in the case of the adsorption of the iron atoms on the graphene at different densities [**296**], [**302**]. This observed increasing in the optimal vertical distance is due to the stronger mutual TM (Fe, Co or Ni) interaction leading to a large repulsive interaction between TM (Fe, Co or Ni) 3d and Carbon p electrons. This will turn on an influence on the intrinsic properties of the electronic and the magnetic structure of both TM (Fe, Co or Ni) and the graphene having a double hexagonal structure appearing in the G_2 symmetry.

6.4. Results and discussions

Based on the equilibrium position parameters obtained from the relaxation method, we study now the effect of the TM (Fe, Co or Ni) adsorption on the electronic structure and the magnetic properties in the presence of the double hexagonal symmetry.

To inspect such effects on each element of this structure, we start by discussing the magnetic properties. The stability of FM or AFM phases, the total moment per formula unit

(Corresponding to three carbon atoms for each TM one) and the partial moments of each atom have been investigated. Then, we move to examine the electronic structure in order to understand and explain the different observations. Finally, we determine the exchanging coupling parameter to estimate the corresponding Curie temperature using Monte Carlo simulation in or Mean field relation.

To determine the most stable magnetic configuration, we should compute the energy difference between the FM and the AFM states. This energy difference is then given by

$$\Delta E_{(AFM-FM)} = E_{AFM} - E_{FM} \qquad [6.1]$$

This quantity allows one to specify the magnetic phase stability. Indeed, to calculate this quantity, we have considered only two possible spin configurations depending on the alignment of the magnetic atoms. In fact, these two configurations are determined by the parallel and the anti-parallel alignments describing the FM and the AFM states respectively. This has been made only for the first neighbor atoms. A close inspection reveals that such a quantity is positive for the Fe-graphene and the Co-graphene systems, while it vanishes the Ni-graphene system. This feature indicates that the Ni-graphene system is a nonmagnetic material. In the Fe-graphene and Co-graphene systems, however, we have found that the FM state is more stable than the AFM state. This property correlates with the results of the total magnetic moments per formula unit obtained in the Fe-graphene, Co-graphene and the Ni-graphene systems, where the corresponding values are equal to 0.648 μ_B, 0.399 μ_B and 0.0258 μ_B respectively. Indeed, the obtained values of the partial magnetic moment for Fe are 2.55029 μ_B and 2.15029 μ_B associated with FM and AFM states respectively. In in the case of Co, it has been observed that these values are 1.625 μ_B and 1.333μ_B associated with FM and AFM states respectively. Moreover, in the case of Ni these values are 0.09446μ_B and 0.00020 μ_B for FM and AFM states respectively. Theses obtained values show the reduction of the magnetic moment at $T = 0\,K$ which reflects, essentially, the main effect of the quantum fluctuations on the studied systems. It is worth noting that this effect has been found in the lower dimensional model appearing in the condensed matter physic. In particular, this effect can be more relevant in the AFM state and the systems that involve a small magnetic moment (spin) values, see [**303**], [**304**], [**305**] and references therein.

Now, to examine the thermodynamic stability of the above stable state (Fe-graphene, Co-graphene, Ni-graphene systems), we should compute the binding energy of TM (Fe, Co or Ni) stretched to the graphene surfaces. Indeed, we determine this energy of the graphene–like nanostructure using the following equation [**32**]:

$$E_{binding} = E_{graphene} + E_{TM-layer} - E_{TM-graphene} \quad [6.2]$$

In this equation, E_{graphene} represents the total energy of a graphene sheet, $E_{TM\text{-}Layer}$ describes the energy of the TM (Fe, Co or Ni) layer, and $E_{TM\text{-}graphene}$ is the total energy of such a nanostructure. This energy quantity can be explored to analyze the stabilization of the studied systems. In particular, the positive value of this quantity indicates an energetically stable nanostructure, which can be exothermically synthesized. However, the negative value shows a non-stable nanostructure. Calculating this quantity for both nanostructures, we get $+0.84eV$ $+1.0eV$ and $+0.98eV$ for Fe, Co and Ni-like systems respectively.

In order to understand and explain the reason behind the more stabilized FM and the non-magnetic behaviors for the Fe-graphene, Co-graphene and the Ni-graphene systems respectively, we analyze the electronic structure. Indeed, Figure 6.2 and Figure 6.3 present respectively the total (TDOS) and the partial density of state (PDOS) the Fe-graphene system while (see Figure 6.4 (a, b)) presents respectively the total and the partial density of state (TDOS) of the both Co-graphene and the Ni-graphene systems with a double hexagonal structure at coverage of 0.666 ML for the TM atoms. It follows from TDOS that the intrinsic electronic structure of the pure graphene has been modified. In fact, the double hexagonal structure shows that the Fe-graphene and Co-graphene systems behave like ferromagnetic metals with strong spin polarization values which equal respectively to 83.5% and 79 % at Fermi level. This quantity is calculated via the following expression

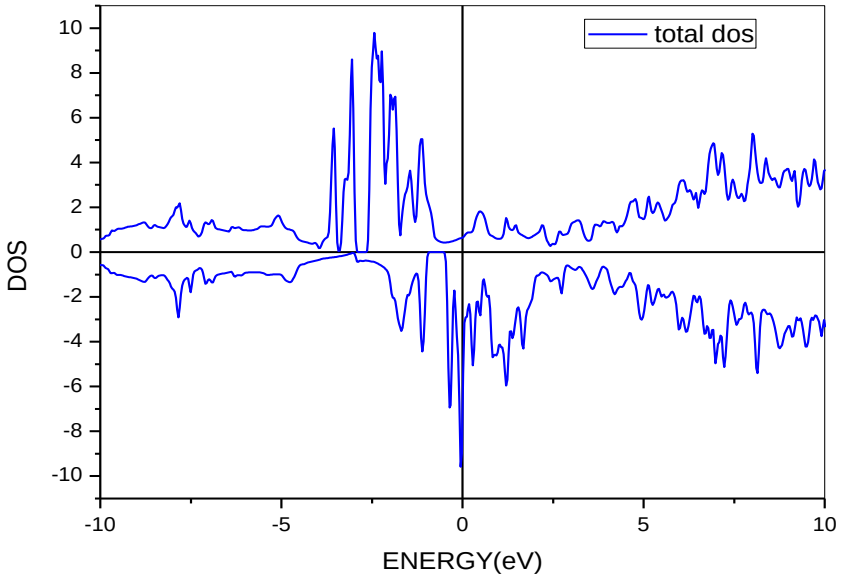

Figure 6.2: Total DOS of iron adatom adsorption on the graphene.

(a) (b)

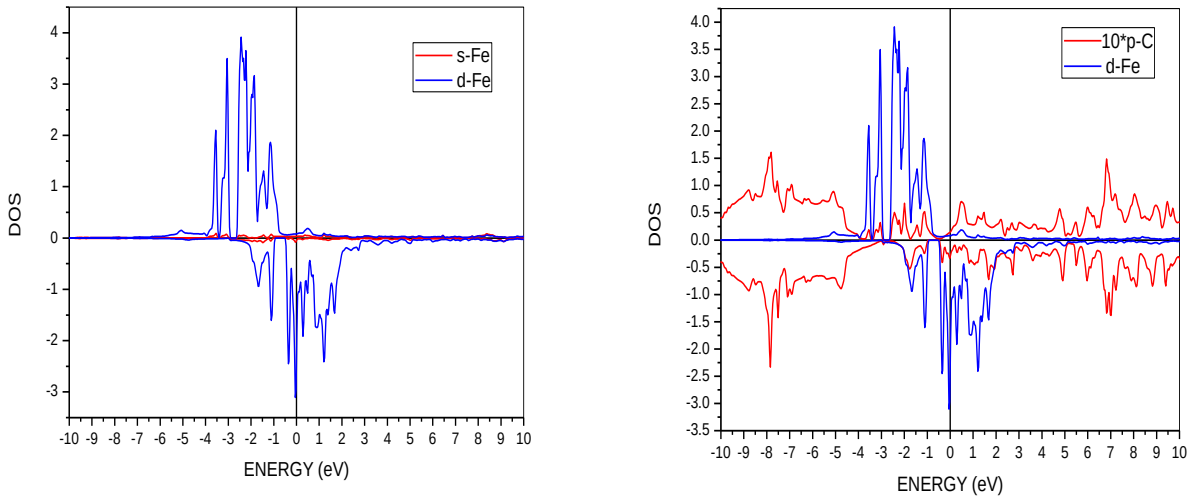

Figure 6.3: (a) Partial DOS of iron atoms adsorbed on graphene (b) red line represents p states of Carbon atom multiply by 10 and the blue one represents d states of iron atom.

$$P = \frac{N_{\uparrow}(E_F) - N_{\downarrow}(E_F)}{N_{\uparrow}(E_F) + N_{\downarrow}(E_F)} \qquad [6.3]$$

Where $N_{\uparrow}(E_F)$ and $N_{\downarrow}(E_F)$ describe the up and down state density for each system at Fermi level respectively. However, the Ni-graphene system is considered as a nonmagnetic metal (see Figure 6.4). To explain this behavior between the present studied models, we have analyzed the partial densities of them (TDOS) (see Figure 6.4). It is clear that there is an overlapping between the valence and the conductor bands showing a non-symmetric behavior between the densities of states of the spin up and down for the Fe and Co adatoms. This behavior is almost symmetrical for the Ni atoms. This feature supports first the mentioned behaviors appearing in the present systems, and also the small magnetic moments obtained in the case of the Ni-graphene system. Thus, we can deduce that the origin of the magnetism properties is due, essentially, to the strong splitting in the case of the Fe-graphene and Co-graphene systems. This splitting almost vanishes in the case of the Ni-graphene system.

Moreover, we observe an overlapping between s and d orbitals of the TM (Fe or Co) atoms and p orbital of the C atoms. Inspired from the electronic configuration of the isolated TM (Fe or Co) atoms and comparing the partial magnetic moment values of the Co atoms interacting with the graphene, we see a reduction of the local magnetic moments of the adsorbed TM (Fe or Co) atoms with respect to the isolated ones. This is due to the $4s \leftrightarrow 3d$ transition. More precisely, it follows from the values of such a variation in the magnetic moments that the electronic configuration of the iron atom $4S^2 3d^6$ is converted to $4S^1 3d^{7,}$ and the electronic configuration of the Co atom $4S^2 3d^7$ is also converted to $4S^1 3d^8$. Effectively, it has been shown that the filling of the d orbitals of the TM atoms occurs in the competition between the d and s states [**296**], [**306**]. Indeed, when the atom comes closer to the surface, the occupation of the 3d shell becomes more favorable due to the reduction of the Coulomb repulsion, whereas the occupation of the 4s shell becomes less favorable due to the increasing Pauli repulsion between the 4s and p electrons. This gives rise to the $3d^8 4s^1$ and $3d^9$ configurations of the Co atoms as shown in [**306**] . The DOS calculation shows a strong hybridization between the p-electrons of the carbon and d-electrons of the TM (Fe or Co) atoms.

The responsible mechanism for the magnetism between the TM (Fe or Co) atoms is the magnetic interaction. In fact, there are two interaction types. The first one is associated with the direct interaction, while the second one corresponds to the indirect interaction one via the carbon atoms. More precisely, the direct interaction is the dominant one with ferromagnetic type. Indeed, this could be explained form the fact that the distance between TM-TM (Fe or Co) atoms, in the studied model, is close to the neighbor distance in its hexagonal structure [**300**], as we mentioned in above. The indirect one is a weak anti-ferromagnetic reducing the intensity of the direct exchange compared to the isolated hexagonal structure of the TM (Fe or Co) atoms.

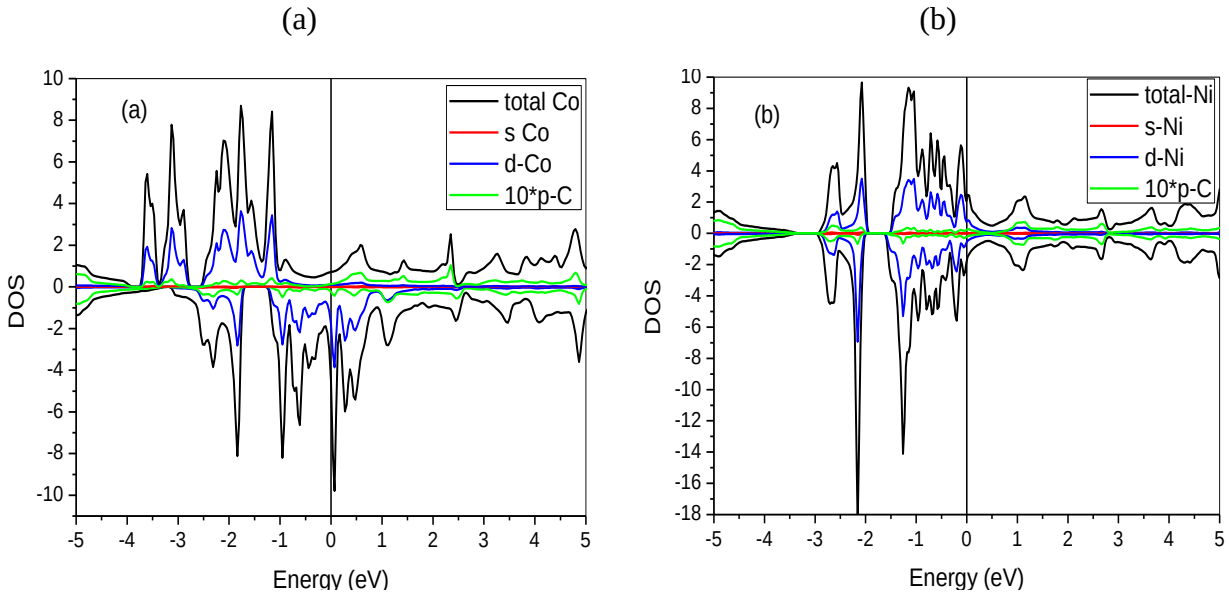

Figure 6.4: Total and partial DOS for (a) Co and (b) Ni adatom adsorption on graphene.

Now, it should be interesting to determine the Curie temperature T_C controlling the ferromagnetic phase transition observed in the Fe-graphene system Co-graphene systems. To estimate such a thermodynamic variable, a priori there are many approaches. Some of them are the molecular filed approximation and the Monte Carlo simulation. T_o estimate such a thermodynamic variable in the Fe-graphene system; we used an approach based on the molecular filed approximation used in the study of the Ising model. Following this method, we can determine the Curie temperature via the following equation

$$T_c = \frac{2}{3}\frac{zJS(S+1)}{k}. \quad [6.4]$$

In the above equation, J and S are the exchanging coupling parameter and the spin respectively. k is the Boltzmann constant and the variable z denotes the number of the nearest neighbor atoms having magnetic moments. Using a numerical calculation, we have found that the total magnetic moment per formula is $0.648\ \mu_B$. This value could be considered as a good one for the Nano magnetic material applications. Moreover, it has been observed that the values of the magnetic moments are $2.55029\ \mu_B$ and $-0.00873\ \mu_B$ for the carbon and the iron atoms respectively. It is clear that the carbons have no relevant magnetic moments and play no role in the elaborating the model. However, they provide an indirect interaction between the iron atoms. In this approximation, the relevant moment is the one associated with the iron atoms. For this reason, the magnetic structure of the system will relay on the symmetry associated with the big hexagon occupied only by the iron atoms.

To get the above parameters, we will use a Hamiltonian formalism describing a hexagonal geometry of the iron atoms. The Hamiltonian read as

$$H = -\sum_{i,j} JS_i S_j . \quad [6.5]$$

Where J now describes the effective exchanging coupling parameter controlling the direct interaction between the Fe-Fe atoms and the indirect interaction between the C-Fe atoms. According to [**230**], [**228**], [**231**], [**232**] , this quantity is given by

$$J_{eff} = \frac{1}{2NZS^2}\Delta E_{(AFM-FM)}. \quad [6.6]$$

In this equation, N indicates the number of the magnetic atoms. The values of the magnetic moments give approximately the value of the spin. More precisely, the spin is fixed to $S = \frac{3}{2}$. Taking z to 3, we obtain $T_c = 367\,\mathrm{K}$.

Moreover, for the Co-graphene system, we used the Monte Carlo calculations. This choice is motivated by the result obtained in the literature dealing with the magnetic statistical models. It is worth noting that this method provides a good estimation for the transition temperature compared with the other alternative methods. To do so, we first determine the magnetic structure for the Co-graphene system. Using the DFT calculation, we find that the partial moment for the Co and the carbon atoms are $1.625\ \mu_B$ and $-0.0035\ \mu_B$ respectively.

This means that the carbon atoms do not have relevant magnetic moments and thus they will not be taken into account during the elaboration of the model. They produce, however, an indirect interaction between the Co atoms. For this reason, the magnetic structure of the present system will be based on the hexagonal symmetry formed only by the Co atoms. For this calculation, we consider also the following Hamiltonian

$$H = -\sum_{i,j} J S_i S_j \qquad [6.7]$$

The values of the magnetic moments give approximately the possible spin value. More precisely, the spin is fixed to $S = 1$.In the above equation; J describes the effective exchanging coupling parameter controlling the direct interaction between the Co-Co atoms and the indirect interaction between the C-Co atoms. Similar to the case of Fe-graphene system and according to [**230**], [**228**], [**231**], [**232**], this quantity is also given by

$$J_{eff} = \frac{1}{2NZS^2} \Delta E_{(AFM-FM)} \qquad [6.8]$$

In this equation, N indicates the number of the magnetic atoms and z denotes the number of nearest neighbors of the Co atoms.

Second, using the Metropolis algorithm, we compute the Magnetization (m) and the Binder cumulant (U) [**229**] for different sizes (L). This will be used to determine the value of T_C from an indirect way through the curve of the magnetization in terms of the temperature. These quantities are given respectively by

$$m = \frac{1}{N}\sum_{i=1}^{N} S_i, \qquad U_4 = 1 - \frac{\langle m^4 \rangle}{3\langle m^2 \rangle^2} \qquad [6.9]$$

Where N is the total number of the spin sites corresponding to the lattice size while m is the magnetization per spin site.

The variation of the magnetization and the Binder cumulant as a function of the temperature for different system sizes are plotted in Figure 6.5 (a, b)). The magnetization vanishes continuously at the critical temperature. This indicates that the transition is the second order. It follows from the Figure 6.5 (b)) that the intersection point gives a good estimation of T_C that equals to $438\ K$. This value can be explored to implement experimentally the Co-graphene system. We expect that this system will bring new interesting features for the spintronic applications and in the elaboration of the Nano magnetic materials as well.

It is worth noting that this calculation has been made only for the first neighbor atoms in both systems. To give a complete picture, the magnetic anisotropy and the exchanging couplings of next nearest neighbors should be implemented in the calculation [**231**]. This feature needs a deeper study. We leave this issue for the future work. We hope to report on this issue elsewhere.

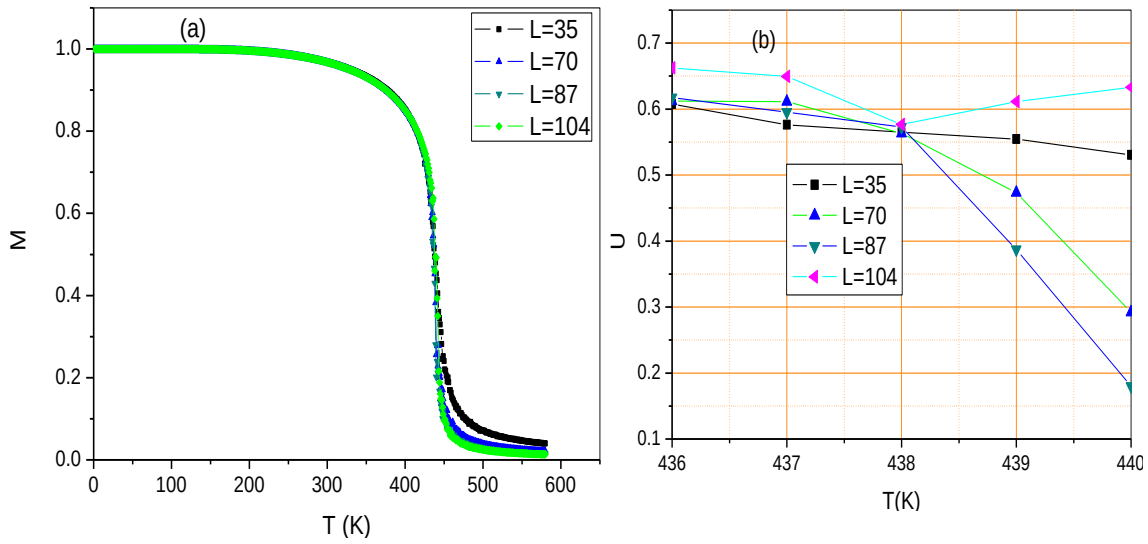

Figure 6.5: (a) The magnetization and (b) the Binder cumulant as a function of the temperature for different system sizes

6.5. Conclusion

In this chapter, we have engineered a model based on the adsorbed materials. This system is obtained by considering a graphene sheet interacting with the TM (Fe, Co, or Ni) atoms. We have found that the system exhibits a nice geometrical shape having a double hexagonal structure required by coverage of 0.666 monolayer placed at H sites. Motivated by recent works dealing with the graphene, the silicene and the nanotube adsorptions, we have built a stable configuration obtained by the relaxation method using the Wien2k code based on DFT method. A close inspection shows that the FM state is more stable than AFM state with the in the presence of strong spin polarizations in the case of Fe-graphene and Co-graphene systems. However, the derived Ni-system remains a non-magnetic metal.

The responsible mechanism for the magnetism between the TM (Fe or Co) atoms is the interaction contribution. It has been realized that there are two types. The first one is associated with the direct interaction between the TM (Fe or Co) atoms. The second contribution corresponds to an indirect interaction between the TM (Fe or Co) atoms via carbon ones. The Curie temperature and the spin polarization have been also estimated. In order to improve the obtained results, other quantities like the magnetic anisotropy and the exchanging couplings of the next nearest neighbors should be included in the calculation.

7. Chapter 5: New Hexagonal Structure for C, Si and Ge Atoms

7.1. Introduction

Recently, there has been a quite remarkable interest in the understanding of the silicene material since it involves properties similar to those of the graphene. Theoretical computations reveal that, near the so-called Dirac points, the corresponding low energy excitations of the flat silicene are described by the Dirac equation dealing with two dimensional (2D) massless fermions [**22**]. More recently, it has been obtained an unexpected $(\sqrt{3}\times\sqrt{3})$R30° superstructure on the silicene geometry instead of the usual (1×1) structure appearing in the single hexagonal structure [**41**]. In particular, it has been found a linear energy dispersion relation and a large Fermi velocity for such silicon atomic configurations.

This unexpected superstructure has been found also in epitaxial graphene [**41**], [**42**]. In these systems, the hexagonal symmetry develops an unexpected hexagonal superstructure. In particular, an experimental work on the silicene by low temperature STM and scanning tunneling spectroscopy (STS) has been investigated leading to a $(\sqrt{3}\times\sqrt{3})$R30° superstructure on the silicene sheet, in contrast to the (1×1) usual structure. For this new structure, it has been shown that the electronic property measured by STS is in good agreement with theoretical result providing a new support for silicene applications. Moreover, it has been found quasi particle interference (QPI) patterns suggesting intervalley and intravalley scattering of charge carriers [**41**]. The same hexagonal structure has been dealt with in the study of epitaxial graphene doped with oxygen using various method including Low Energy Electron Microscopy, microprobe Low Energy Electron Diffraction and microprobe Angle Resolved Photoemission. In this work, the $(\sqrt{3}\times\sqrt{3})$R30° structure has been also found on a different localization of the material suggesting that the oxygen can intercalate between the interface and the first graphene layers without producing covalent bounds with other layers [**42**].

The aim of this chapter is to contribute to these activities by presenting new materials having both (1×1) and $(\sqrt{3}\times\sqrt{3})$ R30° superstructures on the same atomic surface. In this new monolayer atomic representation, it appears a double hexagonal structure of unequal side length

at angle 30° supported by a two dimensional root system of the exceptional Lie algebra G_2. In this engineering method, the principal hexagonal unit cell of the double hexagonal structure is associated with the G_2 root system. It contains twelve atoms instead of the usual configuration involving only six ones.

The general study is beyond the scope of the present work, though we will consider two explicit examples with a flat geometry. Extended geometries including the buckled one will be dealt with in a future work. In particular, we give a numerical study dealing with the electronic structure of carbon, silicon and germanium. Using the density functional theory with the structural optimizations based on Ab-initio calculations relaying on FPLO9.00-34 code, we calculate the electronic structures of such materials. As a result, we show that the implementation of the double hexagonal structure modify the usual electronic properties and the size of the lattices. More precisely, the lattice parameters are increased and the corresponding materials are converted to a conductor, in contrast to the one involves only a single hexagonal geometry.

7.2. Models with double hexagonal structure and methodology

In this section, we engineer new materials with a double hexagonal symmetry. Then, we consider the study of the corresponding electronic structures. These atomic monolayers are assumed to be in a flat geometry. Indeed, motivated by the unexpected observation in the experimental result dealing with the silicon atoms where it appears the $(\sqrt{3}\times\sqrt{3})$R30° superstructure [**41**], we implement a new structure in Nano-materials based on atomic monolayers described by IV group elements. This superstructure is inspired from a special symmetry appearing in the Lie algebra classification of rank two [**216**] . Before going ahead, let us note that the present study assumes some basic knowledge on Lie algebras and their root systems. Indeed, a Lie algebra g is a vector space together with an antisymmetric bilinear bracket [,]: g.g → g satisfying the Jacobi identity $([a,[b,c]] + [c,[a,b]] + [b,[c,a]] = 0)$. It turns out that any semi-simple Lie algebra can be viewed as a direct sum of simple Lie algebras. The Cartan sub-algebra H is generated by the all semi-simple elements. It is worth noting that g may then be written as the direct sum of H and the subspaces $g = H \oplus \{\oplus_\alpha g_\alpha\}$ where $g_\alpha = \{x \in g, [h,x] = \alpha(x)x\}$. Here the vectors α ranges over all elements of the dual of H. In Lie

theory, these vectors are called roots and they form a set known by a root system of g. It has been realized that many information on the algebra are hidden in such a set. Roughly speaking, it has been shown that there is a nice classification of Lie algebras producing four different Lie algebras with rank two. One of them is called G_2. The index 2 refers to the rank two of this algebra being the dimension of the corresponding H sub-algebra. This is the group of the automorphisms for the octonionic algebra [**216**], [**307**], [**308**], [**309**], [**310**]. In the connection with the building of the root system, the G_2 symmetry has two hexagons of unequal side length generated by two simple unequal roots at angle $120° + 30° = 150°$. The length of the corresponding two simples roots α_1 and α_2 are constrained by $\frac{|\alpha_2|^2}{|\alpha_1|^2} = 3$. Each simple root generates a single hexagon. The small one is generated by the root set $\pm\alpha_1, \pm(\alpha_1 + \alpha_2), \pm(2\alpha_1 + \alpha_2)$ while the second one is generated by $\pm\alpha_2, \pm(3\alpha_1 + \alpha_2), \pm(3\alpha_1 + 2\alpha_2)$. It is interesting to note that the small one can be identified with the hexagonal structure associated with the su (3) symmetry since it is a G_2 subsymmetry. The remaining one should be associated with the unexpected observation found in [**41**].

Having introduced the mathematical backgrounds, now we build new materials with a double hexagonal structure. To do so, let us first discuss the atomic configuration based on monolayer geometry with the single hexagonal structure given in Figure 7.1. In fact, the six atoms of each unit cell are associated with the six nonzero roots of the su (3) Lie algebra. These roots are obtained from the simple ones with the sum and the opposed forming the single hexagon. They are given by $\pm\alpha_1, \pm\alpha_2, \pm(\alpha_1 + \alpha_2)$.

The new atom configuration will be associated with the root system of the G_2 symmetry. More specifically, to each non zero root we associate a single atom of the IV group elements. In this way, the principal cell consists of twelve atoms instead of six appearing in the single hexagonal structure material. Inspired from the G_2 root system, the unit cell involves two hexagons of unequal side length at angle 30°. The corresponding lattice parameters, which will be noted here as a_1 and a_2, are associated respectively with α_1 and α_2 and they are constrained by $|a_2|^2 = 3|a_1|^2$ required by the Lie symmetry classification [**216**]. The general configuration of the corresponding materials can be obtained from the fact the double hexagonal structure can also

tessellate the flat plane. This allows one to engineer two possible superstructures given by (1×1) and $(\sqrt{3}\times\sqrt{3})$R30°, forming a new unit cell for a monolayer atomic configuration with the double hexagonal symmetry. This monolayer structure is shown in Figure 7.2.

At this level an interesting comment may be done. The double hexagonal configuration develops $D_6 \times Z_2$ group symmetry of order twelve which acts transitively on the two hexagons independently. It is worth noting that D_6 is the dihedral group leaving a regular hexagon invariant.

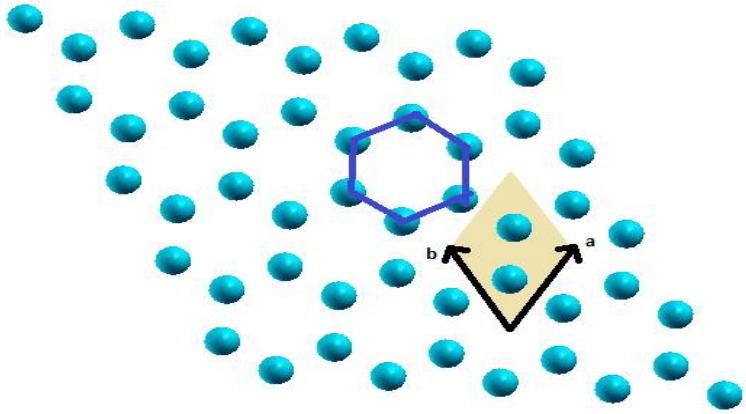

Figure 7.1: Two dimensional flat materials with single hexagonal structure.

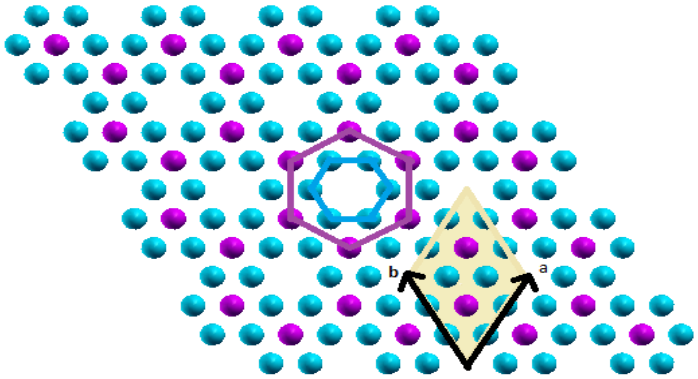

Figure 7.2: Monolayer of two dimensional flat materials with double hexagonal structure.

To study the electronic structure of such new materials having the double hexagonal geometry, we use *ab* intio calculations based on the all-electron full-potential local-orbital minimum-basis scheme FPLO9.00-34 [**196**], [**197**]. This method has been performed to solve the Kohn-Sham equations using the scalar-relativistic scheme. The parameterizations of the exchange-correlation energy have been done within the generalized gradient approximation (GGA) [**149**]. To ensure a high accuracy in our performed computations, we take both self-consistent criterions of the energy and the density together with a precision of 10^{-8} Ha and 10^{-6} respectively. To accurate the Brillouin zone integrations, we consider the tetrahedron scheme and the centered 48x48x1 K-point mesh.

In what follows, we consider the electronic structure of materials in the presence of the hexagonal structures. In all calculations, the atoms are located on the flat geometries which are formed by the two translation vectors. In particular, we use unit cells that are presented in the (Figure 7.1 and Figure 7.2). The calculations have been made for a monolayer geometry. Moreover, 40 Å is used as a vacuum spacing along the z-direction (perpendicular) to avoid the interactions of the unit cell with its periodic images. Multilayer systems will be dealt with in future.

In this work, we present only the carbon silicon and germanium atoms. We believe that this method can be applied for all elements sharing the characters of IV group elements. It is worth noting that the valence basis state sets are $(1s, 2s, 2p, 3s, 3p, 3d)$, $(2s, 2p, 3s, 3p, 3d, 4s, 4p)$ and $(3s, 3p, 3d, 4s, 4p, 4d, 5s)$ for the carbon, silicon and the germanium atoms respectively.

7.3. Results and Discussions

Before considering the numerical computation for the electronic structure of such materials, we first determine the equilibrium lattice parameters using the relaxation method for both the single and the double hexagonal structures. These parameters will be used later for calculating the density of states. Indeed, using the GGA approximation and the fitting with respect to a generic polynomial of the second order, we obtain the equilibrium positions corresponding to the single and the double hexagonal structure for the considered atoms. For the single hexagonal structure, we find that the lattice equilibriums take the value $a_C = 2.46 \pm 0.01$Å

a_{Si}=3.91 ± 0.01Å, and $a_{Ge} = 4.12 \pm 0.01$Å for the graphene, silicene and the germanene respectively. These lattice parameters are in a good agreement with the results obtained in the literature using the GGA approximation [**10**], [**238**]. For the double hexagonal structure, we get new values. In the case of the carbon, we obtain $a_1(C) = 2.89 \pm 0.01$Å for the small hexagonal and $a_2(C) = 5.00 \pm 0.01$Å $= \sqrt{3}a_1(C)$ for the big hexagonal and In the case of double hexagonal structure of silicon atoms, we find $a_1(Si)$=4.278 ± 0.01Å for the small hexagonal and $a_2(Si)$==7.410 ± 0.01Å=$\sqrt{3a_1(Si)}$; while for the germanene, we have $a_1(Ge) = 4.74 \pm 0.01$Å for the small hexagonal and $a_2(Ge) = 8.21 \pm 0.01$Å $= \sqrt{3}a_1(Ge)$ for the big hexagonal. It follows that the introduction of the double hexagonal structure affects the lattice parameters. Therefore, it increases the lattice parameter of the small hexagon. The effect of the double hexagonal structure on the lattice parameter behavior can be interpreted as a homogenous doping procedure around 67 % of atoms in the interstitial site. This is due the presence of interstitial atoms which provides a local geometric deformation of the corresponding lattice. This feature pushes the atoms to move and relax in order to get a new stable position. This observation could be supported by the known results dealing with the interstitial doping which increases the lattice parameters [**311**], [**312**].

(a) (b)

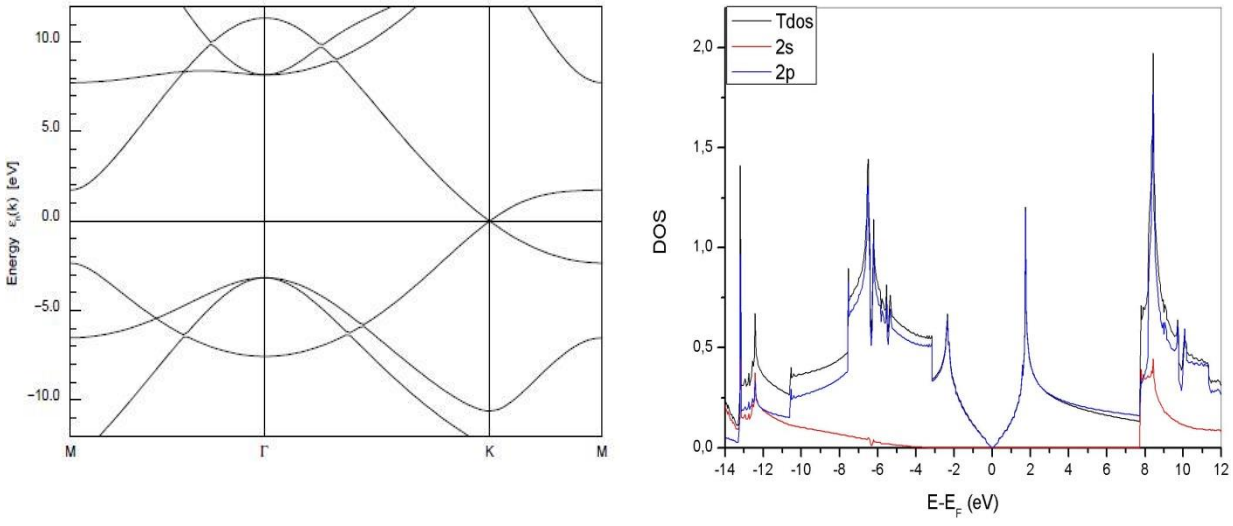

Figure 7.3: (a) Band structure and (b) density of states of graphene sheet.

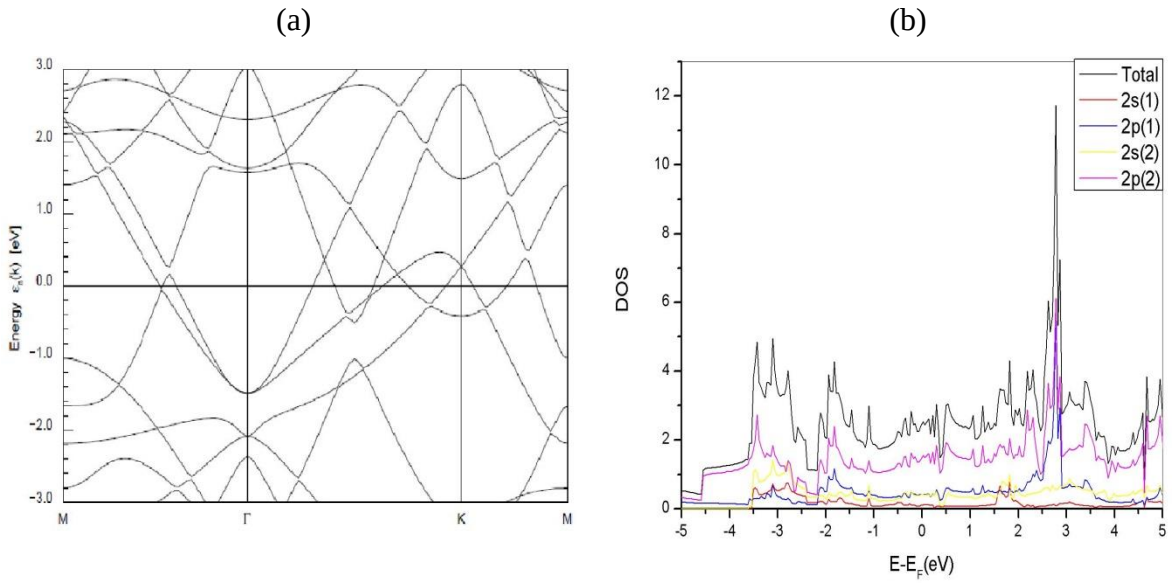

Figure 7.4: (a) Band structure and (b) density of states for double hexagonal of carbon.

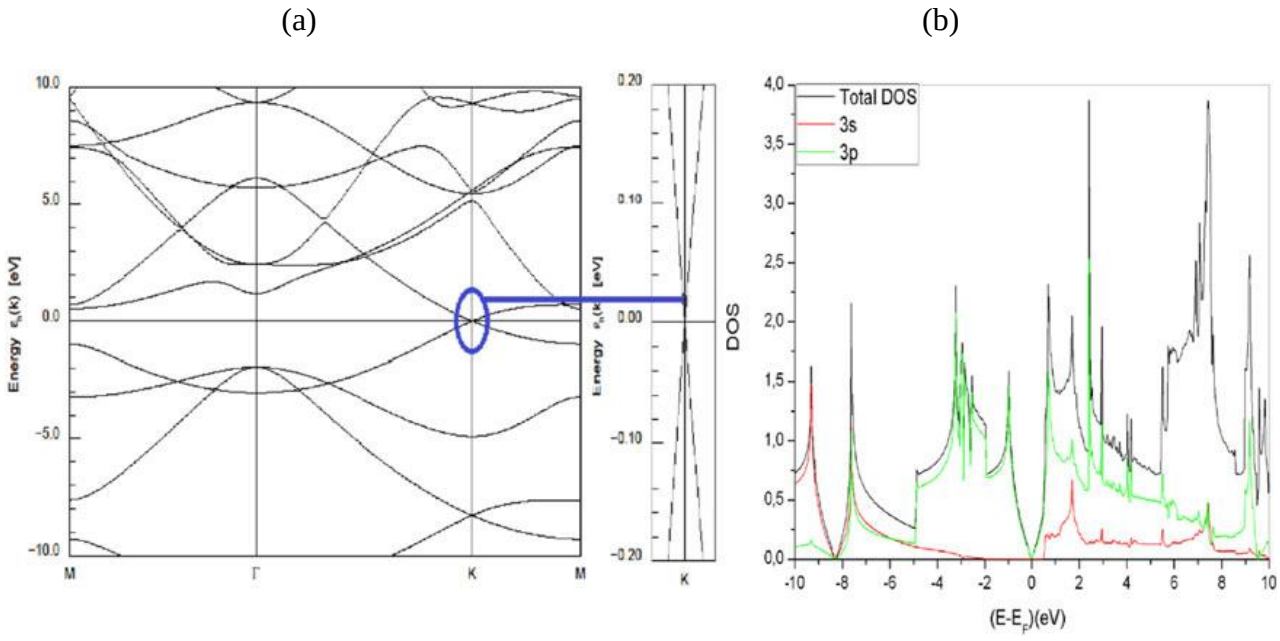

Figure 7.5: (a) Band structure and (b) density of states for silicene sheet.

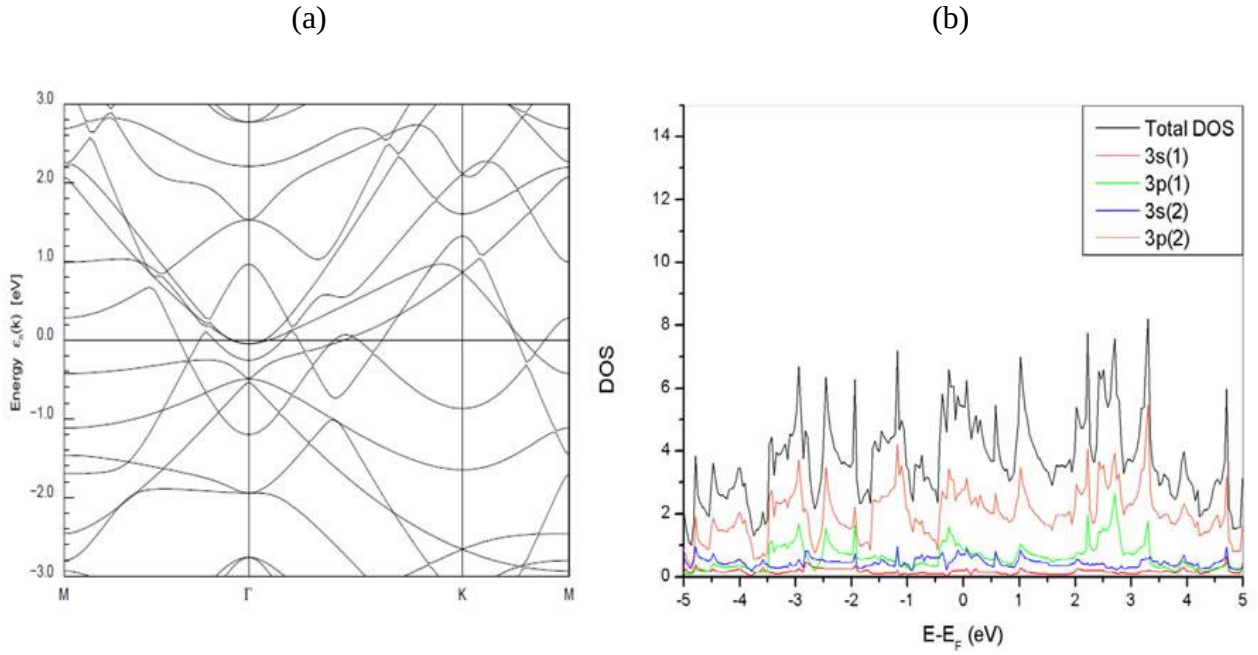

Figure 7.6: (a) Band structure and (b) density of states for the double hexagonal of silicon.

Based on the equilibrium position parameters obtained from the relaxation method, we study the electronic structures for the carbon, silicon and the germanium atomic configurations based on the double hexagonal. Using FPLO9.00-34 code, we first calculate the density of states (DOS) and the structure bands for the proposed materials. In particular, we plot in Figure 7.3 , Figure 7.4, Figure 7.5, Figure 7.6, Figure 7.7 and Figure 7.8, our results for DOS and band structures respectively. From Figure 7.3, we find similar results obtained in the literature [**10**], [**238**]. The energy dispersion is linear $\mathrm{E} = \pm h v_F k$ where k and v_F are momentum and Fermi velocity respectively. It is recalled that the linear dispersion behavior indicates that the charge carriers near the Dirac point become like massless fermionic fields satisfying the relativistic Dirac-like equation. On K-points, the usual graphene material is considered as a semi-conductor with zero gap energy.

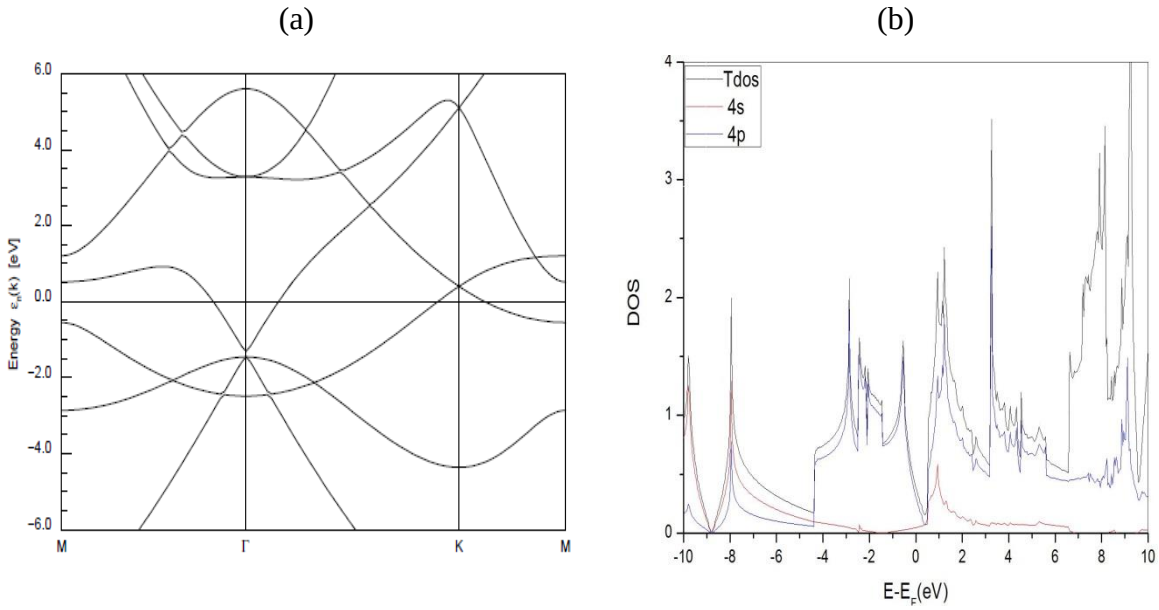

Figure 7.7: (a) Band structure and (b) density of states of germanene sheet.

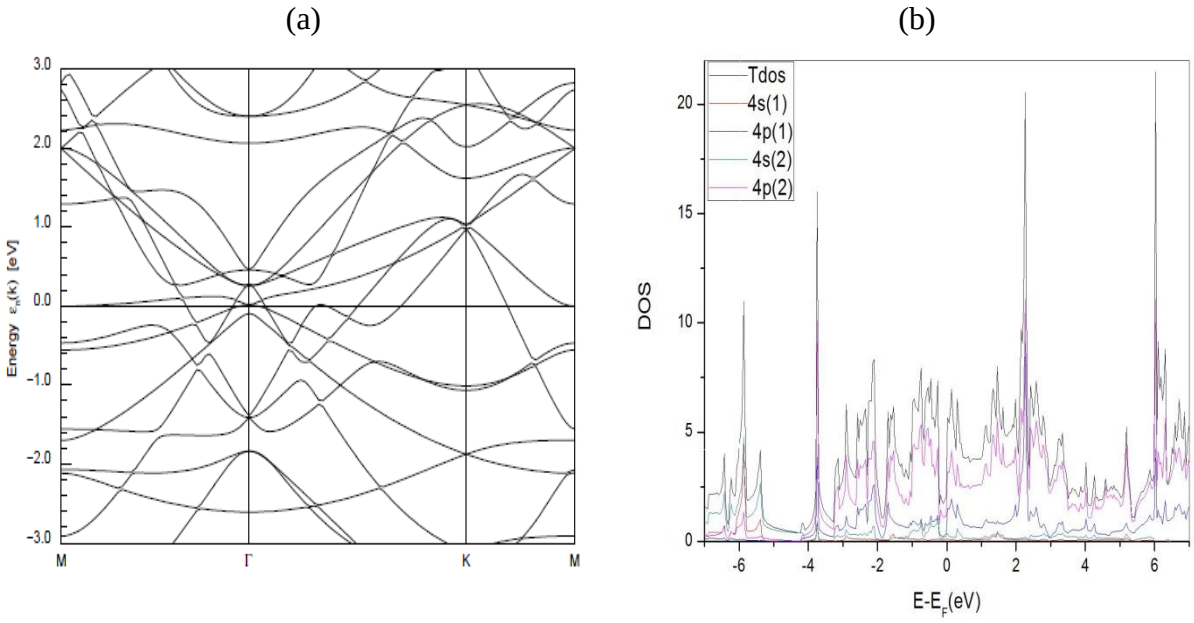

Figure 7.8: (a) Band structure and (b) density of states for the double hexagonal of germanium.

However, in the case of the carbon structure with the double hexagonal geometry, the system behavior has been modified compared with the usual one. Indeed, it follows from the (Figure 7.4) that there is an overlapping between the valence and the conductor bands indicating that the system has been converted to a metal. This is due to the effect of the double hexagonal structure which modify the number of neighbor interacting atoms for the small and the big hexagons. These numbers become five and six respectively instead of the three ones appearing in the usual single hexagonal materials. The increasing of these numbers creates new states around the Fermi energy. This leads to an overlapping between the valence and the conductor bands indicating the system becomes metal.

For the case of the silicon, we present our results in the (Figure 7.5) and (Figure 7.6). As shown clearly from these figures that the silicon atoms behave in both structure like the carbon atoms. In fact, they have almost the same analyses and discussions. The results of silicene are close to those obtained by other groups. [**10**], [**238**]

In the case of the germanium atoms, our results for single and double hexagonal structures are shown in the (Figure 7.7 and Figure 7.8) respectively. For the single hexagonal structure of the germanene, the conduction band and the valence band meet at K points which are now situated little higher than the Fermi energy. This result shows that the atomic monolayer of the germanene is a semimetal. This calculation agrees with the result obtained in literature using the Gaussian 03 package [**238**]. However, for the germanene with the double hexagonal geometry the behavior has been modified like the case of the graphene. From (Figure 7.7), one can observe easily that the material behaves like a metal.

7.4. Conclusion

In this work, we have discussed monolayer materials with a new hexagonal structure. This extended structure is based on a double hexagonal flat geometry. The geometry is associated with the two dimensional root system of the exceptional Lie algebra G_2. The principal hexagonal unit cell is related to the G_2 root system. The double hexagonal structure contains twelve atoms, instead of the usual one involves only six ones. This leads to two different (1×1) and $(\sqrt{3}\times\sqrt{3})R30°$ superstructures placed at the material sheet. More precisely, we have presented a numerical study using the density functional theory with structural optimizations based on Ab-

initio calculations relying on FPLO9.00-34 code with GGA approximations. The calculations have been made for the case of the graphene and the germanene. In particular, we have found that the usual electronic properties and the lattice parameters, appearing in the single hexagonal geometries, are modified. This is due to the fact that double hexagonal structure changes the number of the neighbor interacting atoms for the small and the big hexagons. These numbers are five and six respectively instead of the three ones appearing in the single hexagonal geometry. This augmentation of these numbers creates new states around the Fermi energy. This leads to an overlapping between the valence and conductor bands showing that the system behaves as a metal.

General Conclusion and Outlook

General Conclusion and Outlook

In the present thesis, we theoretically investigated, mainly, the electronic properties of graphene nanostructures. Furthermore, the electronic properties of silicene and germanene mono and bi layer also have been studied. Besides that, theoretical model of new hexagonal structure for the carbon, silicon and germanium is also investigated.

In the first chapter, we present the introduction to this work. A brief review on graphene as crystalline carbon allotrope, its properties and counterparts is given. A few methods to obtain graphene samples are presented along with some experimental techniques. In order to give an idea of how graphene may be useful, we discuss some applications of graphene either that already have been realized or in the future.

The second chapter is devoted to introduce the theoretical frame that we use and to explain some of the approximations and approaches used further on in this thesis.

In chapter 3 we provide an examination on the single layer materials models, and the calculation methods and making contact with the literature. In fact, these models can be flat in all cases or buckled as the case of silicene and germanene only. An examination of the method for these models is very important before undertaking the calculation corresponding to other effects on the electronic structure. For that, we have modeled systems corresponding to a single layer of graphene, silicene and germanene with appropriate approximations using FPLO9.00-34 code. Then, we determine the relaxed lattice parameter and the corresponding density of states and band structures as well. The obtained results show also that, the buckled model is most stable in the case of silicene and germanene. . This calculation agrees with the result obtained in literature. This is a good agreement allowing the validation of our modeling approximations based on FPLO using the LDA parameterizations.

In chapter 4, we have studied the electronic structure of the two parallel sheets of graphene using ab initio calculations implemented in FPLO9.00-34 code. The studied systems are based on

a static single layer interacting with an additional layer placed at distance d along the normal direction z forming with the first one a (AB) stacking arrangement. Indeed, we have first discussed the effect of the dynamic layer on the bilayer system by varying the vertical distance d starting from a distance around the van der Waals bond length. In particular, we have shown that the variation of the vertical distance does not modify the energy gap. In particular, the behavior of the band structure at K point has been changed from a linear to a parabolic one. This means that the charge carries become slightly massive. Moreover, we have found that such a distance variation can be used only to control the lattice size deformation.

However, we have shown that a diagonal distance variation of the graphene bilayer affects the electronic properties that drastically depend on intermediate stacking arrangements between the (AA) and the (AB) configurations. It has been shown that bilayer system behaves like two isolated graphene planes for large vertical distances. For small vertical distances, states in the Dirac cones belonging to the two layers interact between them. These interactions lead to the opening of the energy gap.

In chapter 5, we have discussed the electronic band structure of two parallel planes of silicene and germanene having hexagonal geometries using first-principles calculations based on FPLO9.00-34 code. For each material, we have reported an explicit computational study of a static single layer in the presence of an extra dynamic one. The latter one is located at distance *d* along the normal direction z forming with the first one a (AA1) and reversed (AA2) stacking arrangements. It has been shown that band gap can be opened by simply varying the distance between two parallel layers of silicone only for the distance greater than Van der Waals bond length. But, in the germanene case, the flat geometry does not respond to such a distance variation. However the band gap can be opened by simply varying the distance between two parallel layers of germanene for two different buckled geometries. The existence of the energy gap behavior is due to the transition from delocalized to localized states in pz orbitals. We believe that our results present the first systematical study on germanene and silicene like bilayers.

In chapter 6, we have engineered a model based on the adsorbed materials. This system is obtained by considering a graphene sheet interacting with the TM (Fe, Co, or Ni) atoms. We have found that the system exhibits a nice geometrical shape having a double hexagonal structure required by coverage of 0.666 monolayer placed at H sites. Motivated by recent works dealing

with the graphene, the silicene and the nanotube adsorptions, we have built a stable configuration obtained by the relaxation method using the Wien2k code based on DFT method. A close inspection shows that the FM state is more stable than AFM state with the in the presence of strong spin polarizations in the case of Fe-graphene and Co-graphene systems. However, the derived Ni-system remains a non-magnetic metal.

The responsible mechanism for the magnetism between the TM (Fe or Co) atoms is the interaction contribution. It has been realized that there are two types. The first one is associated with the direct interaction between the TM (Fe or Co) atoms. The second contribution corresponds to an indirect interaction between the TM (Fe or Co) atoms via carbon ones. The Curie temperature and the spin polarization have been also estimated. In order to improve the obtained results, other quantities like the magnetic anisotropy and the exchanging couplings of the next nearest neighbors should be included in the calculation.

In chapter 7, we have discussed monolayer materials with a new hexagonal structure. This extended structure is based on a double hexagonal flat geometry. The geometry is associated with the two dimensional root system of the exceptional Lie algebra G_2. The principal hexagonal unit cell is related to the G_2 root system. The double hexagonal structure contains twelve atoms, instead of the usual one involves only six ones. This leads to two different (1×1) and $(\sqrt{3}\times\sqrt{3}$)R30° superstructures placed at the material sheet. More precisely, we have presented a numerical study using the density functional theory with structural optimizations based on Ab-initio calculations relying on FPLO9.00-34 code with GGA approximations. The calculations have been made for the case of the graphene and the germanene. In particular, we have found that the usual electronic properties and the lattice parameters, appearing in the single hexagonal geometries, are modified. This is due to the fact that double hexagonal structure changes the number of the neighbor interacting atoms for the small and the big hexagons. These numbers are five and six respectively instead of the three ones appearing in the single hexagonal geometry. This augmentation of these numbers creates new states around the Fermi energy. This leads to an overlapping between the valence and conductor bands showing that the system behaves as a metal.

Outlook

To give a complete picture, many of the calculations of like-bilayer systems that were performed in this thesis should be improved by including explicitly van der Waals interaction in the DFT calculations, especially, for the large distances.

Another improvement would be the correction of the band gap calculations using more accurate approximations like TB-mBJ and methods like GW and the correction of the strong correlation for the transition metals. Furthermore, In order to improve the critical temperature in TM-graphene systems, other quantities like the magnetic anisotropy and the exchanging couplings of the next nearest neighbors should be included in the calculations.

As sake of completeness to these work, further studies, should consider the effect of substrate, contact, magnetic and electric fields and temperature

Moreover, the extension of graphene works in this thesis to silicene and germanene and other possible 0D, 1D and 2D materials. Other calculations including the optical properties, energy conversion and storage should be investigated.

Bibliography

Bibliography

[1] K. S. Novoselov et. al., *Science*, vol. 306, p. 666, 2004.

[2] A. K. Geim and K. S. Novoselov, *Nat. Mater.* , vol. 6 183, p. 183, 2007.

[3] A. H. Castro Neto et. al, *Rev. Mod. Phys*, vol. 81, p. 109, 2009.

[4] G. G. Guzmán-Verri and L. C. Lew Yan Voon, *Phys. Rev. B*, vol. 76, p. 07513191, 2997.

[5] A. Kara et. al, *J. Supercond. Novel Magn*, vol. 22, p. 259, 2009.

[6] B. Aufray, A. Kara et. al., *Appl. Phys. Lett.* , vol. 96, p. 183102, 2010.

[7] S. Naji, A. Belhaj, H. Labrim, A. Benyoussef, A. El Kenz, *The European Physical Journal B*, vol. 85, p. 273, 2012.

[8] S. Naji, A. Belhaj, H. Labrim, A. Benyoussef, A. El Kenz, " ," *Mod. Phys. Lett. B*, vol. 27, p. 1350212 , 2013.

[9] N. D. Drummond, V. Zólyomi, and V. I. Fal'ko, *Phys. Rev. B* , vol. 85, p. 075423 , 2012.

[10] H. Behera and G. Mukhopadhyay, *AIP Conf. Proc.*, vol. 1313, p. 152, 2010.

[11] S. Cahangirov, M. Topsakal, E. Akturk, H. Sahin, S. Ciraci, *Phys. Rev. Lett.*, vol. 102, p. 236804, 2009.

[12] A. Kara, H. Enriquez, A.P. Seitsonen, L. C. Lew Yan Voon, S. Vizzini, B. Aufray, H. Oughaddou, *Surf. Sci. Rep.* , vol. 67, pp. 1-18, 2012.

[13] A. S. Mayorov et al., *Nano Lett.*, vol. 11, p. 2396, 2011.

[14] C. Lee at al., *Science* , vol. 321, p. 385, 2008.

[15] R. R. Nair et al., *Science* , vol. 320, p. 1308, 2008.

[16] J. S. Bunch et al., *Nano Lett.* , vol. 8, p. 2458, 2008.

[17] J. Moser, A. Barreiro, A. Bachtold, *Appl. Phys. Lett.* , vol. 91, p. 163513 , 2007.

[18] K. Takeda and K. Shiraishi, *Phys. Rev. B* , vol. 50, p. 14916, 1994.

[19] Y. Zhang et al., *Nature*, vol. 438, p. 201, 2005.

[20] L. Li,S.-z. Lu,J. Pan,Z. Qin, Y. Wang, Y. Wang, G. Cao, S. Du, H. Gao , *Adv. Mater*, vol. 26, p. 4820, 2014.

[21] M.E. Dávila, L. Xian, S. Cahangirov, A. Rubio, G. Le Lay, *arXiv:1406.2488*, 2014.

[22] A. H. Castro Neto, F. Guinea, N. M. R. Peres, K. S. Novoselov, A. K. Geim, *Rev. Mod. Phys.*, vol. 81, p. 109, 2009.

[23] M.A. H. Vozmediano, F. Guinea, *arXiv:1108.0580.*, 2011.

[24] Y.-M. Lin et al., *Nano Lett.* , vol. 9, p. 422, 2009.

[25] Y.-M. Lin et al., *Science* , vol. 327, p. 662, 2010.

[26] F. Schwierz , *Nat Nanotechnol* , vol. 5, p. 487, 2010.

[27] Z. Y. Rong and P. Kuiper, *Phys. Rev. B* , vol. 48, p. 17427, 1993.

[28] W. T. Pong, and C. Durkan, *J. Phys. D : Appl. Phys.*, vol. 38 , p. R329 , 2005.

[29] L. Guohong, A. Luican, J. M. B. Lopes dos Santos, A. H. Castro Neto, et al., *Nature Physics* , vol. 6, p. 109, 2010.

[30] M. Chaichian et al., *Phys. Rev. A* , vol. 86, p. 012515, 2012.

[31] T. Wassmann et al., *Phys. Rev. Lett.*, vol. 101, p. 096402, 2008.

[32] V. Q. Bui et al., *J.Phys.Chem.C.*, vol. 117 , p. 3605, 2013.

[33] J. Yu, Z. Zhang, W. Guo, *J. Appl. Phys.* , vol. 113, p. 133701, 2013.

[34] R. Decker et al., *Phys. Rev. B*, vol. 87, p. 041403, 2013.

[35] J. Fernandez-Rossier,J. Palacios , *J. Phys. Rev. Lett*, vol. 99, p. 177204, 2007.

[36] F. Zhang et al., *J. Phys. Chem. C*, vol. 117, p. 14659, 2013.

[37] Z.H. Zhang et al., *Appl. Phys. Lett.* , vol. 97, p. 183105 , 2010.

[38] S. Datta and B. Das, *Appl. Phys. Lett.* , vol. 56, p. 665, 1990.

[39] V. F. Motsnyi et al., *Appl. Phys. Lett.*, vol. 81, p. 265, 2002.

[40] J. Akerman, *Science* , vol. 308, p. 508, 2005.

[41] L. Chen et al., *Rev. Lett.* , vol. 109, p. 056804, 2012.

[42] C. Mathieu et al., *Phys. Rev. B* , vol. 86, p. 035435 , 2012.

[43] E. H. L. Falcao and F. Wudl, *J. Chem. Tech. Biotech.*, vol. 82, p. 524, 2007.

[44] A. A. Radzig and B. M. Smirnov , *Reference Data on Atoms, Molecules and*. Berlin: Springer, 1985.

[45] S. Iijima, *nature*, vol. 354, p. 6348, 1991.

[46] M. Terronesa et al., *Nano Today* , vol. 5, p. 351, 2012.

[47] I. Snook and A. Barnard, *Physics and applications of graphene-theory*, S. Mikhailov, Ed. Rijeka, Croatia: InTech , 2011.

[48] Y.Son et al., *Phys. Rev. lett.*, vol. 97, p. 216803, 2006.

[49] Y. Li et al., *Phys. Rev. Lett.*, vol. 99, p. 186801, 2007.

[50] F. Wu et al, *Appl. Phys. Lett.*, vol. 94, p. 223105, 2009.

[51] T. J. Booth et al., *Nano Lett*, vol. 8, no. 8, p. 2442, 2008.

[52] S. Mikhailov, Ed., *Physics and applications of graphene-Experiments*. Rijeka, Croatia: InTech, 2011.

[53] S. Mikhailov, Ed., *Physics and applications of graphene-theory*. Rijeka, Croatia: InTech, 2011.

[54] X. Li et al., *Science*, vol. 319 , no. 5867, p. 1229, 2008.

[55] K. S. Kim et al., *Nature* , vol. 457, p. 706, 2009.

[56] M. Liu et al., *Nature* , vol. 474, p. 64, 2011.

[57] Y. W. Zhu et al., *Science*, vol. 332, p. 1537, 2011.

[58] M. F. El-Kady et al., *Science*, vol. 335, p. 6074, 2012.

[59] K. S. Novoselov et al., *Nature*, vol. 490, p. 192, 2012.

[60] F. Bonaccorso et al., *Nature Photonics*, vol. 4, no. 9, p. 611, 2010.

[61] R. E. Peierls, *Ann. Inst. Henri Poincare*, vol. 5, p. 177, 1935.

[62] L. D. Landau, *Phys. Z. Sowjetunion* , vol. 11, p. 26, 1937.

[63] N. D. Mermin and H. Wagner, *Phys. Rev. Lett.* , vol. 17, p. 1133, 1966.

[64] N. D. Mermin, *Phys. Rev.* , vol. 176, p. 250, 1968.

[65] J. C. Meyer, A. K. Geim, M. I. Katsnelson, K. S. Novoselov, T. J. Booth, and S. Roth, *Nature*, vol. 446, p. 60, 2006.

[66] A. Fasolino, J. H. Los, M. I. Katsnelson, *Nature Materials* , vol. 6, p. 858, 2007.

[67] P. R. Wallace, *Phys. Rev.* , vol. 71, p. 622, 1947.

[68] J. W. McClure, *Phys. Rev.*, vol. 108, p. 612, 1957.

[69] J. S. Slonczewski and P. R. Weiss, *Phys. Rev.*, vol. 109, p. 272, 1958.

[70] G. W. Semenoff, *Phys. Rev. Lett.* , vol. 53, p. 2449, 1984.

[71] K. S. Novoselov et al., *Nature*, vol. 438, p. 197, 2005.

[72] Y. Zhang, Y. -W. Tan, H. L. Stormer, P. Kim, *Nature* , vol. 438, p. 7065, 2005.

[73] M. I. KATSNELSON, *GRAPHENE Carbon in Two Dimensions*. Cambridge, UK: Cambridge University Press, 2012.

[74] F. R. Gamble and B. G. Silbernagel, *J. Chem. Phys.* , vol. 63, p. 2544, 1975.

[75] M. R. Lang et al., *ACS Nano*, vol. 6, p. 295, 2012.

[76] H. B. Zhang et al., *Adv. Mater.*, vol. 24, p. 132, 2012.

[77] X. F. Tang et al, *Appl. Phys. Lett.* , vol. 90, p. 012102, 2007.

[78] B. Feng, Z. Ding, S. Meng, Y. Yao, X. He, P. Cheng, L. Chen, K. Wu, *Nano Lett.*, vol. 3507, no. 7, p. 12, 2012.

[79] M. Houssa, G. Pourtois, V. V. Afanasev, A. Stesmans, *Appl. Phys. Lett*, vol. 97, p. 112106, 2011.

[80] S. Lebegue and O. Eriksson, *Phys. Rev. B* , vol. 79, p. 115409, 2009.

[81] N. Y. Dzade, K. O. Obodo, S. K. Adjokatse, A. C. Ashu, E. Amankwah, C. D. Atiso, A. A. Bello, E. Igumbor, S. B. Nzabarinda, J. T. Obodo, A. O. Ogbuu, O. E. Femi, J. O. Udeigwe, U. V. Waghmare, *J. Phys.: Condens. Matter*, vol. 22, p. 375502, 2010.

[82] D. Jose and A. Datta, *Phys. Chem. Chem. Phys.*, vol. 13, p. 7304 , 2011.

[83] C.-C. Liu, W. Feng, Y. Yao, *Phys. Rev. Lett.* , vol. 107, p. 076802 , 2011.

[84] M. Ezawa, *New J. Phys.* , vol. 14, p. 033003 , 2012.

[85] S. Lebegue O. Eriksson, *Phys. Rev. B* , vol. 79, p. 115409 , 2009.

[86] H. Behera and G. Mukhopadhyay, *AIP Conference Proceedings* , vol. 1349, p. 823, 2011.

[87] L.C. Lew Yan Voon, E. Sandberg, R.S. Aga, A.A. Farajian, *arXiv:1007.2110.*, 2110.

[88] M. Houssa, G. Pourtois, V.V Afanasev, A. Stesmans, *Appl. Phys. Lett.* , vol. 96, p. 082111 , 2010.

[89] S. Wang, *J. Phys. Soc. Jpn.* , vol. 79, p. 064602, 2010.

[90] T. Enoki and C. N. R. Rao S. K. Pati, Ed., *Graphene and Fascinating Attributes*. Singapore: World Scientific , 2011.

[91] X. Li et al., *Science* , vol. 1312, p. 324, 2009.

[92] S. Bae et al., *Nature Nanotechnol.* , vol. 5, p. 574, 2010.

[93] S. Lee et al., *Nano Lett.* , vol. 10, p. 4702, 2010.

[94] J. D. Roy-Mayhew and I. A. Aksay, *Chem. Rev*, vol. 114, no. 12, p. 6323, 2014.

[95] M. P. Ramuz et al., *ACS Nano*, vol. 6, p. 10384, 2012.

[96] L. A. Ponomarenko et al., *Science*, vol. 320, p. 356, 2008.

[97] C. Stampfer et al., *Nano Lett.* , vol. 8, p. 2378, 2008.

[98] J. Cai et al., *Nature*, vol. 466, p. 470, 2010.

[99] M. Y. Han et al., *Phys. Rev. Lett.*, vol. 98, p. 206805 , 2007.

[100] J. M. Pereira Jr., P. Vasilopoulos, F. M. Peeters, *Nano Lett.* , vol. 7, p. 946, 2007.

[101] T. Ohta et al., *Science 313* , vol. 313, p. 951, 2006.

[102] J. B. Oostinga et al., *Nature Mater.*, vol. 7, p. 151 , 2008.

[103] R. R. Nair et al., *Small 6, 2877 (2010*, vol. 6, p. 2877, 2010.

[104] D. C. Elias et al., *Science 323, 610 (2009*, vol. 323, p. 610, 2009.

[105] L. Britnell et al., *Science* , vol. 335, p. 947 , 2012.

[106] C. R. Dean et al., *Nat. Nanotech.*, vol. 5, p. 722, 2010.

[107] L. Liao et al., *Nature*, vol. 467 , p. 305, 2010.

[108] L. Liao et al., *Nano Lett.* , vol. 10, p. 3952, 2010.

[109] H. Dery et al., *IEEE Trans. Electron Devices*, vol. 59, p. 259, 2012.

[110] T. O. Wehling et al., *Nano Lett.* , vol. 8, p. 173, 2008.

[111] F. Fchedin et al., *Nat.Mater.* , vol. 6, p. 652 , 2007.

[112] E.W. Hill, A. Vijayaragahvan, K. Novoselov, *IEEE Sensors J.*, vol. 11, p. 3161, 2011.

[113] A. Tzalenchuk et al., *Nat. Nanotechnol.* , vol. 5, p. 186, 2010.

[114] T. J. B. M. Janssen et al., *Metrologia*, vol. 49, p. 294 , 2012.

[115] K. S. Novoselov et al., *Science* , vol. 315, p. 1379, 2007.

[116] A. Abouimrane et al., *J. Phys. Chem. C*, vol. 114 , p. 12800, 2010.

[117] P. Simon and Y. Gogotsi, *Nature Mater.* , vol. 7, p. 845 , 2008.

[118] B. A. CIPRA, "The Best of the 20th Century: Editors Name Top 10 Algorithms," *SIAM News*, vol. 33, no. 4, 2000.

[119] J. Dongarra and F. Sullivan, *Comp. in Sci. Eng*, vol. 2, no. 22, 2000.

[120] C.A. Mead, *Journal of VLSI Sig. Process.* , vol. 8, no. 9, 1994.

[121] R. Kurzweil, *The Age of Spiritual Machines*. New York: Penguin Putnam, 2000.

[122] R. M. Martin, *Electronic structure: Basic theory and practical methods*. Cambridge: Cambridge University Press, 2004.

[123] M. Born and J.R. Oppenheimer, "Ann. Physik," vol. 87, no. 457, 1927.

[124] D. R. Hartree, *Proc. Cambridge Phil. Soc.* , vol. 24, no. 89,111,426, 1928.

[125] V. Fock, *Z. Physik* , vol. 61, no. 126, 1930.

[126] J. C. Slater, *Phys. Rev.*, vol. 34, no. 10, p. 1293, 1929.

[127] C. D. Sherrill and H. F. Schaefer III, *Advances in quantum chemistry* , vol. 34, no. 143, 1999.

[128] H.Kümmel, *Theoretica chimica acta*, vol. 80, no. 2,3, 1991.

[129] Chr. Møller and M. S. Plesset, *Phys. Rev. 46, 618*, vol. 46, no. 7, p. 618, 1934.

[130] J. A. Pople, M. Head-Gordon, K. Raghavachari , *J. Chem. Phys.* , vol. 87, no. 10, p. 5968 , 1987.

[131] C. Angeli1, R. Cimiraglia, S. Evangelisti, T. Leininger, J.-P. Malrieu, *J. Chem. Phys.* , vol. 114, no. 23, p. 10252, 2001.

[132] C. Trindle and D. Shillady, *Electronic Structure Modeling: Connections Between Theory and Software*. NW: CRC Press, 2008.

[133] L. H. Thomas, *Proc. Cambridge Phil. Roy. Soc.* , vol. 23, p. 542, 1927.

[134] E. Fermi, *Rend. Accad. Naz. Lincei* , vol. 6, p. 602, 1927.

[135] P. A. M. Dirac, *Proc. Cambridge Phil. Roy. Soc.* , vol. 26, p. 376, 1930.

[136] C. F. von Weizsacker, *Z. Phys.*, vol. 96, p. 431, 1935.

[137] E. Wigner, *Trans. Faraday Soc.* , vol. 34, p. 678, 1938.

[138] R. P. Feynman, N. Metropolis, and E. Teller, *Phys. Rev.* , vol. 75, p. 1561, 1949.

[139] P. Hohenberg and W. Kohn, *Phys. Rev.* , vol. 136, p. B864, 1964.

[140] N. C. Handy, *Lecture Notes in Quantum Chemistry II*, B. O. Roos, Ed. Heidelberg: Springer, 1994.

[141] E.H. Lieb, *Int. J. Quantum Chem.* , vol. 24, no. 3, p. 243 , 1983.

[142] M. Levy, *Proc. Nat. Acad. Sci. USA*, vol. 76, p. 6062, 1979.

[143] N. D. Mermin, *Phys. Rev*, vol. 137, p. A1441, 1965.

[144] W. Kohn and L. J. Sham, *Phys. Rev.* , vol. 140, p. A1133, 1965.

[145] J. C. Slater, *Phys. Rev.*, vol. 81, p. 385, 1951.

[146] D. M. Ceperley and B. J. Alder, *Phys. Rev. Lett*, vol. 45, p. 566, 1980.

[147] J. P. Perdew and Y.Wang, *Phys. Rev. B*, vol. 45, p. 13244, 1992.

[148] J. P. Perdew, *Int. J. Quantum Chem*, vol. 28, p. 497, 1985.

[149] J. P. Perdew, K. Burke, M. Ernzerhof, *Phys. Rev. Lett*, vol. 77, p. 3865, 1996.

[150] C. S. Wang, B. M. Klein, H. Krakauer, *Phys. Rev. Lett.*, vol. 54, p. 1852, 1985.

[151] T. C. Leung, C. T. Chan, B. N. Harmon, *Phys. Rev. B*, vol. 44, p. 2923, 1991.

[152] A. D. Becke, *Phys. Rev. A*, vol. 38, p. 3098, 1988.

[153] C. Lee, W. Yang, R. G. Parr, *Phys. Rev. B*, vol. 37, p. 785, 1988.

[154] H. J. Monkhorst and J. D. Pack, *Phys. Rev. B*, vol. 13, p. 5188, 1976.

[155] H. Hellmann, *Einfuhrung in die Quantumchemie*. Leipzig: Franz Duetsche, 1937.

[156] R. P. Feynman, *Phys. Rev.*, vol. 56, p. 340 , 1939.

[157] T. L. Beck, *Rev. Mod. Phys.*, vol. 72, p. 1041, 2000.

[158] H. Hellmann, *J. Chem. Phys.*, vol. 3, p. 61, 1935.

[159] H. Hellmann, *J. Chem. Phys.* , vol. 4, p. 324, 1936.

[160] R. Car and M. Parrinello, *Phys. Rev. Lett.* , vol. 55, p. 2471, 1985.

[161] M. C. Payne, M. P. Teter, D. C. Allan, T. A. Arias, J. D. Joannopoulos, *Rev. Mod. Phys.*, vol. 64, p. 1045, 1992.

[162] W. C. Topp and J. J. Hopfield, *Phys. Rev. B* , vol. 7, p. 1295 , 1973.

[163] D. R. Hamann, M. Schlüter, C. Chiang, *Phys. Rev. Lett.* , vol. 43, p. 1494, 1979.

[164] W. C. Herring, *Phys. Rev.* , vol. 57, p. 1169, 1940.

[165] W. C. Herring and A. G. Hill, *Phys. Rev.*, vol. 58, p. 132, 1940.

[166] E. Antoncik, *Czech. J. Phys.*, vol. 4, p. 439, 1954.

[167] E. Antoncik, *J. Phys. Chem. Solids* , vol. 10, p. 314 , 1959.

[168] J. C. Phillips and L. Kleinman, *Phys. Rev.*, vol. 116, p. 287 , 1959.

[169] P. E. Blöchl, *Phys. Rev. B* , vol. 41, p. 5414 , 1990.

[170] D. Vanderbilt, *Phys. Rev. B* , vol. 41, p. 7892, 1990.

[171] P. E. Blöchl, *Phys. Rev. B* , vol. 50, p. 17953, 1994.

[172] G. Kresse and D. Joubert, *Phys. Rev. B*, vol. 59, p. 1758, 1999.

[173] N. A. W. Holzwarth, G. E. Matthews, A. R. Tackett, R. B. Dunning, *Phys. Rev. B* , vol. 55, p. 2005, 1997.

[174] F. Bloch, *Z. Phys.* , vol. 52, p. 555 , 1928.

[175] H. Jones, N. Mott, Skinner, *Phys. Rev.* , vol. 45, p. 379, 1934.

[176] J. C. Slater and G. F. Koster, *Phys. Rev.* , vol. 94, p. 1498, 1954.

[177] R. D. McWeeny and B. T. Sutcliffe, *Methods of Molecular Quantum Mechanics*, second edition ed. New York: Academic Press, 1976.

[178] F. Jensen, *An Introduction to Computational Chemistry*. New York: John Wiley and Sons, 1998.

[179] C. J. Cramer, *Essentials of Computational Chemistry: Theories and Models*. New York: Wiley, 2002.

[180] H. Eschrig, *Optimized LCAO Methods*. Berlin: Springer, 1987.

[181] J. C. Slater, *Phys. Rev.*, vol. 51, p. 846, 1937.

[182] V. L. Moruzzi, A. R. Williams, J. F. Janak, *Phys. Rev. B* , vol. 15, p. 2854, 1977.

[183] V. L. Moruzzi, J. F. Janak, A. R. Williams, *Calculated Electronic Properties of Metals*. New York : Pergamon Press, 1978.

[184] O. K. Andersen, *In Computational Methods in Band Theory*, J. F. Janak, A. R. Williams P. M. Marcus, Ed. New York: Plenum, 1971.

[185] D. J. Singh, *Planewaves, Pseudopotentials, and the APW Method*. Boston: Kluwer Academic Publishers, 1994.

[186] P. Blaha, K. Schwarz, P. Sorantin, S.B. Trickey, *Computer Phys. Commun.* , vol. 59, no. 2, p. 399, 1990.

[187] D. D. Koelling and G. O. Arbman, *J. Phys. F: Met. Phys.*, vol. 5, p. 2041, 1975.

[188] H. Krakauer, M. Posternak, and A. J. Freeman, *Phys. Rev. B* , vol. 19 , p. 1706, 1979.

[189] M. Weinert, E. Wimmer, A. J. Freeman, *Phys. Rev. B* , vol. 26, p. 4571, 1982.

[190] L. F. Mattheiss and D. R. Hamann, *Phys. Rev. B* , vol. 33, p. 823, 1986.

[191] H. Skriver, *The LMTO Method*. New York: Springer, 1984.

[192] O. K. Andersen, *Phys. Rev. B* , vol. 12, p. 3060, 1975.

[193] K. H. Weyrich, *Phys. Rev. B*, vol. 37, p. 10269 , 1988.

[194] O. K. Andersen, T. Saha-Dasgupta, R. Tank, C. Arcangeli, O. Jepsen, G. Krier, *Iin Electronic Structure and Physical Properties of Solids*, H. Dreysse, Ed. Berlin: Springer, 1998.

[195] O. K. Andersen and T. Saha-Dasgupta, *Phys. Rev. B* , vol. 62, p. R16219, 2000.

[196] K. Koepernik and H. Eschrig, *Phys. Rev. B* , vol. 59 , p. 1743, 1999.

[197] I. Opahle, K. Koepernik, H. Eschrig, *Phys. Rev. B* , vol. 60, p. 14035 , 1999.

[198] H. Eschrig, *The Fundamentals of Density Functional Theory*, 2nd ed. Leipzig: Edition am Gutenbergplatz, 2003.

[199] D. Singh, *Phys.Rev. B*, vol. 43, p. 6388, 1991.

[200] E. Sjöstedt, L. Nordström, D. J. Singh , *Solid State Commun.*, vol. 114, p. 15 , 2000.

[201] D. P. Landau and K. Binder, *A Guide to Monte Carlo Methods in Statistical Physics*. Cambridge: Cambridge University Press, 2000.

[202] M. E. J. Newman, G. T. Barkema, *Monte Carlo Methods in Statistical Physics*. Oxford: Clarendon Press , 1999.

[203] W.Janke, *Computational Many-Particle Physics, in: Lect. Notes Phys*, R. Schneider, A. Weiße H. Fehske, Ed. Berlin Heidelberg: Springer, 2008, vol. 739.

[204] C. Domb, *Phase Transitions and Critical Phenomena*, M. S. Green, J. Lebowitz C. Domb, Ed. London: Academic Press, 1974-2000, vol. 1-20.

[205] H. E. Stanley, *Introduction to Phase Transitions and critical phenomena*. Oxford: Oxford University Press, 1971.

[206] M. Yeomans, *Statistical Mechanics of Phase Transitions*. Oxford: Oxford University Press, 1993.

[207] O. Kahn, J.S. Miller, F. Palacio D. Gatteschi, Ed., *Magnetic Molecular Materials*. Plenum: NATO ASI E 198, 1991.

[208] P. Weiss, *J. Phys. Radium* , vol. 6, p. 661, 1907.

[209] R. Honmura and T. Kaneyoshi, *J. Phys. C: Solid State Phys.* , vol. 12, p. 3979 , 1979.

[210] N. Boccara, *Phys. Lett.A* , vol. 94, p. 185, 1983.

[211] A. Benyoussef and N. Boccara, *J. Appl. Phys* , vol. 55, p. 1667 , 1985.

[212] K.G. Wilson, *Phys. Rev. B* , vol. 4, p. 3184, 1971.

[213] J. Oitmaa, *Phys. Lett. A* , vol. 33, p. 230, 1970.

[214] K. Binder and P.C. Hohenberg, *Phys. Rev. B*, vol. 9, p. 2194, 1974.

[215] I. Syozi, *Progr. Theor. Phys.* , vol. 6, p. 341 , 1951.

[216] J. E.Humphreys, *Introduction to Lie Algebras and Representation Theory*. New York: Sauteur-Verlag, 1978.

[217] A. Belhaj, *Symétrie en Physique: Algèbres de Lie, Théorie des groupes et Représentations*.: arXiv:1205.3335, 2012.

[218] S. Naji, A. Belhaj, H. Labrim, M. Bhihi, A. Benyoussef, A. El Kenz, *Int. J. Mod. Phys. B*, vol. 28, p. 1450086, 2014.

[219] R. J. Baxter, *Exactly solved models in statistical mechanics*.: Academic Press Inc, 1982.

[220] W. Lenz, *Physikalische Zeitschrift* , vol. 21, 1920.

[221] E.Z. Ising, *Phys.* , vol. 31 , p. 253 , 1925.

[222] R. B. Potts, *Proc. Camb. Phil. Soc.* , vol. 48, p. 106, 1952.

[223] J. Ashkin and E. Teller, *Phys. Rev.*, vol. 64, p. 5 , 1943.

[224] H. E. Stanley, *Phys. Rev. Lett.* , vol. 20, p. 589, 1968.

[225] L. Onsager, *Phys. Rev.*, vol. 65, p. 117, 1944.

[226] J. Hammersley and D. Handscomb, *Monte Carlo Methods*. London,New York: Chapman and Hall , 1964.

[227] N. Metropolis, A. Rosenbluth, M. Rosenbluth, A. Teller, E. Teller, *J. Chem. Phys.* , vol. 21, p. 1087, 1953.

[228] S. Naji, A. Belhaj, H. Labrim, M. Bhihi, A. Benyoussef, A. El Kenz, *J. Phys. Chem.C*, vol. 118, no. 9, p. 4924, 2014.

[229] K. Binder and D.W. Heerman, *Monte Carlo Simulation in Statistical Physics*.: Springer Verlag, 1988.

[230] S. Naji, A. Belhaj, H. Labrim, M. Bhihi, A. Benyoussef, A. El Kenz, *Int. J. Quantum Chem.* , vol. 114, p. 463, 2014.

[231] S. Naji, A. Benyoussef, A. El Kenz, H. Ez.Zahraouy, M. Loulidi, *physica A*, vol. 391, p. 3885, 2012.

[232] F. El Hallani, S. Naji, H. Ez-Zahraouy and A. Benyoussef, *J. Appl. Phys.* , vol. 114, p. 163909 , 2013.

[233] R. Glauber, *J. Math. Phys.* , vol. 4, p. 294 , 1963.

[234] U. Wolff, *Phys. Rev. Lett.*, vol. 62, p. 361 , 1989.

[235] R. Swendsen and J.S.Wang, *Phys. Rev. Lett.* , vol. 58, p. 86 , 1987.

[236] S. Naji, A. Belhaj, H. Labrim, A. Benyoussef, A. El Kenz, *The European Physical Journal B*, vol. 85, p. 273, 2012.

[237] H. Şahin, S. Cahangirov, M. Topsakal, E. Bekaroglu, E. Akturk, R. T. Senger, S. Ciraci, *Phys. Rev. B* , vol. 80, p. 155453, 2009.

[238]]. T. Suzuki, Y. Yokomizo, *Physica E* , vol. 42, p. 2820, 2010.

[239] A. Das, S. Pisana, B. Chakraborty, S. Piscanec et al., *Nat. Nanotechnol.*, vol. 3, p. 210, 2008.

[240] Y.B. Zhang, T.T. Tang, C. Girit, Z. Hao, M.C. Martin, A. Zett l et al., *Nature*, vol. 459, p. 820, 2009.

[241] X. Deng et al., *Phys. Lett. A* , vol. 375 , p. 3890 , 2011).

[242] J. E. Santos et al., *Phys. Rev. B* , vol. 84, p. 085430, 2011.

[243] R.H. Miwa et al., *Appl. Phys. Lett.*, vol. 99, p. 163108 , 2011.

[244] T. Kawasaki, *Surf. Rev. Lett.* , vol. 9, p. 1459, 2002.

[245] L.Y. Zhao et al., *Science* , vol. 333, p. 999, 2011.

[246] P. A. Denis, *Chem. Phys. Lett.* , vol. 508 , p. 95, 2011.

[247] W.J. Yu et al., *Nano. Lett.*, vol. 11, p. 4759, 2011.

[248] J. Dai and J. Yuan, *J. Phys. Condens. Matter.* , vol. 22, p. 225501 , 2010.

[249] J. B. Oostinga et al., *Nature Mater*, vol. 7, p. 151, 2007.

[250] E. V. Castro et al., *Phys. Rev. Lett*, vol. 99, p. 216802, 2007.

[251] E. A. Henriksen and J. P. Eisenstein , *Phys. Rev. B*, vol. 82 , p. 041412, 2010.

[252] E. McCann and M. Koshino, *Rep. Prog. Phys.* , vol. 76 , p. 056503 , 2013.

[253] E.V. Gorbar et al., *Phys.Rev. B*, vol. 85, p. 235460, 2012.

[254] B. Roy, *Phys. Rev. B* , vol. 88, p. 075415 , 2013.

[255] R. V. Gorbachev et al., *Phys. Rev. Lett.* , vol. 98, p. 176805, 2007.

[256] M. Nakamura and L. Hirasawa, *Phys. Rev. B*, vol. 77, p. 045429, 2008.

[257] K. F. Mak, J. Shan, T. F. Heinz, *Phys. Rev. Lett.* , vol. 104, p. 176404, 2010.

[258] W. Norimatsu and M. Kusunoki, *Phys. Rev. B*, vol. 81, p. 161410, 2010.

[259] J.-K. Lee, S.-C Lee, J.-P. Ahn, S.-C. Kim, J. I. B. Wilson, P. John, *J. Chem. Phys.* , vol. 129, p. 234709, 2008.

[260] Z. Liu, K. Suenaga, P. J. F. Harris, and S. Iijima, *Phys. Rev. Lett.* , vol. 102, p. 015501, 2009.

[261] G. Trambly, D. Mayou, L. Magaud, *Nano Letters* , vol. 10, p. 804, 2010.

[262] J.-C. Charlier, X. Gonze, J.-P. Michenaud, *Carbon* , vol. 32, p. 289, 1994.

[263] Y.J. Dappe, M. A. Basanta, J. Ortega, F. Flores, *Phys. Rev. B*, vol. 74, p. 205434, 2006.

[264] M. Birowska, K. Milowska, J.A. Majewski, *Acta Physica Polonica A*, vol. 120, p. 845, 2011.

[265] J. Berashevich and T. Chakraborty, *J. Phys. Chem. C*, vol. 115, no. 50, p. 24666, 2011.

[266] T. Yumura and K. Yoshizawa, *Chem. Phys.*, vol. 279 , p. 111, 2002.

[267] J. Berashevich and T. Chakraborty, *Phys. Rev. B* , vol. 84, p. 033403, 2011.

[268] L. M. Zhang, Z. Q. Li, D. N. Basov, M. M. Fogler, Z. Hao, M. C. Martin, *Phys. Rev. B* , vol. 78, p. 235408, 2008.

[269] P. Gava, M. Lazzeri, A. Marco Saitta, F. Mauri, *Phys. Rev. B* , vol. 78, p. 165431, 2009.

[270] D.Tomanek and S. G. Louie, *Phys. Rev. B*, vol. 37, p. 14, 1987.

[271] J.-C. Charlier, X. Gonze, J.-P. Michenaud, *Europhys. Lett.*, vol. 28, p. 403 , 1994.

[272] R. Roldan, J.-N. Fuchs, M. O. Goerbig, *Phys. Rev. B*, vol. 82, p. 205418, 2010.

[273] G. Kresse and J. Furthmuller, *Phys. Rev. B*, vol. 54, p. 11169, 1996.

[274] M. A. Akhukov, A. Fasolino, Y. N. Gornostyrev, M. I. Katsnelson, *Phys. Rev. B*, vol. 85, p. 115407, 2012.

[275] S. Konschuh, M. Gmitra, D. Kochan, J. Fabian, *Phys. Rev. B* , vol. 85, p. 115423, 2012.

[276] M. Ezawa, *Phys. Rev. Lett.* , vol. 109, p. 055502, 2012.

[277] M. Ezawa, *J. Phys. Soc. Jpn*, vol. 81, p. 064705, 2012.

[278] C. Kamal, *arXiv:1202.2636*, 2012.

[279] S. Naji, M. Bhihi, H. Labrim, A. Belhaj, A. Benyoussef, A. El Kenz, M. Loulidi, *Journal of Physics and Chemistry of Solids* , vol. 75, p. 739, 2014.

[280] S.Naji, B.Khalil, H.Labrim, M.Bhihi, A.belhaj, A.Benyoussef, M.Lakhal, A.El Kenz, *J. Phys.: Conf. Ser.* , vol. 491, p. 012006, 2014.

[281] G. A. Tritsaris , E. Kaxiras , S. Meng, E. Wang, *Nano Lett.*, vol. 13, p. 2258, 2013.

[282] M. Mantina , A. C. Chamberlin , R. Valero , C. J. Cramer, D. G. Truhlar, *J. Phys. Chem. A* , vol. 113 , p. 5806, 2009.

[283] M. Mirzadeh and M. Farjam, *J.Phys.: Condens. Matter* , vol. 24, p. 235304, 2012.

[284] C. Ataca, E. Akturk, S. Ciraci, *Phys. Rev. B* , vol. 79, p. 041406, 2009.

[285] A. Saffarzadeh and G. Kirczenow, *Phys. Rev. B* , vol. 85, p. 245429 , 2012.

[286] T. O. Wehling et al., *Appl. Phys. Lett.* , vol. 93, p. 202110 , 2008.

[287] B. C. Wood et al., *J. Chem. Phys.*, vol. 137, p. 054702, 2012.

[288] L. Jean-Nicolas et al., *Appl. Phsy. Lett.* , vol. 101, p. 113117, 2012.

[289] B. L. Beata and L. I. Jae , *J. Korean Phys. Soc.* , vol. 53, p. 717, 2008.

[290] C. Mathieu et al., *Phys. Rev. B* , vol. 86, p. 035435, 2012.

[291] W. Meyer et al., *Phys. Rev. Lett.* , vol. 101, p. 016103, 2008.

[292] W. Meyer et al., *Phys. Rev. B* , vol. 79, p. 121403, 2009.

[293] K.T. Chan, J.B. Neaton, M.L. Cohen , *Phys. Rev. B* , vol. 77, p. 235430, 2008.

[294] S. Naji, A. Belhaj, H. Labrim, A. Benyoussef, A. El Kenz, *Eur. Phys. J. B* , vol. 85, p. 273, 2012.

[295] A. Belhaj et al., *International Journal of Theoretical Physics*, vol. 52, p. 130, 2013.

[296] Y. Yagi et al., *Phys. Rev. B* , vol. 69, p. 075414, 2004.

[297] Y. Mao, J. Yuan, J. Zhong, *J.Phys: Conden. Matter* , vol. 20, p. 115209, 2008.

[298] T. O. Wehling et al., *Phys.Rev.B* , vol. 84, p. 235110, 2011.

[299] H. Valencia et al., *J.Phys.Chem.C*, vol. 114, p. 14141, 2010.

[300] L. E. Sutton et al., *Table of interatomic distances and configuration in molecules and ions*. London: chemical Society, 1965, vol. 18, Supplement 1956-1959, Special publication.

[301] P. Blaha, K. Schwarz, G.K.H. Madsen, D. Kvasnicka, An Augmented Plane Wave + Local Orbitals program for calculating crystal properties, 2001.

[302] F. Ancilotto and F. Toigo , *Phys. Rev. B* , vol. 47, p. 13713, 1993.

[303] O. Janson et al., *Phys. Rev. B* , vol. 82, p. 014424 , 2010.

[304] A. Tsirlin, O. Janson, H. Rosner, *Phys. Rev. B* , vol. 82, p. 144416 , 2010.

[305] O. Janson et al., *Phys. Rev. B* , vol. 87, p. 064417 , 2013.

[306] A. N. Rudenko et al., *Phys. Rev. B* , vol. 86, p. 075422 , 2012.

[307] A. Belhaj, *J.Phys.A*, vol. 35, p. 8903, 2002.

[308] A. Belhaj et al., *J.Phys.A*, vol. 425, p. 325201, 2009.

[309] A. Belhaj et al., *J.Phys. A*, vol. 38, p. 2773, 2005.

[310] D. Joyce, *Compact manifolds of Special Holonom*.: Oxford University Press, 2000.

[311] O. Lagerstedt and B. Monemar, *Phys. Rev. B* , vol. 19, p. 3064, 1979.

[312] B. Baranowski, S. Majchrzak and T.B. Flangan, *J. Phys. F: Met. Phys.*, vol. 1, p. 258.8, 1991.

[313] I. Forbeaux et al., *Phys.Rev. B* , vol. 58, p. 16396 , 1998.

[314] C. Berger et al., *J. Phys. Chem. B*, vol. 108, p. 19912, 2004.

Abstract

In this thesis, we have theoretically investigated, using *ab* initio calculations, the electronic structure of graphene, silicene and germanene nanostructures.

We have shown first that, the inter-distances variation of the graphene bilayer affects the electronic properties that drastically depend on stacking arrangements. The interactions in such system lead to the opening of the band gap energy making this system extremely appealing for electronic devices and optoelectronics applications. A similar study has been also extended to silicene and germanene like bilayer systems which give close behaviors and results.

We have also engineered a double hexagonal structure model based on the adsorbed materials (Fe, Co, or Ni) atoms interacting with a graphene sheet. A close inspection shows that Fe-graphene and Co-graphene systems are ferromagnetic with strong spin polarizations, while Ni-system remains a non-magnetic metal. Monte Carlo calculations show that Co-graphene system has a high critical temperature making it a very useful in spintronic field.

Besides that, we have proposed and examined a new hexagonal structure for C, Si and Ge atoms. It is found that, this new hexagonal structure modified the usual electronic properties, appearing in the single hexagonal geometries.

Keywords: Graphene, silicene and germanene nanostructures, *ab* initio calculations, Monte Carlo simulation, opening of the band gap energy, ferromagnetic with a strong spin polarization